Ohio University

Athens, Ohio

Nonlinear Normal and Axial Force Indicial Responses for a Two Dimensional Airfoil

Department of

Mechanical Engineering

(2)

Nonlinear Normal and Axial Force Indicial Responses for a Two Dimensional Airfoil

by

G. M. Graham
M. Islam
K.C. Fang

Final Report under Grant AFOSR-89-0502

November 1991

REPORT DOCUMENTATION PAGE

Form Approved
OMB No. 0704-0188

1. AGENCY USE ONLY (Leave blank)	2. REPORT DATE	3. REPORT TYPE AND DATES COVERED
	15 November 1991	Final

4. TITLE AND SUBTITLE
Nonlinear Normal and Axial Force Indicial Responses for a Two Dimensional Airfoil

5. FUNDING NUMBERS
2307/CS
61102F
AFOSR-89-0502

6. AUTHOR(S)
Graham, G. M., Islam, M., and Fang, K. C.

7. PERFORMING ORGANIZATION NAME(S) AND ADDRESS(ES)
Ohio University
Mechanical Engineering Department
251 Stocker Center
Athens, Ohio 45701

8. PERFORMING ORGANIZATION REPORT NUMBER

9. SPONSORING / MONITORING AGENCY NAME(S) AND ADDRESS(ES)
AFOSR
Bolling AFB, DC 20332-6448

10. SPONSORING / MONITORING AGENCY REPORT NUMBER
AFOSR-89-0502

11. SUPPLEMENTARY NOTES

12a. DISTRIBUTION / AVAILABILITY STATEMENT
Approved for Public Release
Distribution is Unlimited

12b. DISTRIBUTION CODE

13. ABSTRACT *(Maximum 200 words)*

Normal and axial force indicial responses for a 2-D NACA 0015 airfoil undergoing small step changes in angle of attack have been measured in a tow tank. The airfoil was pitched about the quarter chord and the Reynolds number was 9.5×10^4. "First order" and "second order" tests were conducted. In the first order tests, the angle of attack prior to the step onset was held constant. In the second order study, the airfoil and was ramped up at constant rate to the onset angle. Step onset angles in the range $0^\circ < \alpha < 60^\circ$ were considered. The step responses have been integrated numerically to compute the loading during a ramp-up motion. The integrated results are compared with baseline load data taken with the same airfoil.

14. SUBJECT TERMS	15. NUMBER OF PAGES
Nonlinear Aerodynamics, Indicial Responses	77
	16. PRICE CODE

17. SECURITY CLASSIFICATION OF REPORT	18. SECURITY CLASSIFICATION OF THIS PAGE	19. SECURITY CLASSIFICATION OF ABSTRACT	20. LIMITATION OF ABSTRACT
U	U	U	

Abstract

Normal and axial force indicial responses for a 2-D NACA 0015 airfoil undergoing small step changes in angle of attack have been measured in a tow tank. The airfoil was pitched about the quarter chord and the Reynolds number was 9.5 X 10^4. "First order" and "second order" tests were conducted. In the first order tests, the angle of attack prior to the step onset was held constant. In the second order study, the airfoil and was ramped up at constant rate to the onset angle. Step onset angles in the range $0° < \alpha < 60°$ were considered. The step responses have been integrated numerically to compute the loading during a ramp-up motion. The integrated results are compared with baseline load data taken with the same airfoil.

Table of Contents

I. Introduction

The loading on an airfoil operating at high angle of attack is a nonlinear flight problem. In this context, nonlinear refers to the fact that the loading response to a step change in one or more of the motion variables is influenced by the flow conditions which exist at the onset of the step. The flow conditions at the step onset will be determined by the airfoil motion history prior to the step. Mathematically, the loading response to a step change in a motion variable as the step amplitude approaches zero and wherein an accounting is made of past motion effects is called the nonlinear indicial response[1,2]. The loading on an airfoil in arbitrary motion can, in principle, be computed through a convolution of indicial responses. This report investigates experimentally the nonlinear indicial normal and axial force responses to step changes in angle of attack. The main objectives of this report are to: i) provide some theoretical justification for the experiments undertaken, ii)present experimentally measured normal and axial force responses to step changes in angle of attack, and iii)numerically integrate the experimental responses for certain trial motions. The normal and axial forces acting on a 2-D airfoil undergoing a large-amplitude ramp motion are computed from the experimentally measured nonlinear responses. A saw-tooth motion is also considered. The integrated results are compared with baseline data taken with the same airfoil.

II. The Nonlinear Indicial Response

The normal force loading on a two dimensional airfoil moving in translation and rotation can be computed from the following convolution integral[1]:

$$C_N(t) = C_{No} + \int_0^t \phi_{N\alpha} \left[\frac{d\dot{h}}{d\tau} + \frac{d\alpha}{d\tau} \right] d\tau + \int_0^t \phi_{N\dot{\alpha}} \frac{d\dot{\alpha}}{d\tau} \, d\tau \qquad (1)$$

where C_{No} is the initial force, t is the nondimensional "measuring" time, and τ is a nondimensional time variable of integration. The motion variables α and $\dot{h}$ are measured in the "wind tunnel" axes so that α is the angle between the freestream velocity vector and the airfoil chord line and is positive nose-up, and $\dot{h}$ is the nondimensional rate of plunge perpendicular to the freestream and is positive downward. Both α and $\dot{h}$ are measured at the pitch axis. The term $\dot{\alpha}$ is the rate of change of α by rotation about the pitch axis. The terms $\phi_{N\alpha}$ and $\phi_{N\dot{\alpha}}$ are the

normal force indicial responses which are defined as:

$$\phi_{N\alpha} = \frac{\partial C_N}{\partial \alpha}\Big)_{\dot{h},\dot{\alpha}=\text{const}} = \frac{\partial C_N}{\partial \dot{h}}\Big)_{\alpha,\dot{\alpha}=\text{const}}$$

and $$\phi_{N\dot{\alpha}} = \frac{\partial C_N}{\partial \dot{\alpha}}\Big)_{\alpha,\dot{h}=\text{const}} \qquad (2)$$

In the nonlinear aerodynamics formulation the indicial responses are functionals[1,2] of the airfoil motion. Following the notation of Reference[1], this can be expressed by:

$$\phi_{N\alpha} = \phi_{N\alpha}\,[\alpha(\xi);t,\tau] \qquad \text{and} \qquad \phi_{N\dot{\alpha}} = \phi_{N\dot{\alpha}}\,[\alpha(\xi);t,\tau] \qquad (3)$$

where $\alpha(\xi)$ is a function which describes the airfoil motion. Notice that in the form of Equation 1, the indicial response $\phi_{N\dot{\alpha}}$ may also depend on the location of the pitch axis. By writing the indicial responses as functionals in terms of the airfoil motion $\alpha(\xi)$, past motion effects on the flow field are introduced into the formulation. In the linear formulation, the indicial responses are independent of prior motion events.

As shown in Section III.1, the integrals in Equation 1 can be written in terms of a single nonlinear indicial response functional, $\phi^*_{N\alpha} = \phi^*_{N\alpha}[\alpha(\xi);t,\tau]$, resulting in:

$$C_N(t) = C_{No} + \int_0^t \phi^*_{N\alpha}\,\frac{d\alpha}{d\tau}\,d\tau \qquad (4)$$

where $\phi^*_{N\alpha} = \phi_{N\alpha} - \frac{d\phi_{N\dot{\alpha}}}{d\tau}$. In Section III.2, $\phi^*_{N\alpha}$ is shown to be related to the loading response to a step change in α due to instantaneous rotation about some pitch axis.

The indicial response, $\phi^*_{N\alpha}$, is a derivative which is defined in terms of a "reference" motion and a "step" motion as illustrated in Figure 1[1]. The nonlinear indicial response is given by:

$$\phi^*_{N\alpha}[\alpha(\xi);t,\tau] = \lim_{\Delta\alpha \to 0} \frac{C_{N2}(t) - C_{N1}(t)}{\Delta\alpha} \qquad (5)$$

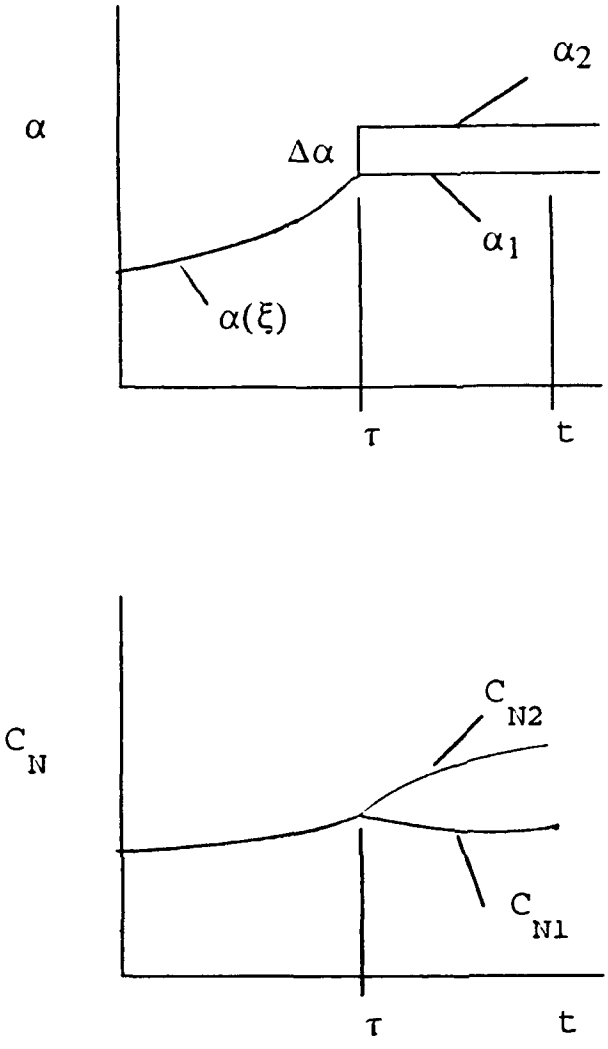

where:

$\alpha(\xi)$ is the "reference motion," defined for $-\infty < t \leq \tau$;

α_1 consists of $\alpha(\xi)$, for $t \leq \tau$, and is held constant at $\alpha(\tau)$ for $t > \tau$;

α_2 consists of $\alpha(\xi)$, for $t \leq \tau$, but jumps instantaneosly to $\alpha(\tau) + \Delta\alpha$, for $t > \tau$.

Figure 1. Motions for Defining the Nonlinear Indicial Response [1].

The form of the indicial response in Equation 5 is not tractable due to the potentially infinite number of reference motions and simplification of the response is needed. Reference[1] suggests that for relatively slow motions the response may be expressed in terms of elapsed time from step onset, $t-\tau$, and a finite number of motion variables at step onset. This can be written:

$$\phi^*_{N\alpha}[\alpha(\xi);t,\tau] \approx \phi^*_{N\alpha}[t-\tau;\ \alpha(\tau), \dot{\alpha}(\tau), \ddot{\alpha}(\tau),\ldots) \qquad (6)$$

where the retention of successively higher order derivatives includes motion events further into the past. The main focus of the present work is the dependence of the indicial response on the first order term, $\alpha(\tau)$, in Equation 6. Second order dependence would include both the $\alpha(\tau)$ and $\dot{\alpha}(\tau)$ terms, and so on.

II.1 Incompressible Case

The present experimental tests were conducted in water at a translational speed of 2 ft/s. Under these conditions the Mach number is nearly zero. In References[3,4] the indicial response is separated into a circulatory component, $\phi^*_{N\alpha_C}$, and a noncirculatrory component, $\phi^*_{N\alpha_I}$:

$$\phi^*_{N\alpha}[t-\tau,\alpha(\tau)] = \phi^*_{N\alpha_C}[t-\tau,\alpha(\tau)] + \phi^*_{N\alpha_I}[t-\tau,\alpha(\tau)] \qquad (7)$$

where we now specify $\phi^*_{N\alpha}$ to be a first order response (i.e. a function of $\alpha(\tau)$). For a thin 2-D airfoil at low angle of attack in an incompressible fluid (and with zero plunge), the noncirculatory normal force response due to an instantaneous positive step change in angle of attack by rotation about the quarter chord is[5]:

$$\phi^*_{N\alpha_I}[t-\tau,\ \alpha(\tau)] = \pi\left[\delta(t-\tau) + \frac{1}{2}\delta'(t-\tau)\right] \qquad (8)$$

The first term on the RHS is the Dirac delta function due to the infinite pitch rate at the step onset, and the second term is the time derivative of the delta function and represents the infinite angular acceleration and deceleration at the beginning and end of the rotation, respectively. The noncirculatory response for incompressible flow is nonzero at the step onset only and Equation 7

can be rewritten:

$$\phi^{*}_{N\alpha}[t-\tau, \alpha(\tau)] = \phi^{*}_{N\alpha_C}[t-\tau, \alpha(\tau)], \quad t-\tau > 0 \tag{9}$$

So that for incompressible flow, there is essentially an uncoupling of the circulatory and noncirculatory effects. Notice, however, that the noncirculatory component will contribute to the integral of Equation 4 due to integration across the delta function at $\tau = t$, giving an apparent mass term proportional to $\dot{\alpha}(t)$ [6].

III. Justification of the Approach

III.1 Alternate Form of the Convolution Integral

To first order, and with zero plunge, the normal force acting on an airfoil is given by the convolution integral:

$$C_N(t) = C_{No} + \int_0^t \phi_{N\alpha}[t-\tau, \alpha(\tau)] \frac{d\alpha}{d\tau} d\tau + \int_0^t \phi_{N\dot{\alpha}}[t-\tau, \alpha(\tau)] \frac{d\dot{\alpha}}{d\tau} d\tau \tag{10}$$

where t and τ are measured in semichords. In what follows an alternate form of Equation 10 is derived. This new form combines the indicial response due to angle of attack ($\phi_{N\alpha}$) and the indicial response due to pitch rate ($\phi_{N\dot{\alpha}}$) into a single response, $\phi^{*}_{N\alpha}$, for a step change in α due to instantaneous rotation about the pitch axis.

A prescribed airfoil motion can be represented by:

$$\alpha(\tau) = \alpha_0 + \mu(\tau) f(\tau) \tag{11}$$

where α_0 is the initial angle of attack, $\mu(\tau)$ is the unit step function which is zero for $\tau < 0$ and is unity for $\tau \geq 0$, and $f(\tau)$ is a nondimensional function describing the motion. The use of the unit step function allows consideration of both continuous and discontinuous motions such as:

$f(\tau) = K\tau$ (instantaneously started ramp motion, K=const.)
$f(\tau) = A \sin \omega\tau$ (harmonic motion)
$f(\tau) = \Delta\alpha$ (instantaneous step change in α)

Notice that for motions which are continuous in α at the origin $f(0) = 0$. In order to evaluate the integrals in Equation 10 we need:

$$\frac{d\alpha}{d\tau} = \mu(\tau)\, f'(\tau) + \delta(\tau)\, f(\tau) \quad \text{and} \quad \frac{d\dot{\alpha}}{d\tau} = \mu(\tau)\, f''(\tau) + 2\delta(\tau)\, f'(\tau) + \delta'(\tau)\, f(\tau) \tag{12}$$

where $\delta(\tau)$ is the delta function, and the ' superscript denotes differentiation with respect to τ. Substituting Equations 12 into Equation 10 and performing the integrations where possible[7] yields:

$$C_N(t) = C_{No} + \int_0^t \phi_{N\alpha}\, f'(\tau)\, d\tau + \int_0^t \phi_{N\dot{\alpha}}\, f''(\tau)\, d\tau + [\phi_{N\alpha} - \phi'_{N\dot{\alpha}}]\, f(\tau)\Big|_{\tau=0} + \phi_{N\dot{\alpha}}\, f'(\tau)\Big|_{\tau=0} \tag{13}$$

where the notation has been shortened using: $\phi_{N\alpha} = \phi_{N\alpha}[t-\tau, \alpha(\tau)]$ and $\phi_{N\dot{\alpha}} = \phi_{N\dot{\alpha}}[t-\tau, \alpha(\tau)]$ and $\phi'_{N\dot{\alpha}} = \frac{d\phi_{N\dot{\alpha}}}{d\tau} = -\frac{d\phi_{N\dot{\alpha}}}{d(t-\tau)}$. The second integral on the RHS of Equation 13 can be integrated by parts to give:

$$\int_0^t \phi_{N\dot{\alpha}}\, f''(\tau)\, d\tau = \phi_{N\dot{\alpha}}\, f'(\tau)\Big|_{\tau=t} - \phi_{N\dot{\alpha}}\, f'(\tau)\Big|_{\tau=0} - \int_0^t \phi'_{N\dot{\alpha}}\, f'(\tau)\, d\tau \tag{14}$$

Substituting Equation 14 into 13 and combining the integrals yields:

$$C_N(t) = C_{No} + \int_0^t [\phi_{N\alpha} - \phi'_{N\dot{\alpha}}]\, f'(\tau) d\tau + [\phi_{N\alpha} - \phi'_{N\dot{\alpha}}]\, f(\tau)\Big|_{\tau=0} + \phi_{N\dot{\alpha}}\, f'(\tau)\Big|_{\tau=t} \tag{15}$$

The integral on the RHS gives the "running" circulatory lift. The third term on the RHS provides for circulatory lift for motions which are discontinuous in α at the origin (i.e. $f(0) \neq 0$). The last term on the RHS is a rate effect at the measuring time, t, and is a consequence of the integration by parts. This term provides for circulatory lift due to pitching at $t = 0$ for motions which are discontinuous in rate (i.e. $f'(0) \neq 0$) such as an instantaneous ramp.

Now, it is proposed to write the convolution integral in an alternate form given by:

$$C_N(t) = C_{No} + \int_0^t \phi^*_{N\alpha}[t-\tau, \alpha(\tau)]\, \frac{d\alpha}{d\tau}\, d\tau \tag{16}$$

where $\phi^*_{N\alpha}$ is a first order response. Substituting the first of Equations 12 into 16 yields:

$$C_N(t) = C_{No} + \int_0^t \phi^*_{N\alpha} f'(\tau)\, d\tau + \phi^*_{N\alpha} f(\tau)\Big|_{\tau=0} \tag{17}$$

Comparing Equation 17 with Equation 15 it can be seen that each formulation will give the same result if $\phi^*_{N\alpha}$ is defined as:

$$\phi^*_{N\alpha}[t-\tau,\alpha(\tau)] = \phi_{N\alpha}[t-\tau,\alpha(\tau)] - \phi'_{N\dot{\alpha}}[t-\tau,\alpha(\tau)] \tag{18}$$

and Equation 16 is amended to read:

$$C_N(t) = C_{No} + \int_0^t \phi^*_{N\alpha}[t-\tau,\alpha(\tau)] \frac{d\alpha}{d\tau}\, d\tau + \phi_{N\dot{\alpha}}[t-\tau,\alpha(\tau)]\, f'(\tau)\Big|_{\tau=t} \tag{19}$$

The convolution integral is thus written in terms of a single response functional, $\phi^*_{N\alpha}$, which is defined by Equation 18 and $f'(\tau)$ depends on the motion as defined by Equation 11. Although the analysis has been done using first order responses, the result is valid for higher order as well as the full nonlinear form.

III.2 The Indicial Response due to Rotation

The response $\phi^*_{N\alpha}$ can be shown to be the response to an instantaneous step change in angle of attack due to rotation. For this motion, in Equation 11, $f(\tau) = f(0) = \Delta\alpha$ and $f'(\tau) = f'(0) = 0$, so that Equation 15 yields:

$$\frac{\Delta C_N(t)}{\Delta\alpha} = \phi_{N\alpha}[t-0,\alpha(0)] - \phi'_{N\dot{\alpha}}[t-0,\alpha(0)] \tag{20}$$

where $\Delta C_N(t) = C_N(t) - C_{No}$. Taking the limit as $\Delta\alpha$ approaches zero in accordance with Equation 5 results in:

$$\frac{\partial C_N(t)}{\partial\alpha}\Big)_{\text{rotation}} = \phi_{N\alpha}[t-0,\alpha(0)] - \phi'_{N\dot{\alpha}}[t-0,\alpha(0)] \tag{21}$$

Setting $\tau = 0$ in Equation 18 and comparing the result with Equation 21 shows that, by definition, the indicial response $\phi^*_{N\alpha}$ is equal to the circulatory response to a step change in angle of attack

due to rotation. The same result is derived somewhat more formally in Appendix A. The response to rotation contains both an angle effect given by the first term on the RHS of Equation 21 and a rate effect given by the second term on the RHS. This result, in combination with the formulation for the loading given by Equation 19, forms the basis of the present experimental study wherein $\phi^*_{N\alpha}$ has been measured approximately. We use the term approximately because the indicial response is defined for an instantaneous step change in α which, of course, is not possible in the laboratory. However, by using water as the working fluid, very rapid step changes relative to the freestream velocity are possible at reasonable Reynolds numbers. Also, it is easier experimentally to impart the motions required to produce the response $\phi^*_{N\alpha}$ than the somewhat more complicated motions to produce $\phi_{N\dot{\alpha}}$[1].

The last term on the RHS of Equation 19 is the product of the indicial response due to a step change in pitch rate (see Equation 2) and the first derivative of the motion function $f(\tau)$ evaluated at time, τ=t. Within the scope of the present study, evaluating this term presents a problem since it is generally not possible to separate the experimental results for $\phi^*_{N\alpha}$ into the $\phi_{N\alpha}$ and $\phi_{N\dot{\alpha}}$ components. Notice, however, that experimentally $\phi_{N\dot{\alpha}}[t-\tau.\alpha(\tau)]$ (or any other experimentally measured response for that matter) will be identically zero at τ=t (i.e. $t-\tau = 0$) due to the cancellation of the reference motion and the step change in $\dot{\alpha}$ motion needed to construct the indicial response. In other words, it is not possible to measure an instantaneous change in circulatory loading. Since our purpose here is to consider integration of experimentally measured indicial responses, this term has been neglected in the force calculations which follow. An estimate of the theoretical magnitude of this term is possible, however, using Wagner's function given by the first of Equations 24 below. For τ=t the expression gives $\phi_{N\dot{\alpha}}(0) = \phi_N(0) = \pi$. Whereas the magnitude of $f'(t)$ will generally be less than 0.05, the product gives : $\phi_{N\dot{\alpha}}(0)\, f'(t) < 0.16$.

III.3 Effect of Step Rate on the Theoretical Response

Obviously, the present experimental approach raises the question: Is a rapid step sufficient to produce a response similar to the indicial response defined for instantaneous motions? We can investigate this possibility using the classical response to a step change in plunge rate given by Wagner's function. Recall from Equation 2 that this is also the response to a step change in α with $\dot{\alpha}$ held constant. For a thin 2-D airfoil undergoing small amplitude motion in an inviscid, incompressible fluid[5]: $\phi_{N\alpha} = \phi_{N\dot{\alpha}} = \phi_N$, where ϕ_N is Wagner's function. The Wagner function is linear and depends on elapsed time only so that $\phi_N = \phi_N(t-\tau)$. From Equation 15 with $C_{N0} = 0$, the circulatory loading due to an instantaneous step change in α by rotation is:

$$C_N(t) = \Delta\alpha\, [\phi_N(t-\tau) - \phi'_N(t-\tau)]\Big|_{\tau=0} \qquad (22)$$

where the step occurs at $\tau = 0$ and t is measured from the step onset. Wagner's function can be approximated by an exponential function of the form:

$$\phi_N(\tau) = 2\pi\,[\mu(\tau) - A\,e^{-a\tau} - B\,e^{-b\tau}] \tag{23}$$

so that:

$$\begin{aligned} \phi_N(t-\tau) &= 2\pi\,[\mu(t-\tau) - A\,e^{-a(t-\tau)} - B\,e^{-b(t-\tau)}] \\ \phi'_N(t-\tau) &= -2\pi\,[\delta(t-\tau) + Aae^{-a(t-\tau)} + Bbe^{-b(t-\tau)}] \end{aligned} \tag{24}$$

also, substituting Equations 24 into 18 yields:

$$\phi^*_{N\alpha}[t-\tau,\alpha(\tau)] = 2\pi\,[\,1 - (1-a)A\,e^{-a(t-\tau)} - (1-b)B\,e^{-b(t-\tau)}]\,,\ \text{for } t > 0 \tag{25}$$

which is the classical linear indicial response due to a step change in alpha by rotation. Notice that while this is based on Wagner's function, it differs from Wagner's function due to the rate effect given by the second of Equations 24. Substituting Equations 24 into 22 yields the ideal(i.e. for instantaneous motion) normal force response:

$$C_{N_{ideal}}(t) = 2\pi\,\Delta\alpha\,[\,1 - (1-a)A\,e^{-at} - (1-b)B\,e^{-bt}]\,,\ \text{for } t > 0 \tag{26}$$

The constants are given by[5]: A=0.165, B=0.335, a=0.0455, and b=0.3.

Of course, real motions are not instantaneous. In practice, however, we can simulate a step change in angle of attack using a small amplitude pitching motion which, using Equation 11, can be approximated by:

$$f(\tau) = K\tau\,[1 - \mu(\tau-\tau_s)] + \Delta\alpha\mu(\tau-\tau_s) \tag{27}$$

where K is the nondimensional pitch rate ($K = \frac{\dot{\alpha}b}{U}$, b=semichord length, U=reference velocity) and is a constant, $\tau = 0$ is when the pitch begins, $\tau = \tau_s$ is when the pitch ends, and $\Delta\alpha$ is the amplitude. Taking the first derivative of Equation 27 and using $\Delta\alpha = K\tau_s$ yields:

$$f'(\tau) = K[1 - \mu(\tau - \tau_s)] \tag{28}$$

Substituting Equations 27 and 28 into Equation 15 and performing the integration results in the following expression for the experimental normal force response:

$$C_{N_{exp}}(t) = 2\pi\,\Delta\alpha\,[1 - (1\text{-}a)A(\frac{e^{a\tau_s} - 1}{a\tau_s})e^{-at} - (1\text{-}b)B(\frac{e^{b\tau_s} - 1}{b\tau_s})e^{-bt}] \quad , \quad \text{for } t > \tau_s \qquad (29)$$

In our experiment we achieve a pitch rate of K = 0.5 and $\Delta\alpha = 1^\circ$ which gives a step duration of $\tau_s = 0.035$ semichords (≈ 0.005 sec in real time). An error which is defined as the difference between the ideal response of Equation 26 and the experimental response of Equation 29, quantity divided by the ideal response is plotted in Figure 2. The point to be made is that the simulation motion of Equation 29 yields a circulatory lift response which is theoretically very close to that for the instantaneous motion of Equation 26.

In summary, the convolution integral for the airfoil loading can be expressed in terms of an indicial response for a step change in α due to rotation. For a rapid step at low angle of attack, the circulatory response is theoretically very similar to the response to an instantaneous step.

IV. Experimental Set-Up

Experiments were conducted in the Ohio University tow-tank. The tank has a length of 30 ft, a width of 12 ft, and a depth of 4 ft. The use of water as a working fluid has several advantages in the types of experiments which were conducted. These include: larger dynamic pressures, very high nondimensional pitch rates are possible at manageable actual pitch rates, and an uncoupling of the circulatory and noncirculatory effects due to incompressibility.

Tests were conducted on a six inch chord NACA 0015 airfoil. The airfoil is suspended vertically from the carriage as shown in Figure 3a. The carriage moves in translation on precision roller bearings and shafts fixed to I-beams which span the tank. The translational speed was 2.03 ft/s which gives a Reynolds number of 9.4×10^4. The airfoil is driven in rotation about the quarter chord by a high power stepper motor. The stepper motor has the rapid starting and stopping capability needed to impart rapid small amplitude changes in angle of attack. The airfoil is connected to the stepper motor via a drive shaft and a 10 to 1 speed reducer. The clearance between the free end of the airfoil and the floor of the tank is one inch.

The normal and axial forces acting on the airfoil are measured using strain gauges mounted on a load cell of rectangular cross section machined on the airfoil drive shaft as illustrated in Figure 3b. The axis of the load cell passes through the quarter chord of the airfoil. The strain gauges are arranged in two Wheatstone bridge configurations. Each bridge is sensitive to the desired force only. The bridges also compensate for torsion. The bridges were calibrated by applying point (quarter chord) loads at the midspan of the submerged part of the airfoil. The bridge output voltages are amplified 200 times using amplifiers located on the carriage. The amplified signals are transmitted via shielded cables to a data acquisition system beside the tank. The system consists of an IBM p.c. equipped with a high-speed A/D converter and scanner. The scanner has a maximum rate of 5 kHz per channel.

Due to the rapid starting and stopping of the airfoil during a step, structural vibrations

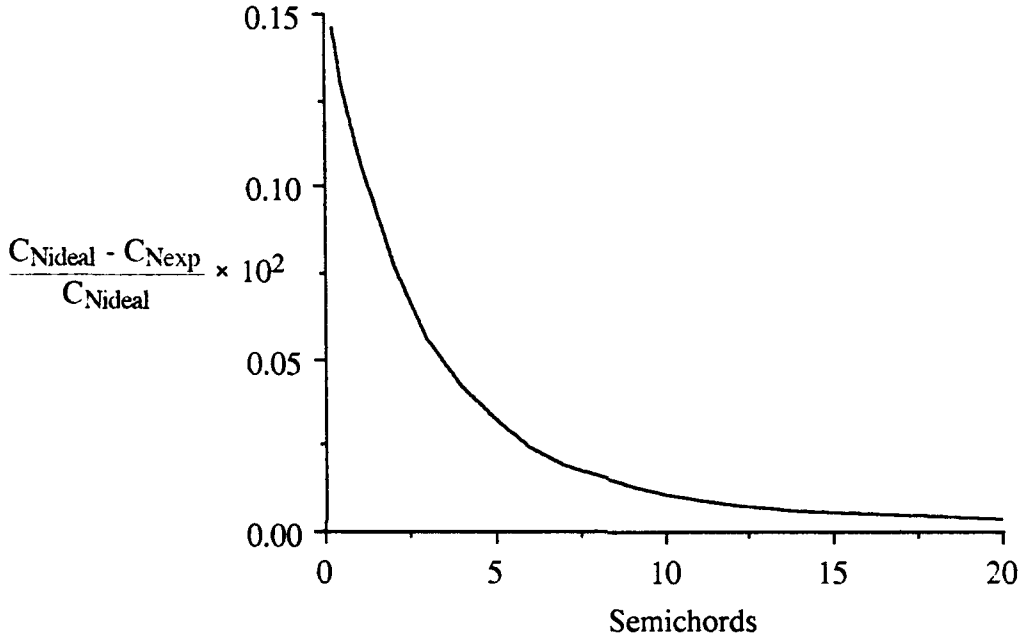

Figure 2. Difference Between the Response due to an Instantaneous Step and the Response due to Step at Finite Rate.

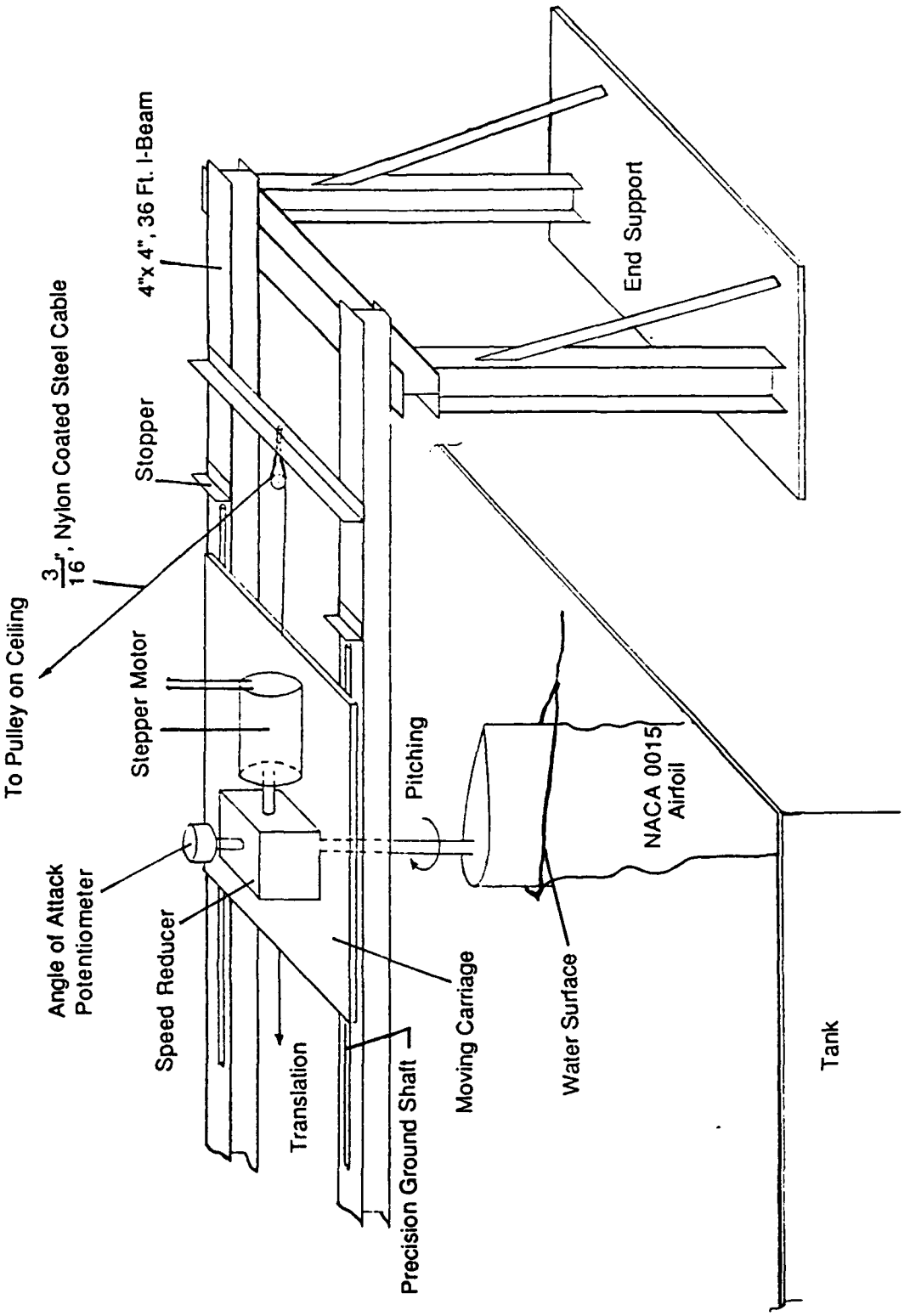

Figure 3a. Tow Tank Facility.

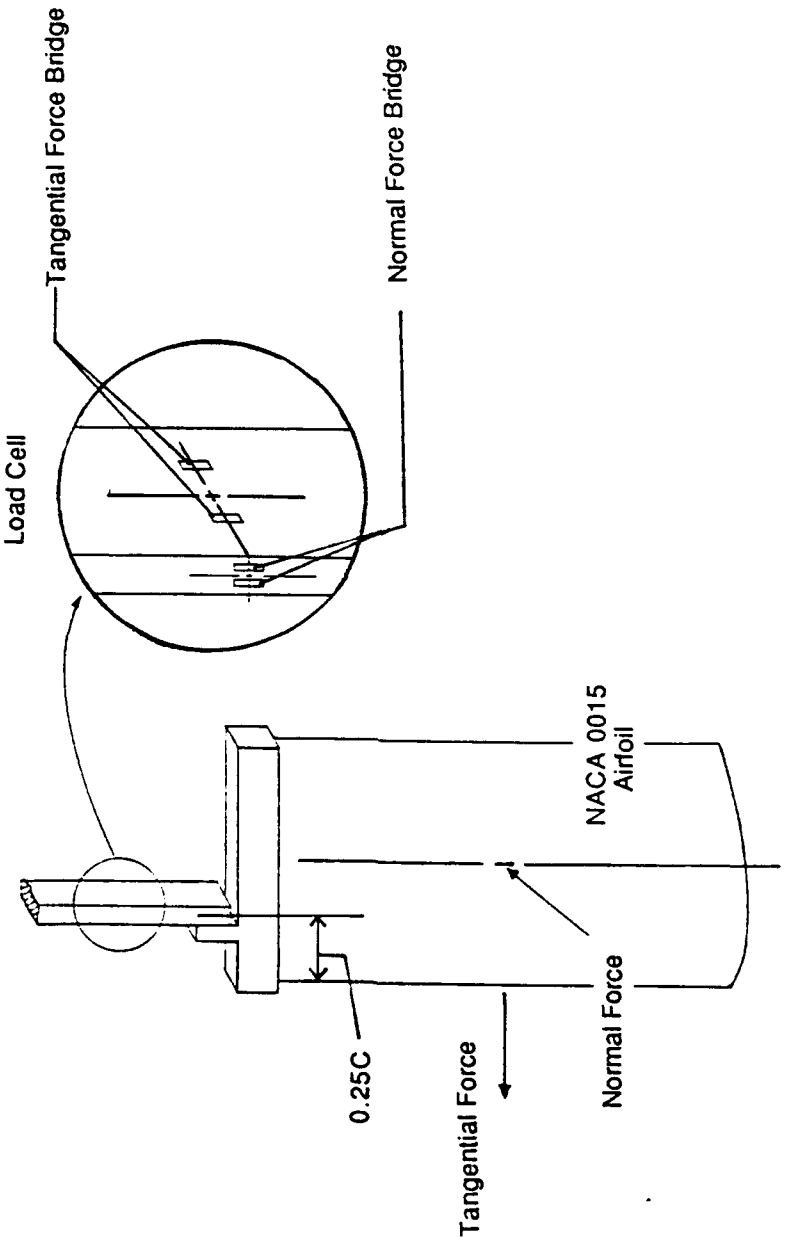

Figure 3b. Strain Gauge Load Cell.

introduced some noise into the bridge outputs. The noise appears at the natural frequencies of the towing structure. The natural vibrational frequencies in the normal and axial force directions were determined by draining the tank and running the airfoil across the tank at various angles of attack. These "empty tank" data where transformed into the frequency domain using FFT where the natural frequencies could be determined from the magnitudes of the Fourier coefficients.

To remove the noise, the strain gauge output signals were low-pass filtered to remove all frequencies above 170 Hz. The data acquisition rate was then set at 340 Hz to ensure detection of any remaining frequencies. The vibrational frequencies were removed from the actual aerodynamic test data in post processing using digital notch filters set at the natural frequencies. The frequencies which were filtered are shown in Table 1. The filters introduce a time lag which has been corrected for in subsequent integrations as described in section IX.1. The time lag is approximately 0.5 chords. The time lag was estimated by assuming that as the step occurs the rise in the force signals would occur at nearly the same frequency as the rise in the signal from the angle of attack sensor. The angle of attack data were passed through the notch filters and the time lag was estimated by comparing the filtered output with the unfiltered input.

V. Calculation of the Indicial Response

The first order normal force indicial response due to angle of attack has been measured by considering the three motions shown in Figure 4. In each motion, the airfoil moves for several chord lengths at constant angle of attack so that in the notation of Figure 1 we have $\alpha(\xi) = \alpha(\tau) = \alpha_o$. In motion 0, the angle is held constant to provide a measure of the static normal force at α_o. An average value of the static force was used by averaging the load data from the twentieth to the twenty fifth chord of travel. In motion 1, the airfoil undergoes a rapid change in angle of attack to $\alpha_o+\Delta\alpha_u$, and in motion 2 to $\alpha_o-\Delta\alpha_d$. The angle of attack parameters α_o, $\Delta\alpha_u$, and $\Delta\alpha_d$ are measured quantities. The distinction between $\Delta\alpha_u$ and $\Delta\alpha_d$ is necessary because the test apparatus is not capable of imparting perfectly symmetric steps about α_o. The time dependent normal force indicial response corresponding to the initial angle α_o was computed using a three point formula given by:

$$\phi^*_{N\alpha}[t-\tau, \alpha_o] = C_{No}[(\Delta\alpha_u-\Delta\alpha_d)(\Delta\alpha_u\Delta\alpha_d)^{-1}] + C_{N+}[\Delta\alpha_d(\Delta\alpha_u(\Delta\alpha_u+\Delta\alpha_d))^{-1}] - C_{N-}[\Delta\alpha_u(\Delta\alpha_d(\Delta\alpha_u+\Delta\alpha_d))^{-1}] \quad (30)$$

where

$C_{No}=C_{No}(\alpha_o)$ = average steady state normal force coefficient during motion 0

$C_{N+}=C_{N+}[t-\tau,\alpha_o]$ = transient normal force coefficient during motion 1

Table 1. Filtered Frequencies in Hz

Normal Force	Axial Force
2.62	2.62
5.46	5.46
7.35	7.35
10.45	10.45
13.93	13.93
46.4	77.4
134.0	
151.7	

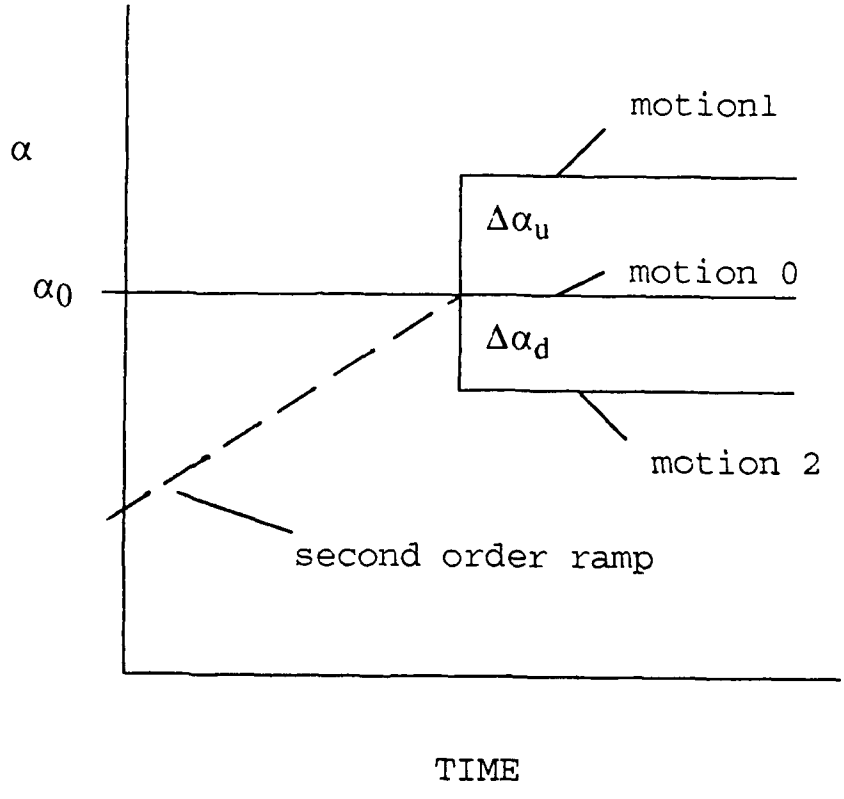

Figure 4. Test Motions for First and Second Order Indicial Responses.

$C_{N-}=C_{N-}[t-\tau,\alpha_o]$ = transient normal force coefficient during motion 2

The same approach has been used for the axial force indicial response. For symmetric steps Equation 30 reduces to a two point central difference. Notice that for zero time from step onset, the measured indicial responses will be zero since an experimental simulation cannot produce an instantaneous change in circulatory loading. As such, the loading for motions 1 and 2 will cancel identically at zero elapsed time. Table 2 is a list of onset angles of attack (α_o) for which the normal and axial force responses were measured.

The uncertainty in the normal force response given by Equation 30 has been estimated to be ±20%. The large uncertainty is primarily due to the uncertainty in $\Delta\alpha_u$ and $\Delta\alpha_d$, and the fact that the magnitudes of these terms themselves are small. Also contributing to the uncertainty is the practice of subtracting two relatively large quantities, namely C_{N+} and C_{N-}, to extract a small residual therefrom. Each response was measured five times to check repeatability and the results were ensemble averaged.

In an attempt to assess the second order rate effects ($\phi^*_{N\alpha} = \phi^*_{N\alpha}[t-\tau,\alpha(\tau),\dot{\alpha}(\tau)]$) for ramp motions, a second series of tests were conducted in which the airfoil undergoes a ramp up motion from a low(substall) angle of attack to the step onset angle of attack as shown in Figure 4. For these tests only a step up and a step down runs were performed and the experimental indicial response was computed using a two point central difference ($(C_{N+}- C_{N-}) / (\Delta\alpha_u+\Delta\alpha_d)$). Three pitch rates were considered, $K = \dot{\alpha}b/U = 0.02$, 0.05, and 0.1, and the step onset angles were very similar to those shown in Table 2.

VI. Angle of Attack and Static Load Data

Representative angle of attack data for a first order response near $\alpha_o = 8°$ are shown in Figure 5a. The steps up and down occur at a reduced pitch rate ($\dot{\alpha}b/U$) of approximately 0.5. In actual physical terms this corresponds to 230 deg/s. For the same airfoil chord length, reduced pitch rate, and Reynolds number the corresponding actual pitch rate in a wind tunnel would be on the order of 3500 deg/s. Figure 5b shows the step up and step down airfoil motion data for a second order ramp-up test with a step onset angle near 21°. The angle of attack data show some electrical noise effects which appear as small spikes. This noise is of no consequence in the calculation of the indicial response since in Equation 30 the $\Delta\alpha$ terms are constants found by first filtering out the high frequency noise and then averaging the angle of attack data over several

Table 2. First Order Onset Angles

α_O = 2.09°	25.65°
4.8°	31.01°
8.33°	35.77°
11.32°	40.24°
14.50°	45.57°
15.47°	51.56°
17.55°	56.16°
20.77°	61.46°

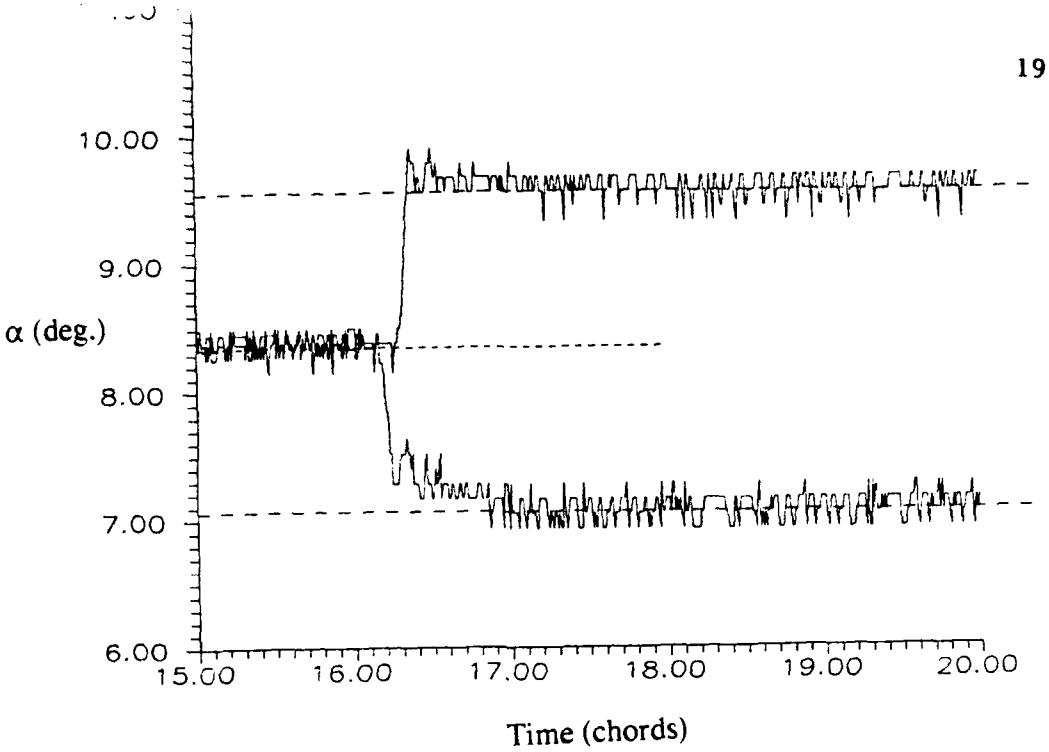

Figure 5a. Angle of Attack Data for First Order Step Up and Step Down Motions at an Onset Angle Near 8°.

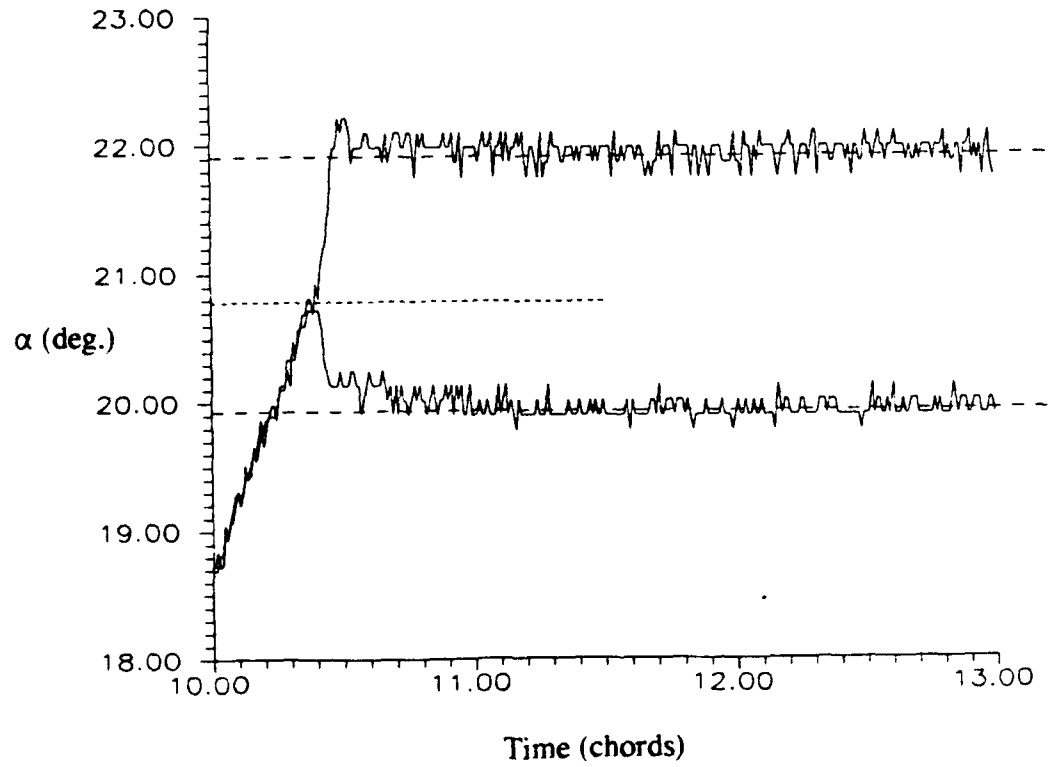

Figure 5b. Angle of Attack Data for Second Order Step Up and Step Down Motions at an Onset Angle Near 21°.

chords before and after the step. The broken lines indicate the average values.

For large values of elapsed time from step onset, the indicial response given by Equation 30 should approach the static force curve slope. The static normal and axial forces have been measured from 0° to 60 ° in 1° to 2° increments and the results are shown in Figures 6a and 6b, respectively. The static slope has been computed from these data using curve fitting over subintervals of alpha and the results are shown in Figures 7a and 7b. These slope data will be compared with the experimental indicial responses at large values of elapsed time.

As a point of reference, the normal force curve slope for a potential flow is also shown on Figure 7a. The potential flow solution obtained using complex variables is[8]:

$$\frac{\partial C_N}{\partial \alpha})_{SS} = 2\pi(1 + 0.77t/c) \quad (= 7.0 \text{ for a NACA 0015}) \tag{31}$$

where t/c is the airfoil thickness ratio. Of course, Equation 31 is only valid for inviscid flow at small angles of attack. The slope data of Figure 7a show nonlinear behavior even at low angles of attack where linear behavior is usually assumed. Surprisingly, there are not many other sources of static section force data at the present Reynolds number ($\approx 10^5$) for comparison. Lift curves from wind tunnel tests on a NACA 0015 are given in Reference[9] for several Reynolds numbers and these data are also plotted on Figure 6a. These data date back to 1937 and are the result of integrated pressure distributions measured using fluid manometers. These data are in graphical form and are rather difficult to quantify accurately--particularly for slope. At a Reynolds number of 84,000 these data appear to show linear behavior in the range $0 \le \alpha \le 6°$ with a slope of approximately 5.9/rad. Notice that this is in rather poor agreement with the theoretical value of 7.0/rad from Equation 31. The difference may be due to viscous losses and wake effects. On the other hand, the data of Reference [9] for a Reynolds number of 42,900 have a nonlinear slope over the same angle of attack range. The slope from in the range of $0 \le \alpha \le 2°$ is on the order of 9.0/rad, while for the range $4° \le \alpha \le 6°$ the slope is near 4.2/rad. Possibly, boundary layer transition plays a role in the low angle of attack nonlinearities in these, as well as the present, static force data. The data of Reference [9] for a NACA 0018 airfoil show a similar Reynolds number dependence. The authors of Reference[9] point out that the accuracy of their data for Reynolds numbers below about 800,000 are put in doubt due to measured

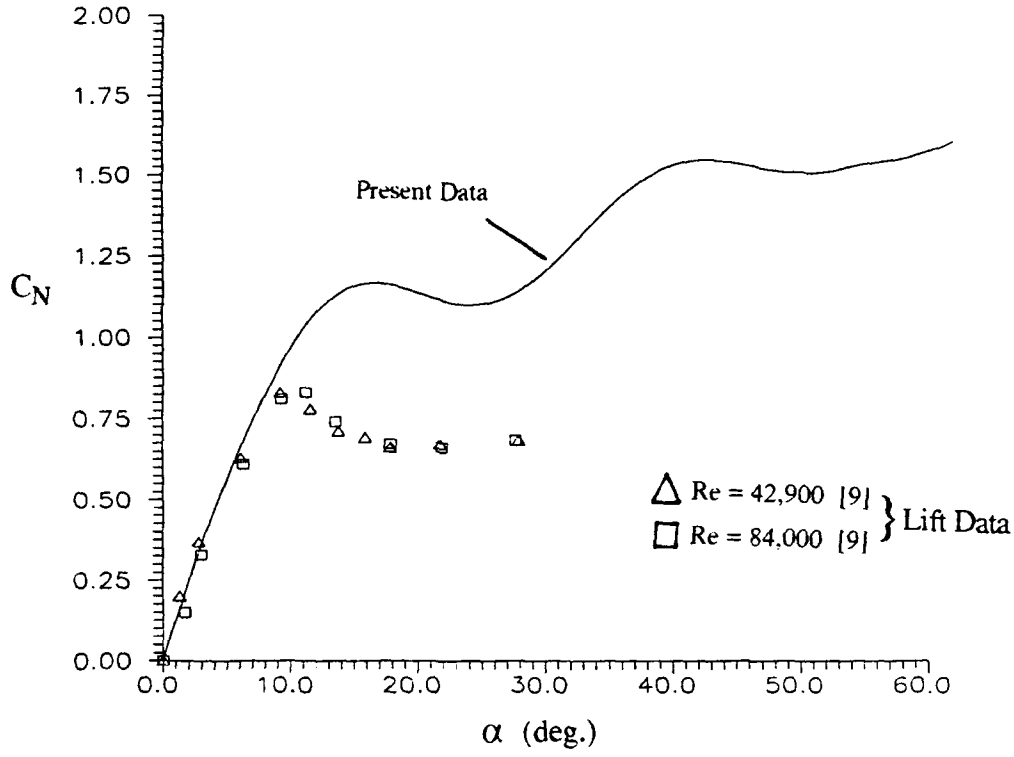

Figure 6a. Steady State Normal Force Results, NACA 0015, Re=9.5 X 10^5.

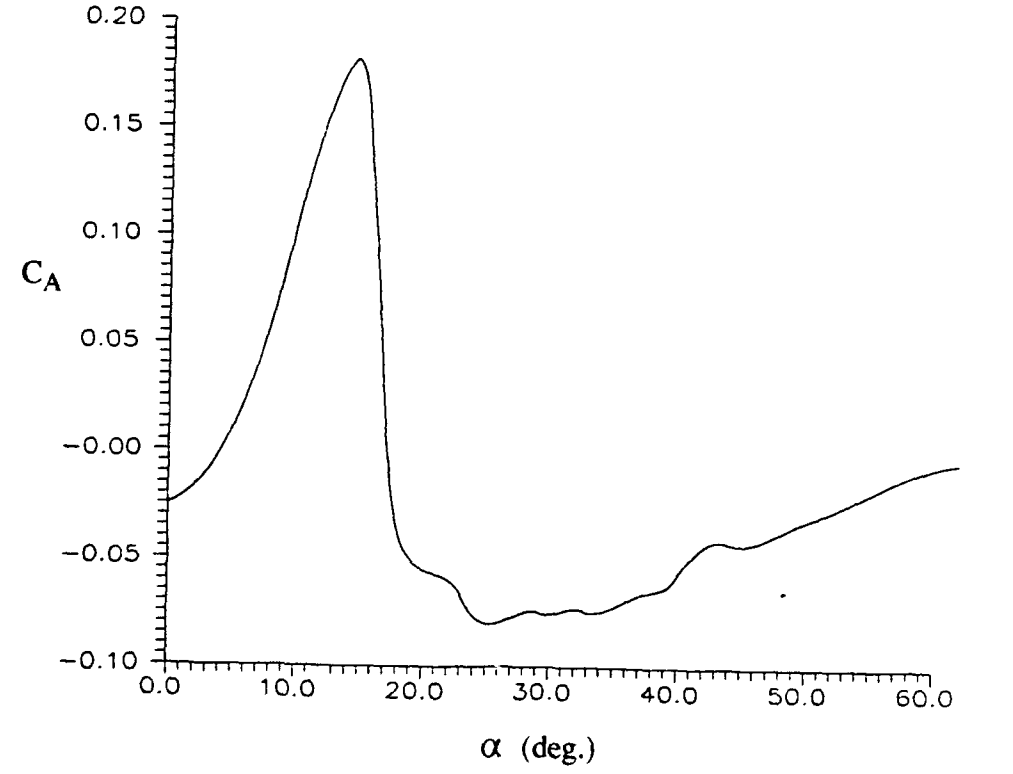

Figure 6b. Steady State Axial Force Results, NACA 0015, Re=9.5 X 10^5.

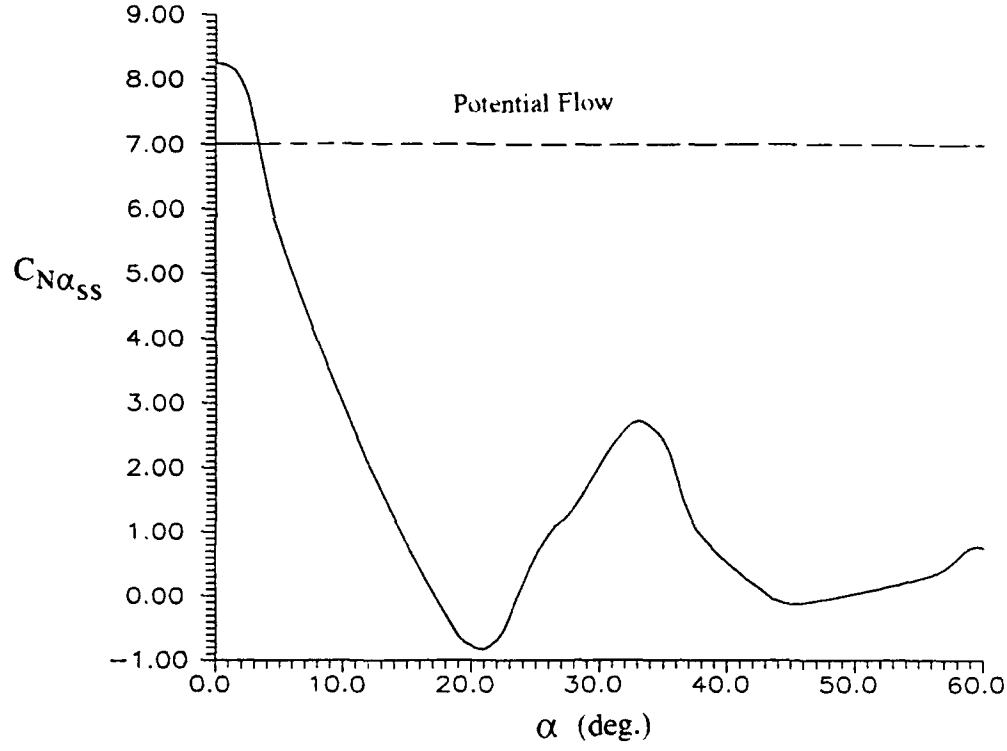

Figure 7a. Slope of Steady State Normal Force Curve.

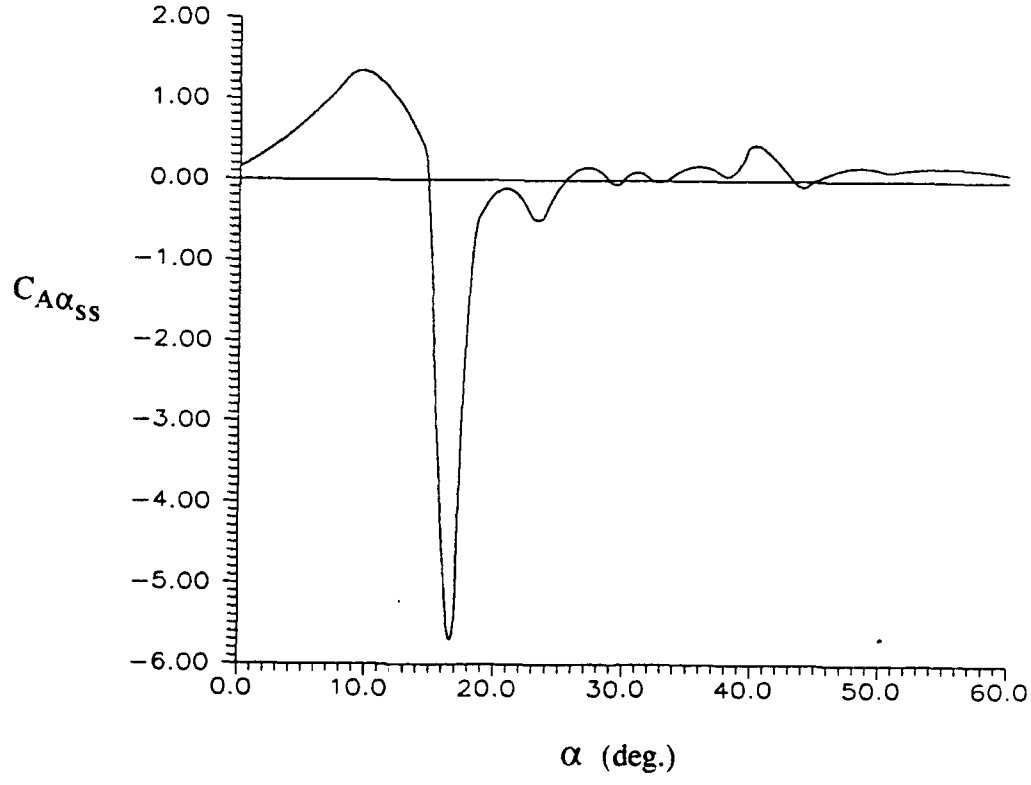

Figure 7b. Slope of Steady State Axial Force Curve.

assymetry in the lift curves for symmetric airfoils for positive and negative angles of attack . In any case, the situation exemplifies the difficulty in comparing section force characteristics from different test rigs and models, as well as inviscid theory. At this point we are satisfied to say that the static slope data of Figures 7a and 7b are in general agreement, as will be shown, with the independently measured steady state indicial response results.

VII. First Order Nonlinear Indicial Response Results

VII.1 First Order Normal Force Responses Based on Static Force Nonlinearities

The normal force indicial response to a step change in α due to rotation has been given by Equation 21. For low angle of attack the response has been evaluated using Wagner's function with Equation 25 as the result. Wagner's function (Equation 23) uses a constant steady state normal force curve slope of 2π. At first, it might be tempting to modify Equation 25 to introduce first order nonlinearities by replacing the 2π with the local value of the static normal force curve slope giving:

$$\phi^{*}_{N\alpha}[t-\tau,\alpha(\tau)] = [C_{N_{\alpha s}}(\alpha(\tau))]\,\phi_T(t-\tau) \qquad (32)$$

where : $$\phi_T(t-\tau) = [\,1 - (1-a)A\,e^{-a(t-\tau)} - (1-b)B\,e^{-b(t-\tau)}]$$

The term in brackets on the RHS of Equation 32 is the static normal force curve slope at $\alpha(\tau)$. Notice that for large values of elapsed time the transient function ϕ_T approaches unity, and the indicial response approaches the local steady state slope--as it must regardless of the relationship used to describe the response. Equation 32 is seen to be a special form of Equation 6 wherein the dependence of the response on $\alpha(\tau)$ is introduced through the steady state normal force curve slope, and the time dependence is contained within the function ϕ_T. While this is nonlinear, it has the disadvantage that the "functional form" of the response, given by ϕ_T, does not itself depend on $\alpha(\tau)$. As such, Equation 32 does not encompass first order dependence in the general sense of Equation 6. Furthermore, the present experimental evidence suggests that for large variations in the onset angle of attack, the first order indicial response cannot be adequately represented by a single "type" of function as in Equation 32.

VII.2 Filtering and Repeatability

The present force data have been filtered using notch filters set at the towing structure natural frequencies. The frequencies were determined in empty-tank tests as discussed in Section IV. Figure 8a illustrates the effect of filtering on the normal force data. Shown are normal force data for a 1° step up at an onset angle of 2°. The main effect of the filter is to remove the large loading shortly after the step onset. The effect of filtering the force data on the computed indicial response is shown in Figure 8b. In Figure 8a the abscissa refers to time measured from the beginning of the test. In Figure 8b, as well as other indicial response results which follow, the abscissa refers to elapsed time from the step onset. Beyond about one chord of travel from the step onset, the filtered and unfiltered responses are virtually the same, insofar as the contribution to the integral of Equation 19 is concerned. The filter also attenuates some of the high frequency electrical noise.

As noted in Section V, the experimental uncertainty in the indicial response can become large. Therefore, some scatter in the data due to uncertainty is expected. Figure 9a shows the normal force indicial response results for an onset angle of 2° for five separate runs. Each run has the same general form, however, they differ in magnitude. Figure 9b is the result of averaging the five individual runs. Notice that the averaged result approaches with reasonable accuracy the proper steady state value which has been measured independently as described in Section VI. Figure 9c shows the results of five runs at an onset angle near 11°. These data are repeatable and each run approaches the correct steady state value.

As the onset angle of attack is increased beyond the static stall angle of attack($\approx$15°) the indicial response results become more erratic, more oscillatory, and less repeatable. This appears to be due to flow separation and energetic vortex shedding. Figure 9d shows three indicial response results for an onset angle of 20°. Five runs were performed and the results were ensemble averaged. Reference [10] notes that for time-variant (oscillatory) equilibrium states, the indicial responses at a particular onset angle may differ in phase due to dissimilar conditions at step onset. Similar observations have been made with regard to the onset angle dependence of axial force indicial responses.

VII.3 First Order Normal Force Indicial Responses at Low Alpha

The average results for five runs at α_0=2° are compared with the theoretical responses

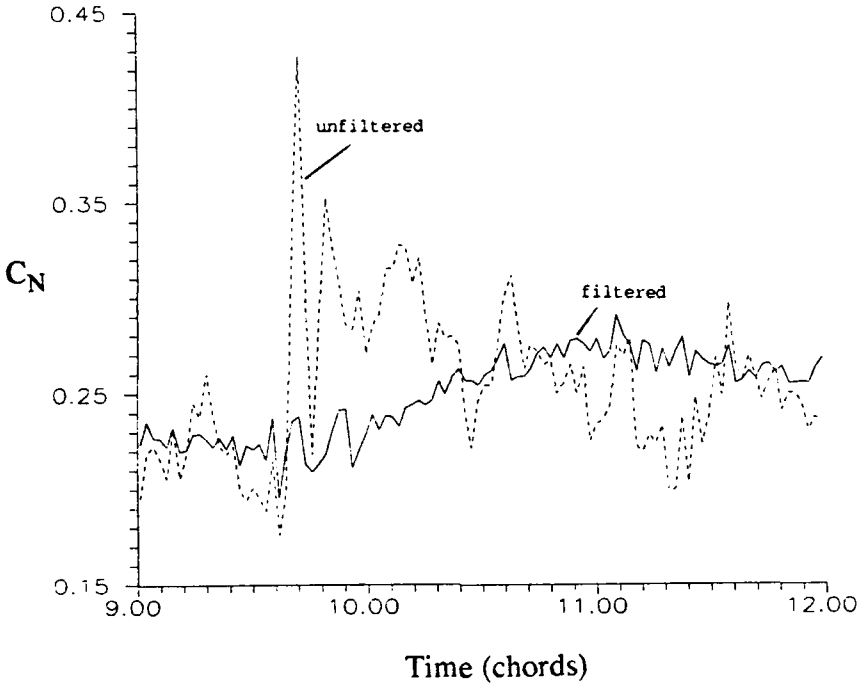

Figure 8a. Effect of Filtering on the Normal Force Response to a Step Up at an Onset Angle near $\alpha_o = 2°$.

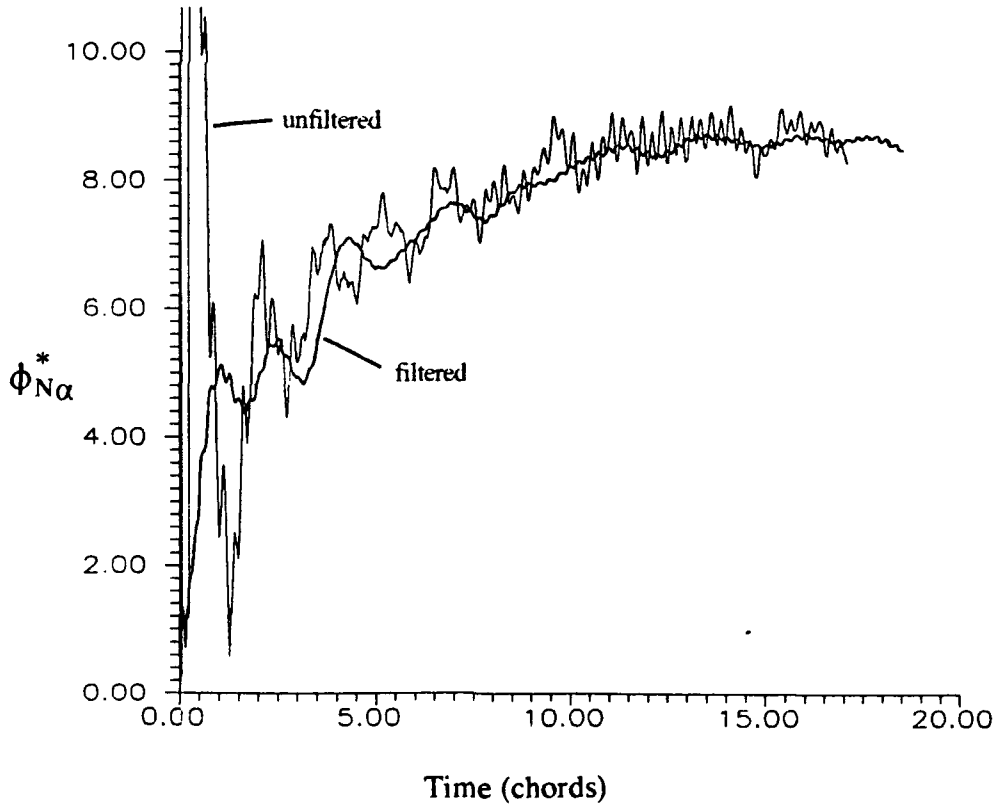

Figure 8b. Effect of Filtering on the Normal Force Indicial Response for an Onset Angle of $\alpha_o = 2°$.

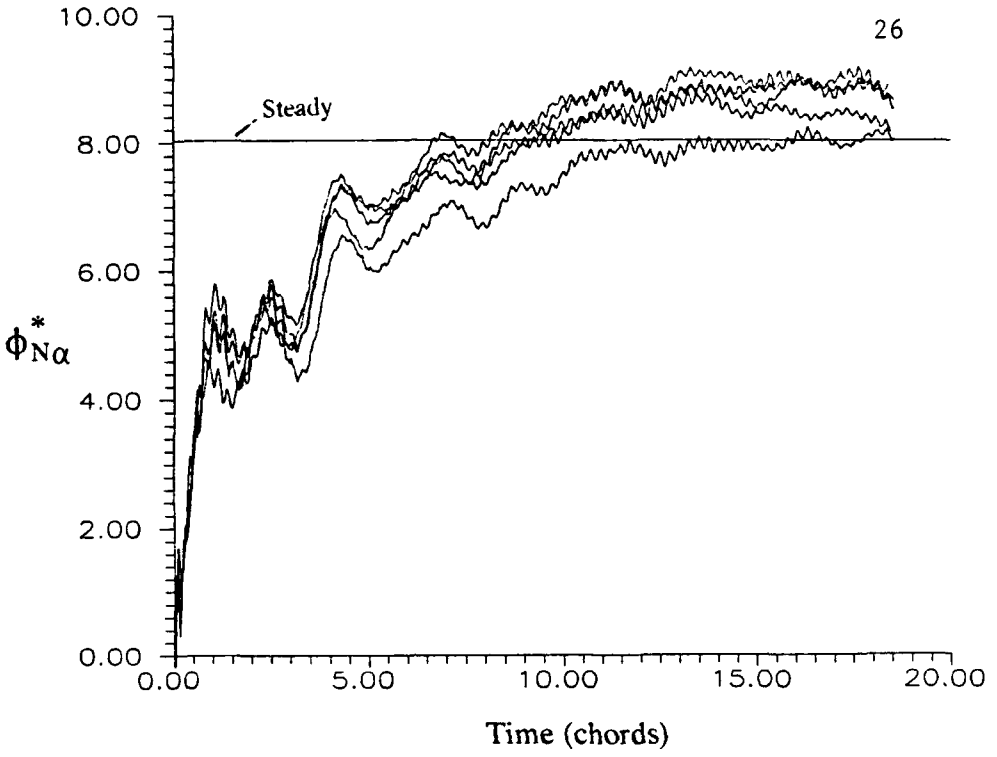

Figure 9a. Five Independent Runs Showing Repeatability of First Order Normal Force Indicial Response for Onset Angles near $\alpha_o = 2°$.

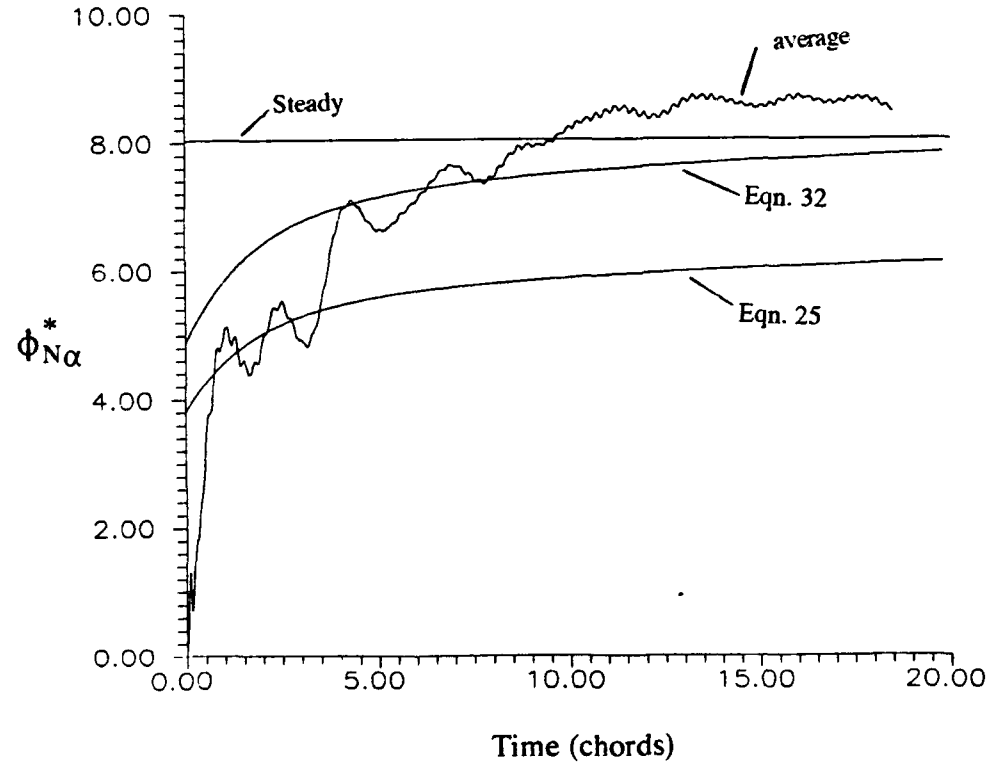

Figure 9b. Average First Order Indicial Response for an Onset Angle of $\alpha_o = 2.09°$.

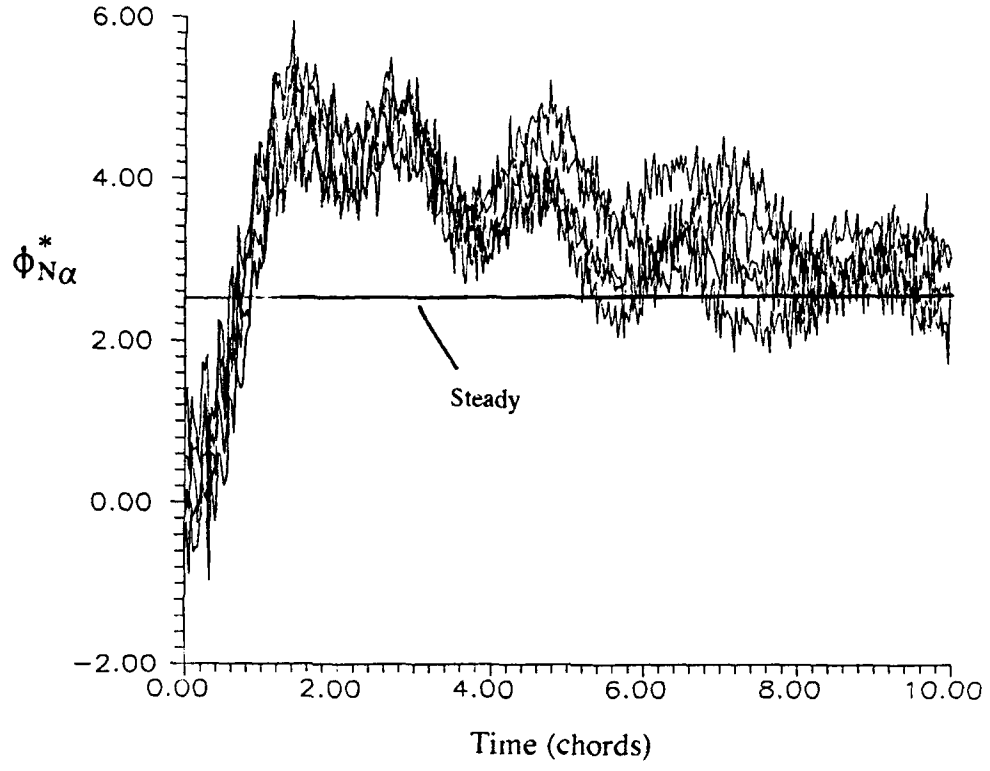

Figure 9c. Five Independent Runs Showing Repeatability of First Order Normal Force Indicial Response for Onset Angles near $\alpha_o = 11°$.

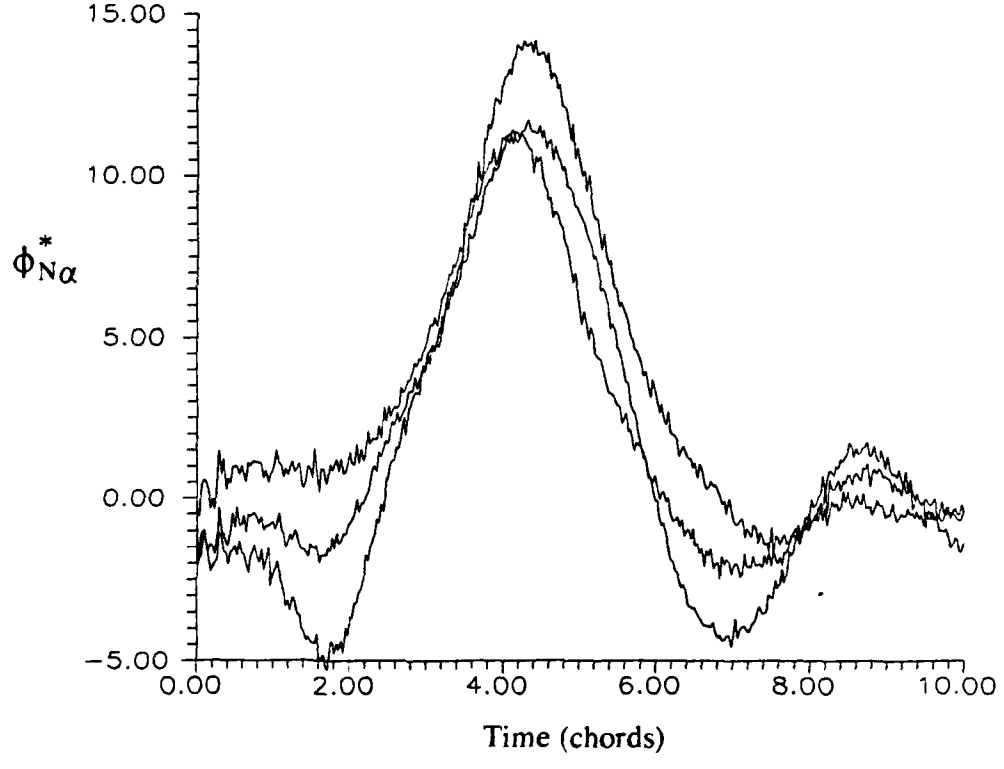

Figure 9d. Three Independent Runs Showing Repeatability of First Order Normal Force Indicial Response for Onset Angles near $\alpha_o = 20°$.

given by Equations 25 and 32 in Figure 9b. Equation 32 was evaluated using the present experimental result for the static normal force curve slope shown in Figure 7a ($C_{N\alpha ss}$ = 8.07/rad at 2°). There is relatively good agreement between the experimental data and Equation 32 over most of the test interval. As discussed earlier, the digital filtering process introduces a time lag in the response of approximately one-half to one chord which is not accounted for in the data of Figure 9b, and other indicial response results which follow. Notice that by shifting the experimental response of Figure 10a to the left to compensate for the time lag, the agreement between the experimental result and the Equation 32 improves. Equation 25, based on a steady state slope of 2π, is seen to give results substantially below the experimental results.

The average normal force response at $\alpha_0 = 4.8°$ is shown in Figure 10a. The response computed from Equation 32 is in reasonably good agreement with the experimental results. Equation 32 has again been evaluated using the present results for the steady state slope given in Figure 7a. Equation 25 is now slightly larger than the steady state experimental result. Increasing α_0 to 8.33° results in the normal force indicial response shown in Figure 10b. The experimental response differs from Equation 32 at elapsed times below 3.0. Equation 25 gives a large overestimate of the steady state normal force response.

Figure 10c shows the normal force indicial response at α_0= 11.32°. Neither Equation 25 or 32 adequately represents the experimental response. Notice, however, that the experimental result still approaches the correct steady state lift curve slope as elapsed time from step onset increases. Furthermore, if Equation 32 rather than the actual response is used in Equation 19 to calculate the normal force, the contribution to the convolution of the response at 11° will be too small for elapsed times less than that for steady state.

Figure 10d is an overlay of the indicial responses for onset angles less than 15°. These responses are similar in that they each appear to approach a single-valued steady state. This is due to the fact that the steady state flow is, more or less, attached. Notice also that the response decreases substantially as the static stall angle is approached, even for small values of elapsed time. Therefore, the present experimental evidence suggests that it may not be valid to assume a response of the form of Equation 25 (i.e. constant steady state slope of 2π) even for relatively low alpha motions.

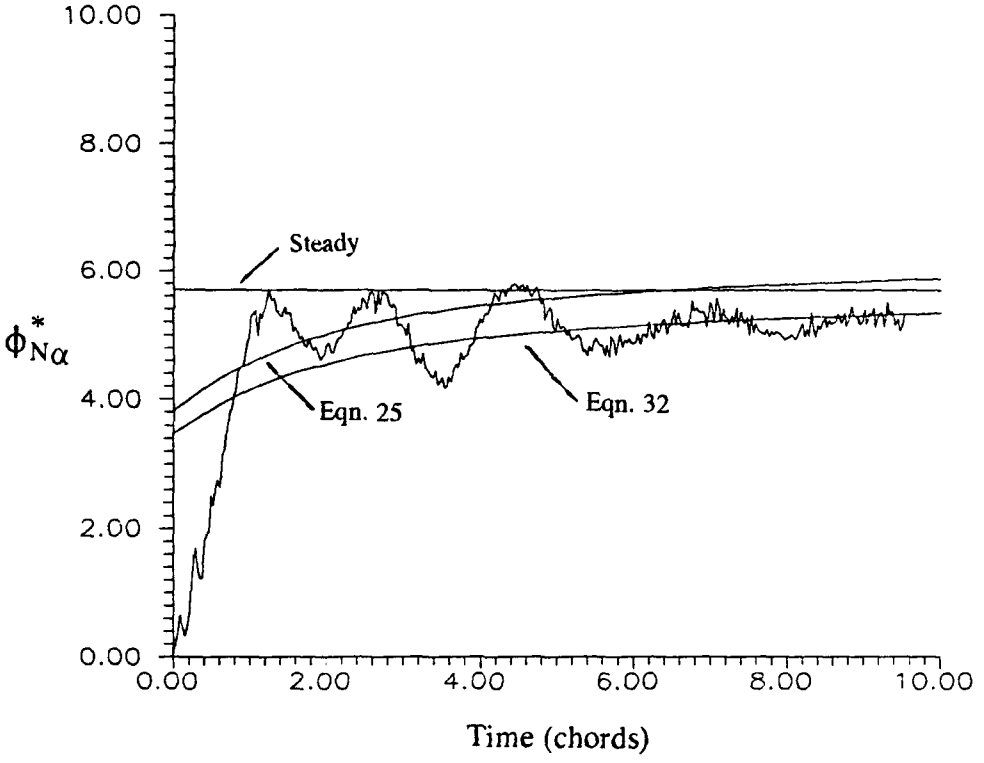

Figure 10a. Average First Order Indicial Response for an Onset Angle of $\alpha_o = 4.8°$.

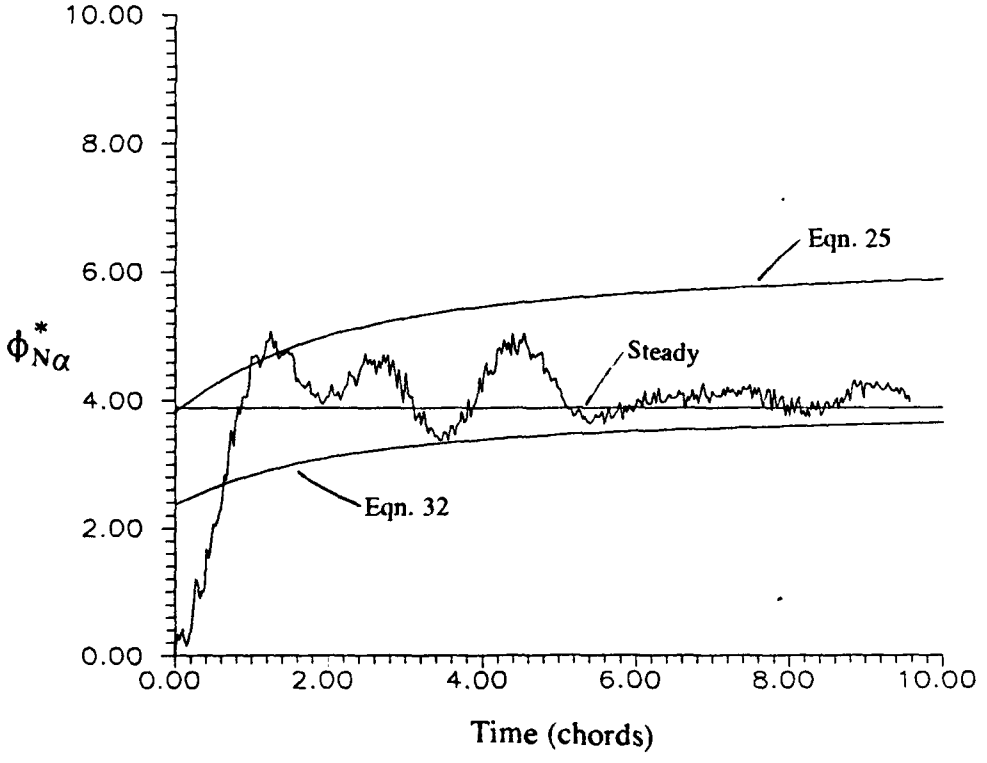

Figure 10b. Average First Order Indicial Response for an Onset Angle of $\alpha_o = 8.33°$.

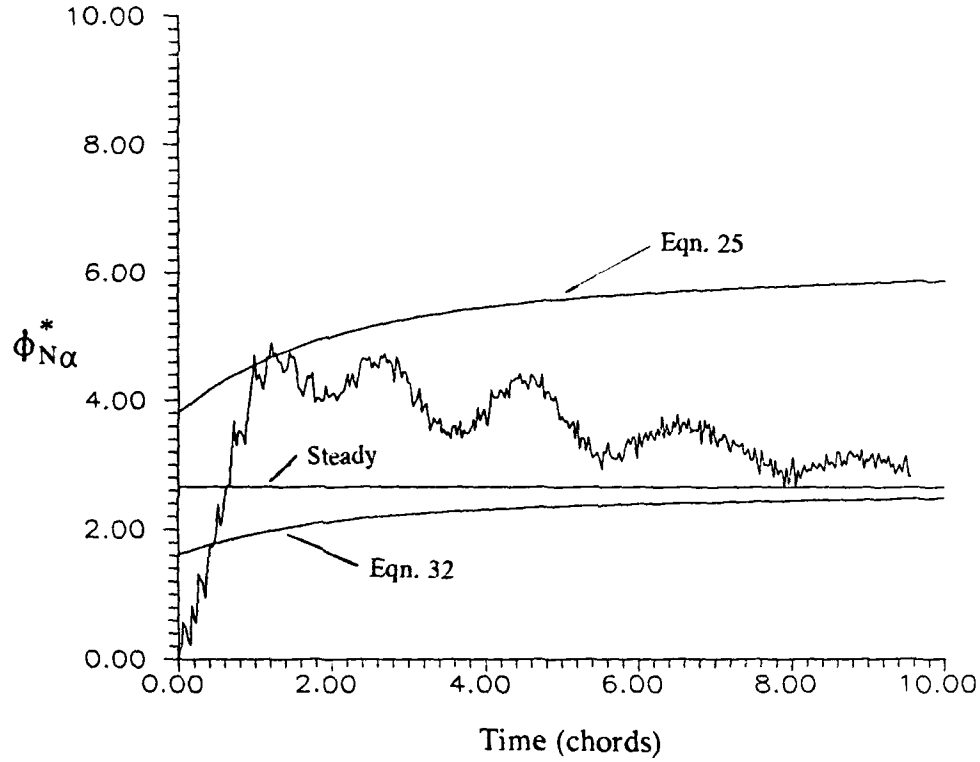

Figure 10c. Average First Order Indicial Response for an Onset Angle of $\alpha_o = 11.32°$.

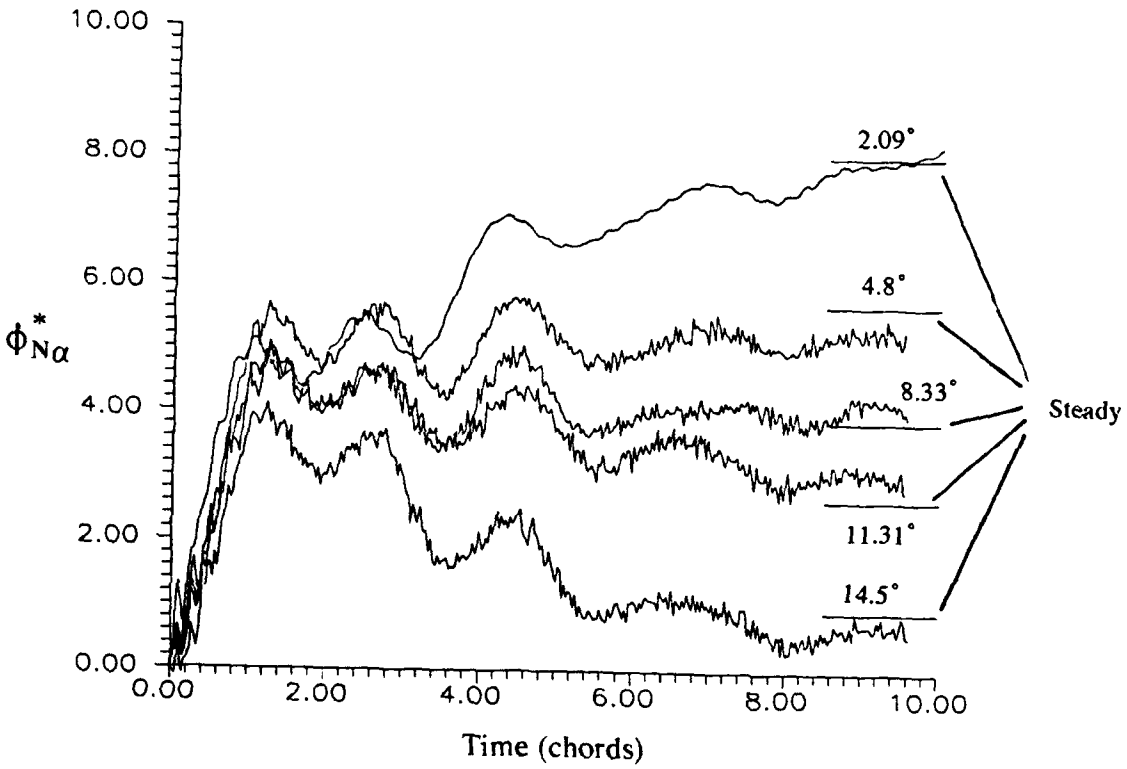

Figure 10d. Overlay of First Order Normal Force Indiciial Responses for Low Onset Angles.

VII.4 First Order Normal Force Indicial Responses at High Alpha

The experimental results for onset angles in the range $15^\circ < \alpha_0 < 26^\circ$ are shown in Figure 11a. Clearly, the responses for $\alpha_0 > 17^\circ$ are fundamentally different than the classical response of Equation 32. Flow visualization studies have shown that for onset angles beyond $\alpha_0 = 15^\circ$ leading edge separation due to static stall has occurred before the step onset. Notice in Figure 7a that the steady state lift curve slope is nearly zero at $\alpha = 15^\circ$ and becomes negative for $\alpha > 15^\circ$, which is another indication of static stall. Referring again to Figure 11a, the indicial response is seen to change substantially in form between $\alpha_0 = 15.47^\circ$ and $\alpha_0 = 17.55^\circ$. This may be indicative of a bifurcation in the aerodynamic response at the static stall angle. This may be further justified by two observations. First, notice that for onset angles less than 15° the indicial response approaches steady state, more-or-less, without oscillations(cf. Figure 10d). For onset angles above 15° the responses have large oscillations which arise due to flow separation and vortex shedding which have been observed in flow visualization movies also taken as part of this study. The oscillations persist for large values of elapsed time(i.e. the steady state may be oscillatory). Oscillations in the steady state response beyond some critical threshold is characteristic of a Hopf bifurcation[10]. Secondly, the responses for $\alpha_0 = 17.55^\circ$ and $\alpha_0 = 20.77^\circ$ appear to have a different time-scale, in terms of the rate at which the responses change with time, than those for $\alpha_0 = 15.47^\circ$ and below. This suggests that the flow has fundamentally changed and the response has undergone a bifurcation to a new flow regime dominated by vortical structures. The time to approach steady state for these responses is clearly longer than the low alpha responses described above. It appears that a longer run time than 10 chords beyond step onset is needed to reach steady state. Significantly longer periods of travel beyond the step onset are not possible in the O.U. tow tank if quasi-steady flow is to be achieved prior to the step. This is particularly true at high alpha where the initial flow is separated. In terms of the convolution integral in Equation 19, however, knowledge of the indicial response for 10 chords of travel is sufficient to consider a number of trial motions of practical interest such as a rapid pull-up.

The responses at $\alpha_0 = 17.55^\circ$ and $\alpha_0 = 20.77^\circ$ display some interesting behavior. First, for elapsed times below 2.0 chords the response magnitudes are small. For small elapsed times these responses will have only small contributions to the convolution integral of Equation 19 which, as will be shown, leads to a significant deficit in the integrated normal force results. As elapsed time increases the responses become extremely large in relation to their respective steady

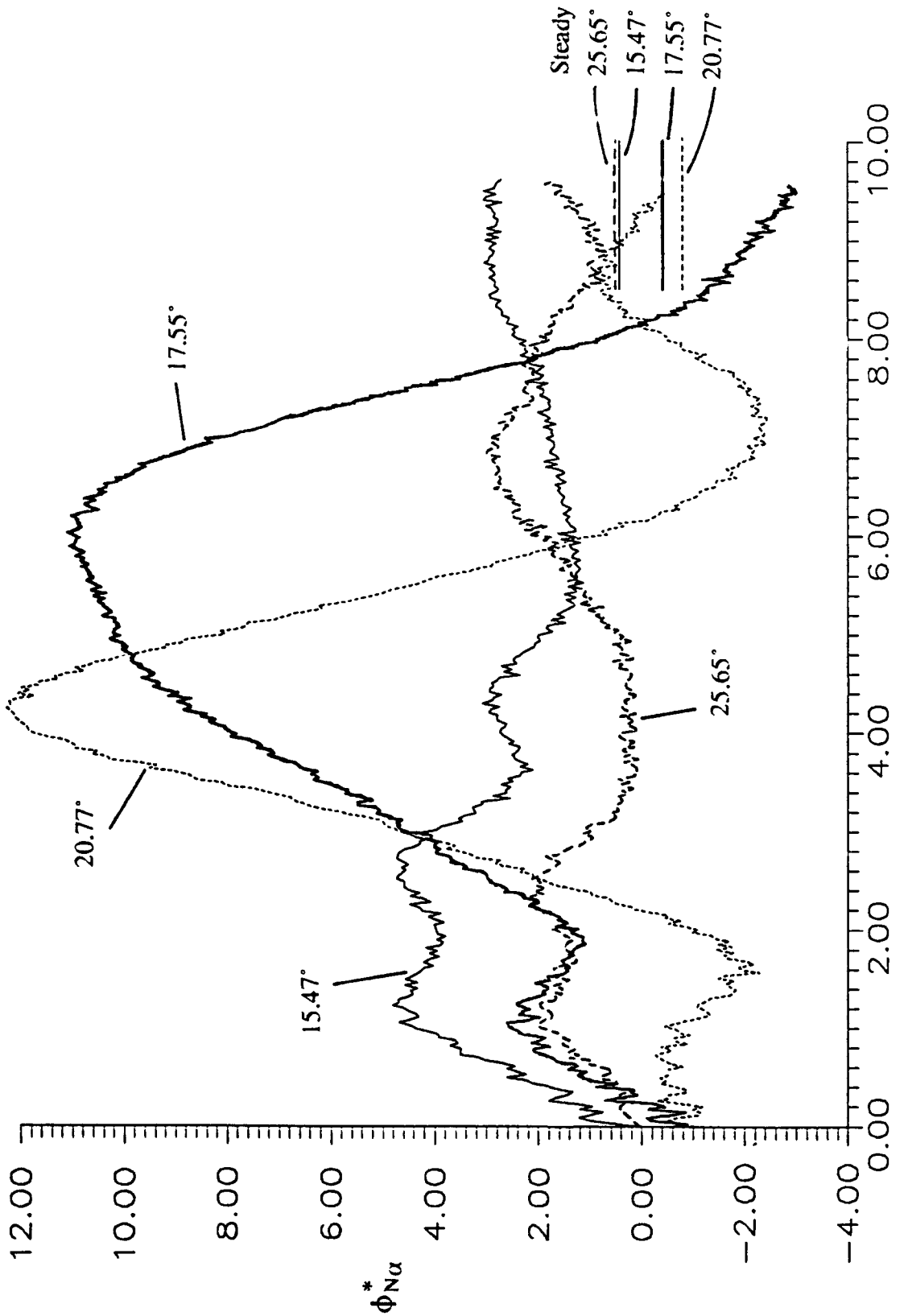

Figure 11a. First Order Normal Force Indicial Responses for Onset Angles in the Range $15° < \alpha_o < 26°$.

state values given in Figure 7a. These large responses will translate into large normal forces for airfoils operating slightly beyond the static stall angle. This is significant from the standpoint of using first order indicial responses to model dynamic stall where it is well known that large forces may ensue. Preliminary results from flow visualizations suggest that the large forces may be due to rapid flow reattachment shortly after the step onset. This flow reattachment may be similar to the phenomenon of flow separation delay in unsteady airfoils, where the delay gives rise to large suction pressures over the upper surface of the airfoil. Assuming these phenomenon are related then this observation would provide some physical grounds for computing dynamic effects using first order indicial responses. Notice, however, that the occurrence of separation delay in dynamic situations will also enter into the nonlinear formulation through attached flow onset conditions. There is then an important distinction between the rapid flow reattachment which has been observed for first order responses at onset angles where the flow is initially separated and separation delay in dynamic situations. Flow reattachment was observed in the range of $17^\circ < \alpha_o < 30^\circ$. At larger angles flow reattachment was not observed and leading edge separation persists throughout the motion.

The responses for $30^\circ < \alpha_o < 46^\circ$ are shown in 11b and those for $50^\circ < \alpha_o < 62^\circ$ are shown in Figure 11c. There is undoubtedly work to be done in interpreting the physical mechanisms involved in the experimental indicial responses. However, the data presented above clearly show that the indicial response is (at least) first order dependent even for moderate angles of attack. Furthermore, for motions with large changes in angle of attack there will be a wide variation in "functional form" of the indicial responses. As has been discussed in connection with Equation 32 in Section VII.1, this eliminates the possibility of simply scaling the classical response according to nonlinearities in the static load slope only.

VIII. First Order Axial Force Responses

The axial loading on an airfoil is, in general, an order of magnitude smaller than the normal force. In rapid unsteady motions, strain gauge measurement of axial loads is generally very susceptible to structural noise due to the required small moment of inertia of the load cell in the axial direction. Measuring axial force indicial responses is a difficult task. Our confidence in the accuracy of the present experimental axial response results stems primarily from the following observations: i) the indicial responses are near to zero at step onset (i.e. the loading for the

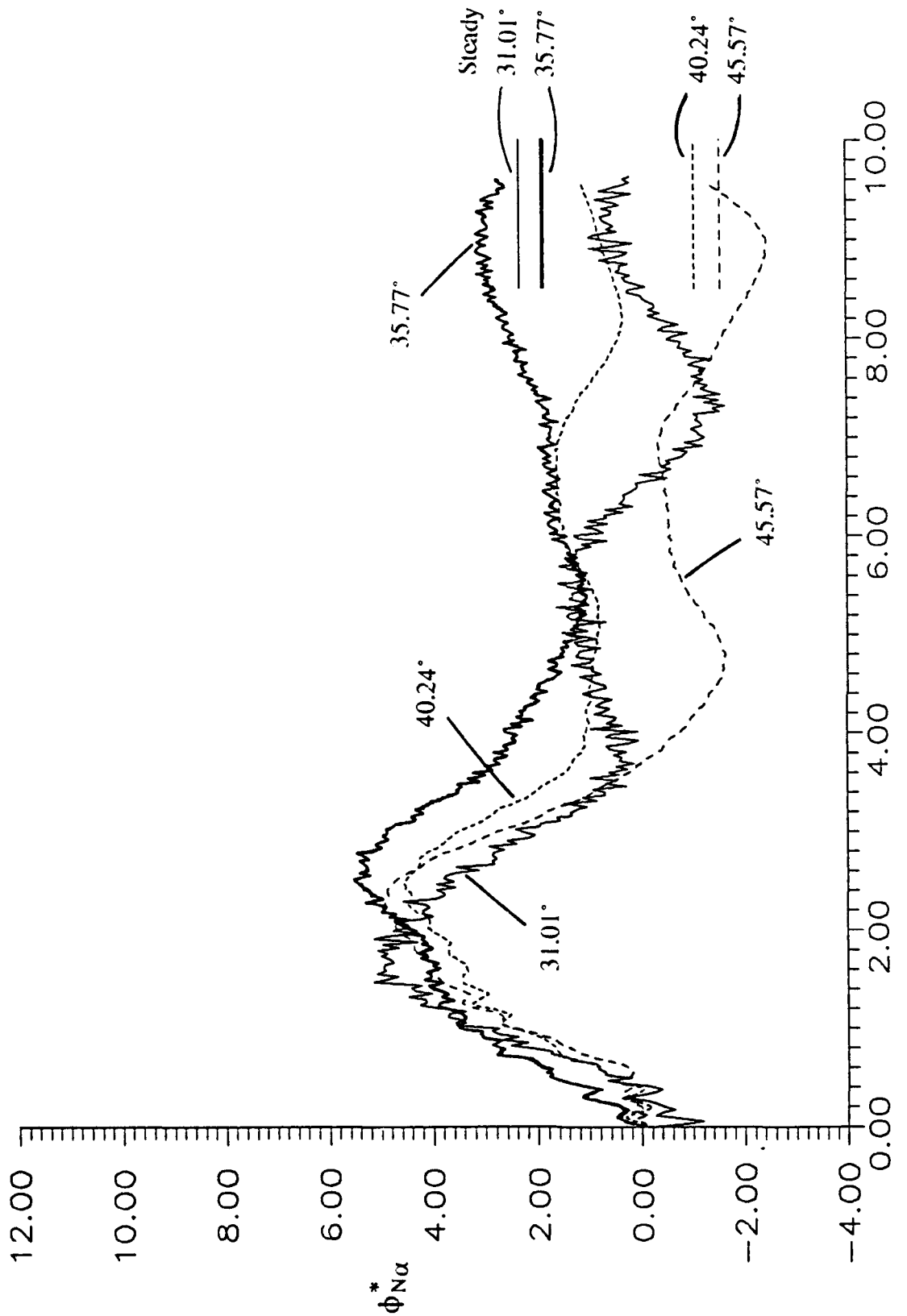

Figure 11b. First Order Normal Force Indicial Responses for Onset Angles in the Range $30° < \alpha_o < 46°$.

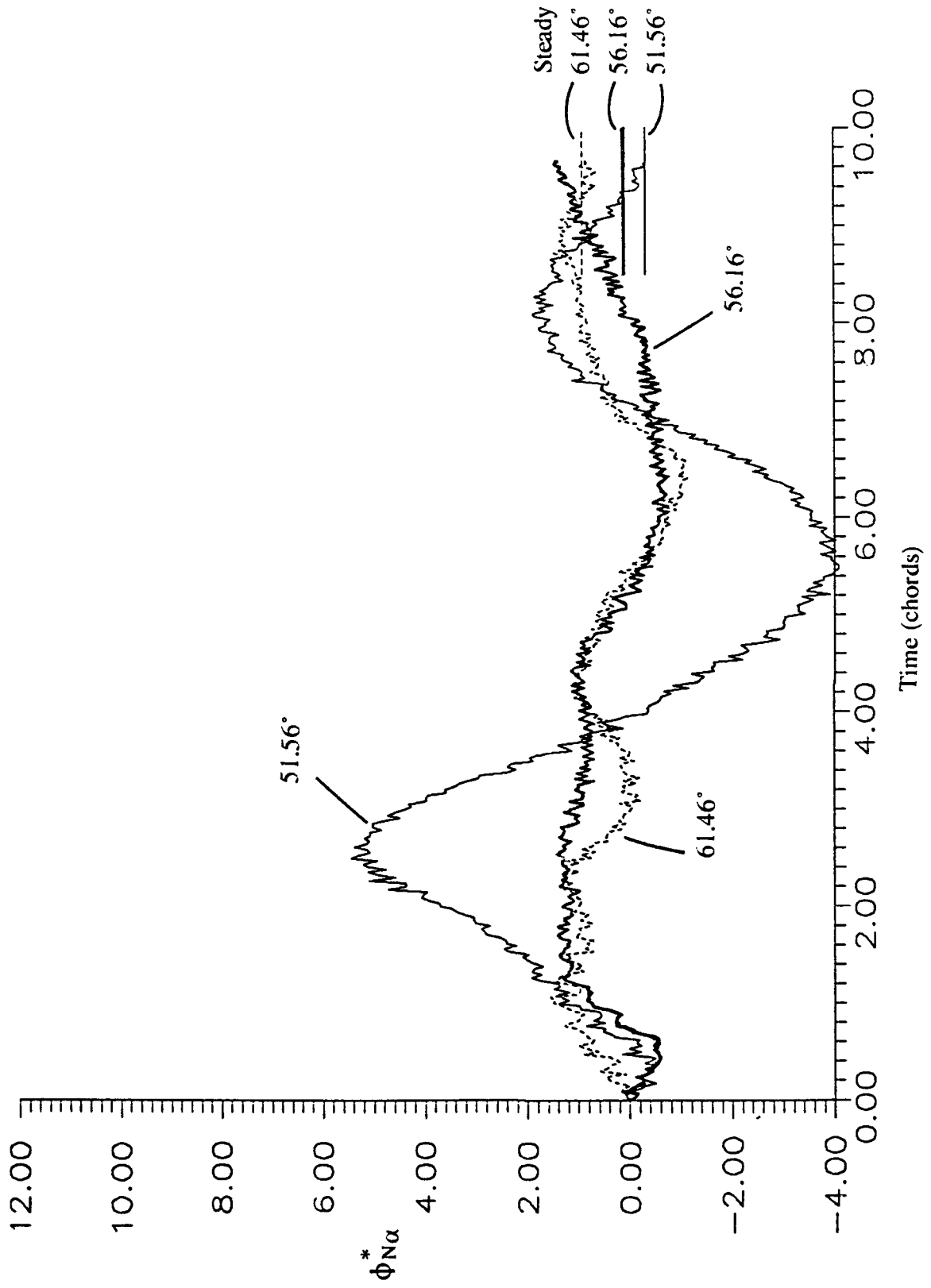

Figure 11c. First Order Normal Force Indicial Responses for Onset Angles in the Range $50° < \alpha_o < 62°$.

motions needed to construct the indicial response cancel at the step onset), ii)in general, the indicial responses approach the correct steady state slope measured in independent tests with the same airfoil as given in Figure 7b, and iii)when integrated for certain trial motions, the results are in reasonable agreement with independently measured trial motion force data. These same observations also apply to the normal force results discussed above. The first order axial force indicial responses are shown in Figures 12a-d. As in the case for the normal force results, the responses for onset angles beyond the static stall angle (≈15°) display oscillatory behavior. Also, the responses near 20° become large relative to their steady state values of Figure 7b.

IX Integration of First Order Responses for Ramp Motion

IX.1 Ramp Up Motion

The integral in Equation 19 has been evaluated numerically for the ramp-up motion given by $K = \dot{\alpha}b/U$ = constant, using the experimental indicial responses. The airfoil begins a $\alpha = 0°$ and ramps up to $\alpha > 30°$. As shown in Figure 13, the motion was approximated by steps of $\Delta\alpha = +1°$. The experimental indicial responses were measured in intervals of at most five degrees alpha(see Table 2). The response at intermediate angles were computed by interpolation between the test data. For example, the indicial response at, say, $\alpha_o = 22°$ was computed by interpolating between the measured responses at $\alpha_o = 20°$ and $\alpha_o = 25°$. The circulatory component of the normal force at some time t and corresponding angle of attack $\alpha(t) = K*t$ is given by:

$$C_N(t) = \sum_{i=1}^{N} \phi^*_{N\alpha}[\tau_{ei}, \alpha_o(\tau_i)]\,\Delta\alpha_i \qquad (33)$$

where $\tau_{ei} = t - \tau_i + \tau_\phi$ and is measured in chords and $\Delta\alpha_i = \pi/180$ radians. The quantity, τ_ϕ, is a correction for the time lag introduced by the filtering process and, in the present study, was found to be nearly equal to 0.5 in chords as discussed in Section IV. Notice that the value of the elapsed time, τ_{ei}, will depend on the pitching rate, and for constant pitch rate (and zero initial angle) may also be expressed as $\tau_{ei} = (\alpha(t) - \alpha_o(\tau_i))/2K + \tau_\phi$. The calculations are relatively insensitive to the time lag for values in the range $0.5 < \tau_\phi < 1.0$ chord. The axial force has been computed in the same way.

The uncertainty in Equation 33 has been estimated on the basis of the uncertainties in

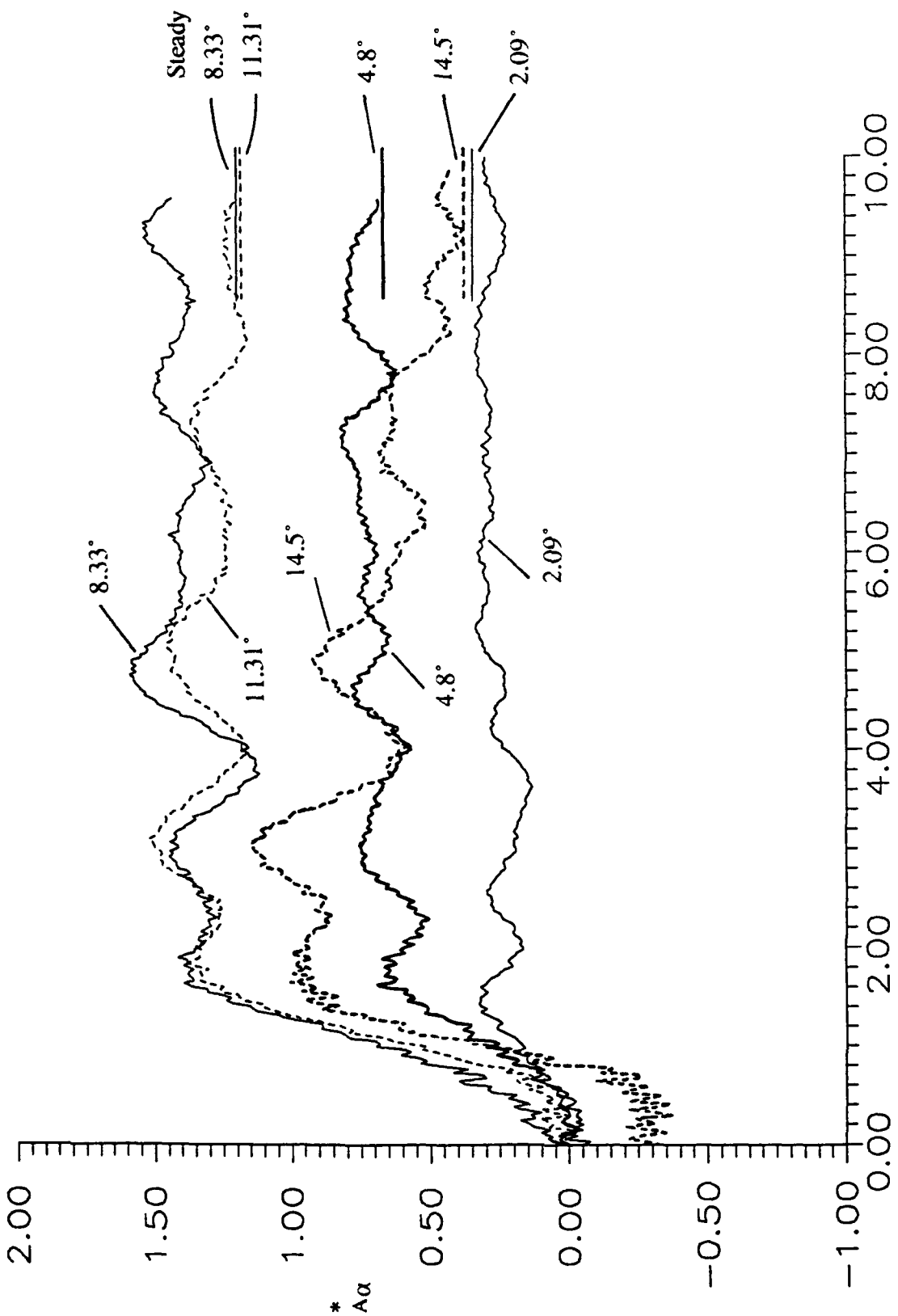

Figure 12a. First Order Axial Force Indicial Responses for Onset Angles in the Range $2° < \alpha_o < 15°$.

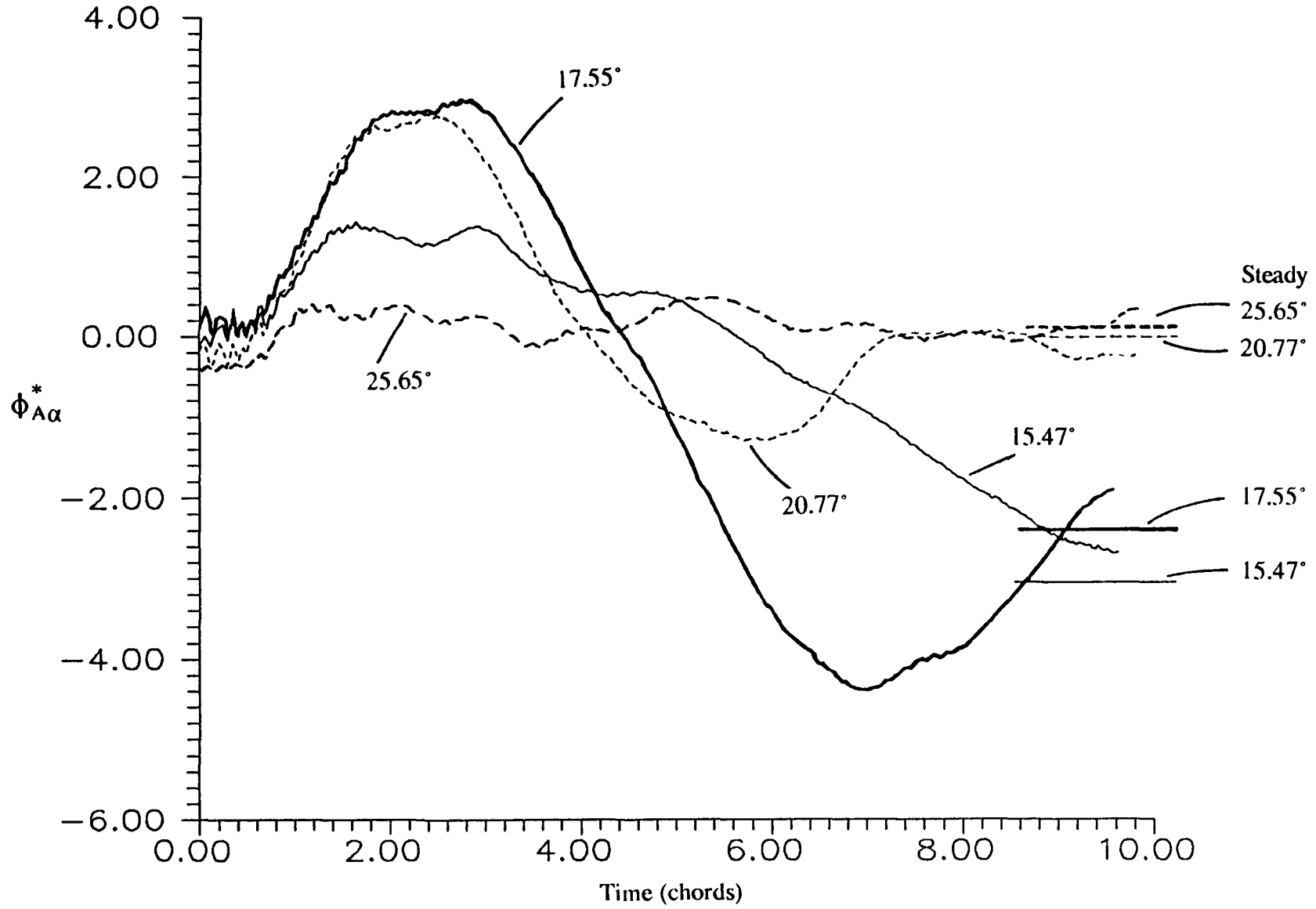

Figure 12b. First Order Axial Force Indicial Responses for Onset Angles in the Range $15° < \alpha_o < 26°$.

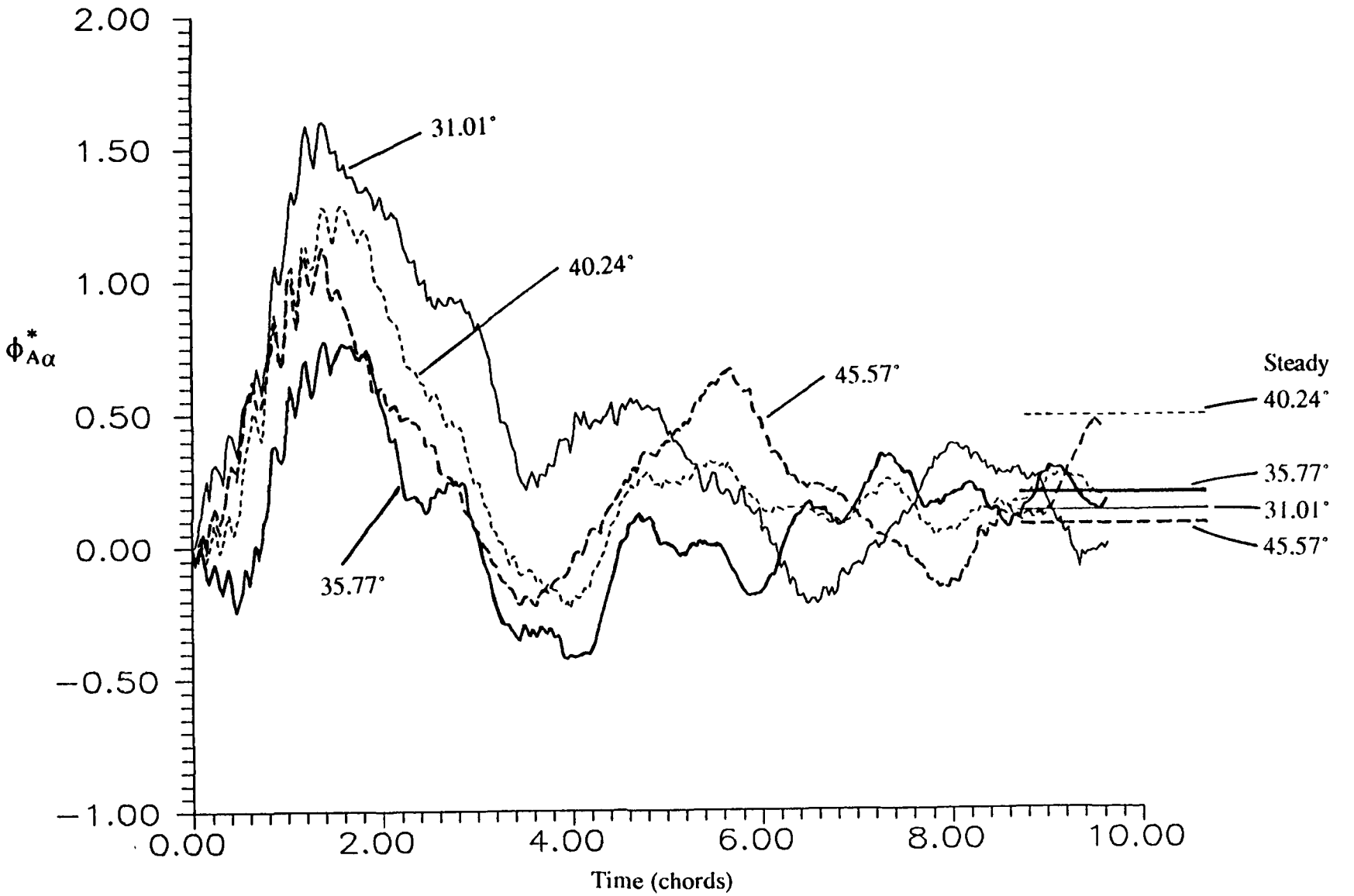

Figure 12c. First Order Axial Force Indicial Responses for Onset Angles in the Range $30° < \alpha_o < 46°$.

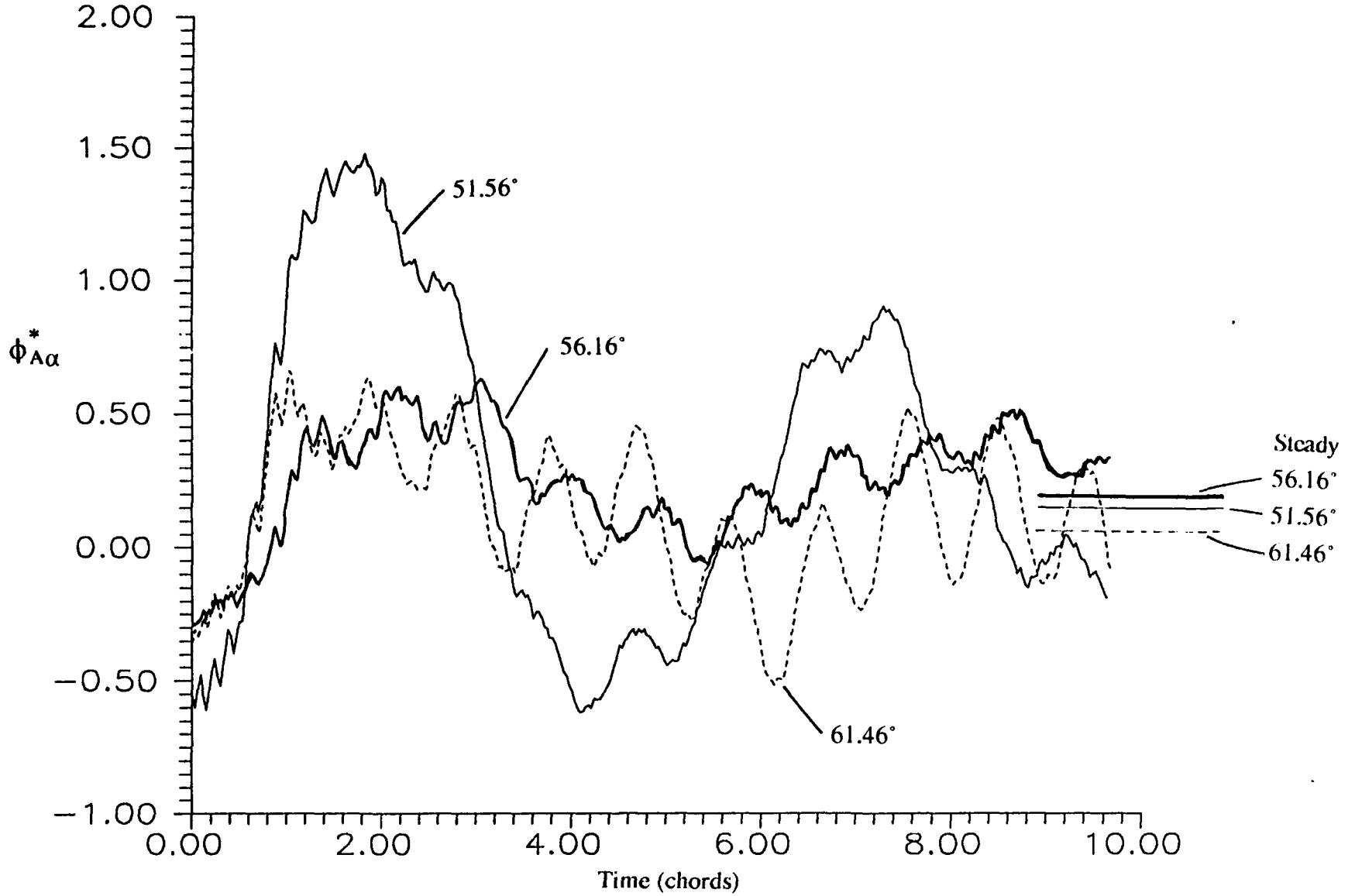

Figure 12d. First Order Axial Force Indicial Responses for Onset Angles in the Range $50° < \alpha_o < 62°$.

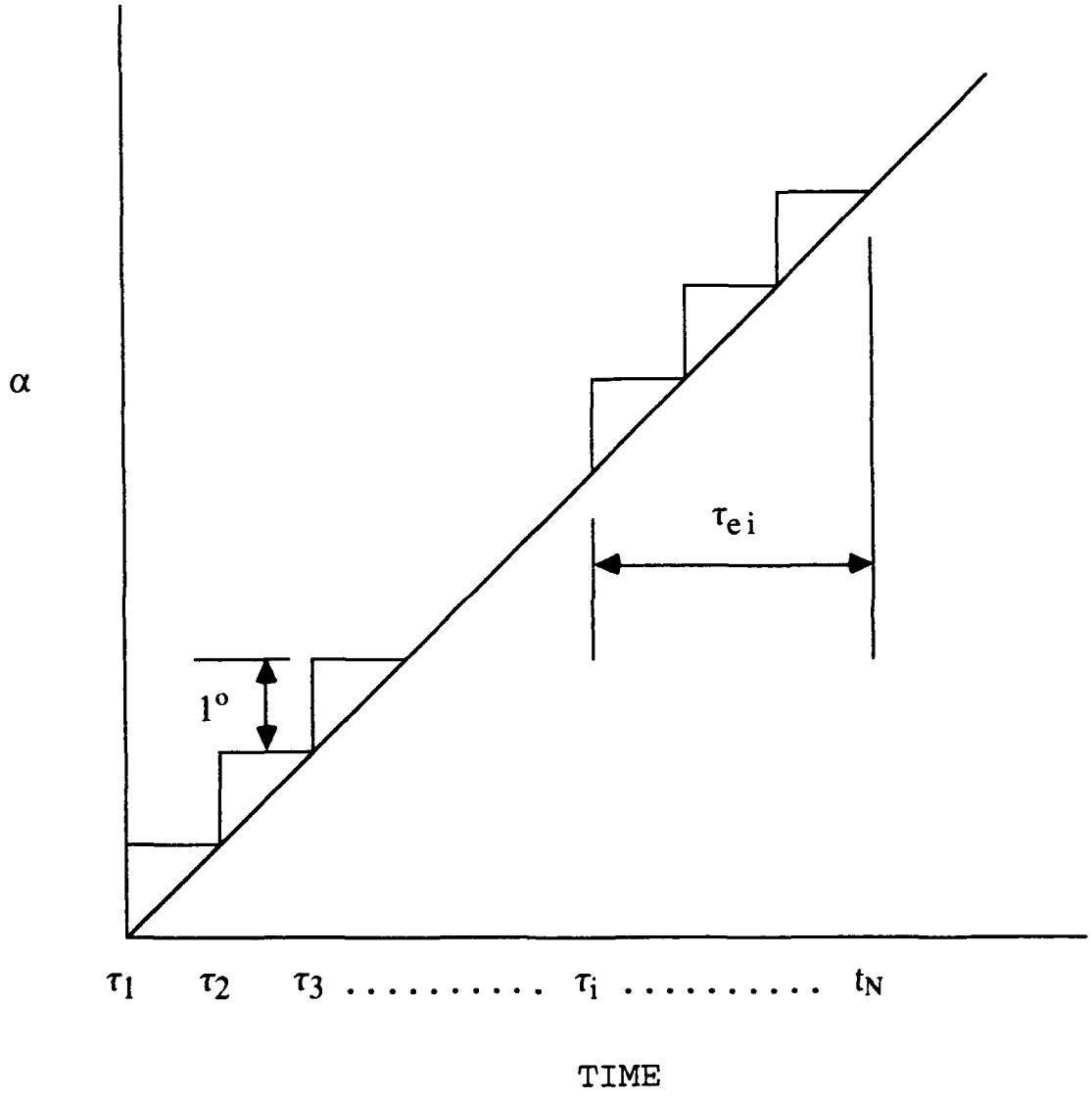

Figure 13. Discretized Motion for Computing the Loading During a Ramp Up Motion.

$\phi^*_{N\alpha}[\tau_{ei}, \alpha_o(\tau_i)]$ and $\Delta\alpha_i$ and will be indicated on the subsequent figures by error bars. The uncertainty analysis indicates that even for relatively accurate angle of attack and force measurements needed to construct the indicial response, the error in the force calculation of Equation 33 can become large(≈20%).

IX.2 Results for Ramp Up at K ≤ 0.01

The computed normal force for K = 0.01 is shown in Figure 14a along with actual ramp motion data taken with the same airfoil used to measure the indicial responses. Forces computed using the linear response based on Equation 25 are also shown. The agreement between the analysis and the ramp data is generally within the experimental uncertainty. At an angle near 16° the integrated indicial response results flatten out while the actual ramp data continue to increase. This appears to be a first order effect embedded within the responses at onset angles above 15° (i.e. separated flow at step onset due to static stall). Returning to Figure 11a, for elapsed times less than about 2 chords the responses at onset angles of 17.55° and 20.77° are small compared to the peak values which occur in the range of 4 to 6 chords. Furthermore, the magnitude of these responses for elapsed time from step onset less than 2 chords are significantly less than those for lower onset angles of attack shown in Figure 10d. This deficiency in the response leads to the flattening of the integrated results near 16°. It will be shown later in this report that including the second order term, $\dot{\alpha}(\tau)$, in Equation 6 will improve these results. In the actual ramp data, the effects of dynamic stall are evident near 25° where the force data flattens out. The nonlinear indicial response model predicts the stall with reasonable accuracy. Not surprisingly, the linear model of Equation 25 is in general agreement with the ramp data at low angle of attack, but does not predict the dynamic stall. The corresponding results for the axial loading during the ramp motion are shown in Figure 14b. There is fair agreement between the integrated first order indicial responses and the actual ramp data. It is not the purpose of this study to investigate aerodynamic stall. However, with regard to the legitimacy of the present indicial response results, it is significant that the loading during this complex flow phenomenon is predicted with some accuracy.

The static force curves for the present airfoil are also shown in Figures 14a and 14b. In each case the dynamic ramp data is substantially larger than the static data--which is a well known result. For the pitch rates considered here the dynamic loads are approximately twice as large as

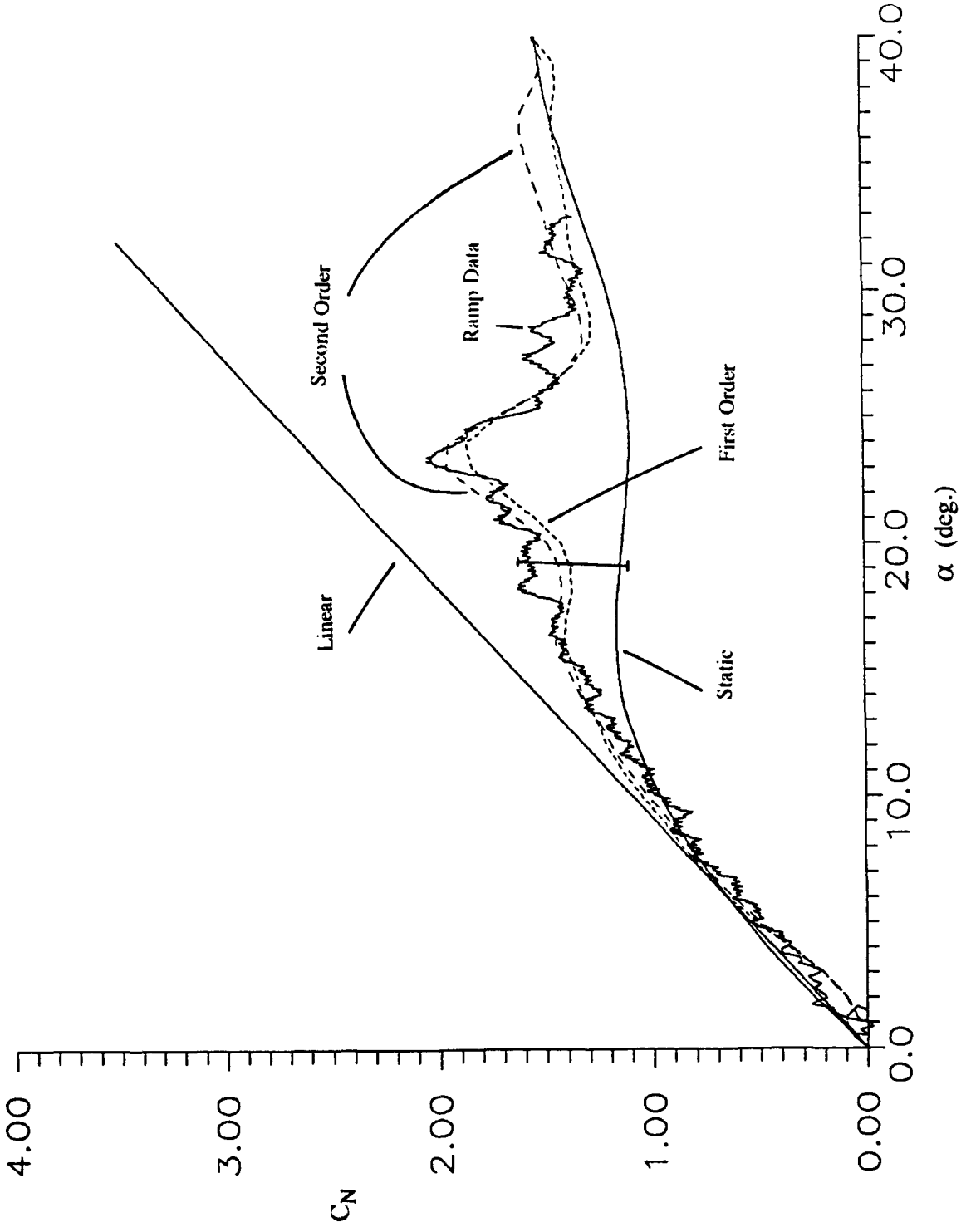

Figure 14a. Integrated Normal Force Results for a Ramp Up Motion at K = 0.01.

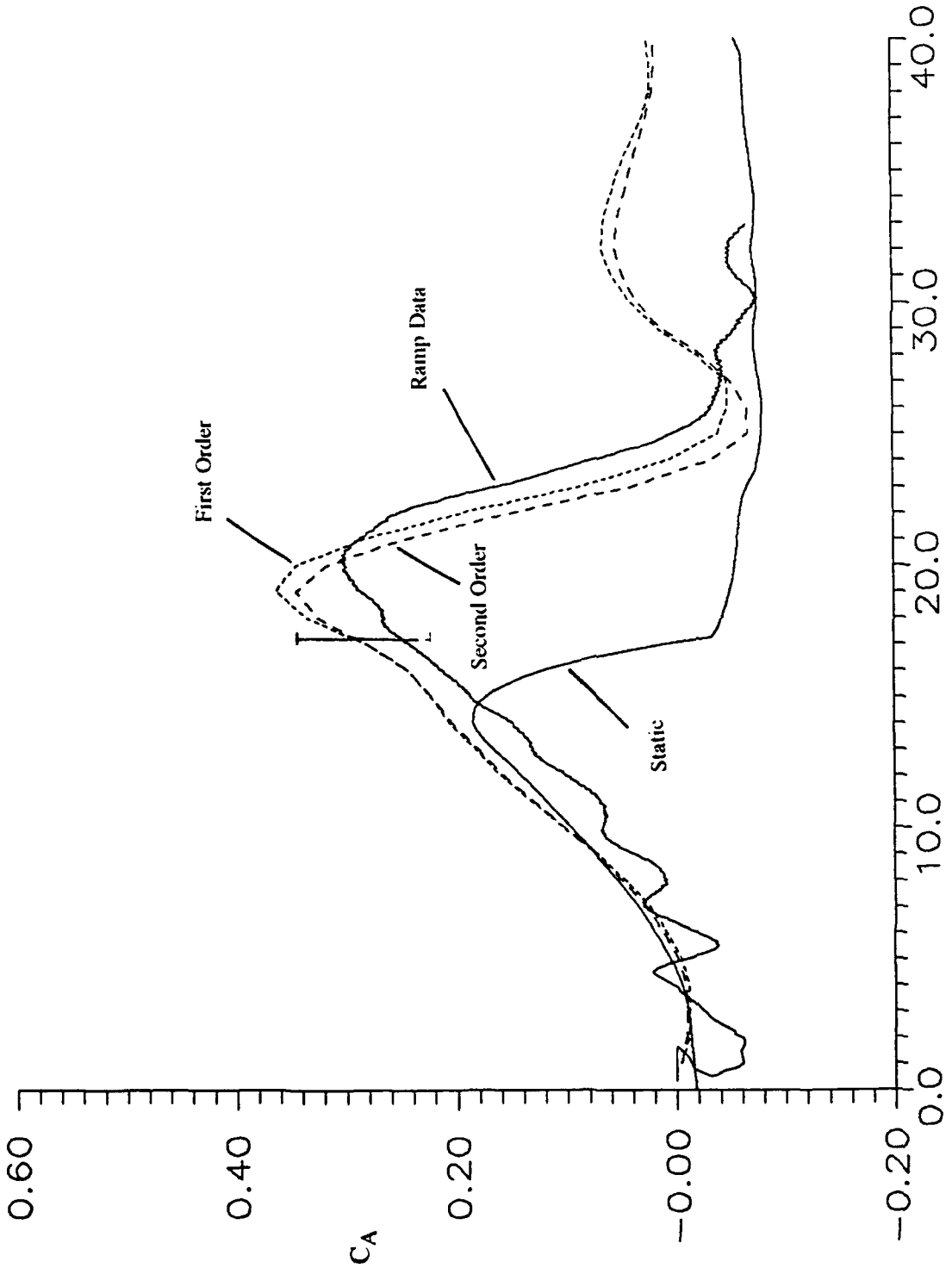

Figure 14b. Integrated Axial Force Results for a Ramp Up Motion at K = 0.01.

their static counterparts. The point to be made is that the first order responses reproduce the dynamic augmentation in the loading and this can be traced directly to the large magnitude indicial responses that occur in the range $16^\circ < \alpha_0 < 30^\circ$, as shown in Figures 11a for the normal force and 12b for the axial force.

The normal force results for K = 0.0075 are shown in Figure 15. In the case of K = 0.0075, the test was started with the airfoil at an initial angle of 8° to provide enough track so that dynamic stall would be reached. The pitching motion was initiated shortly after the motion began so that the steady state had not yet been reached at the inception of the pitch. This explains the discrepancy in the ramp data and the indicial response calculations at the lower angles of attack. On the other hand, by the time the airfoil had reached the dynamic stall angle it had moved approximately 9 chord lengths so that initial angle of attack effects should have diminished. Furthermore, the first order response model predicts the initial loading quite well for K = 0.01 as seen in Figure 14a. In Figure 15 the dynamic stall is again predicted relatively well.

IX.3 Results for Ramp Up at $K \geq 0.015$

Increasing the pitch rate to K = 0.015 results in the normal and axial force data of Figures 16a and 16b, respectively. With regard to the normal force, the initial loading is predicted reasonably well. At angles beyond 20° unsteady effects become increasingly important and flow separation is significantly delayed in the ramp up motion. Flow separation for K = 0.015 occurs near 23°. The first order response model appears to introduces flow separation effects too early in the motion and, as a result, underpredicts the normal force loading during dynamic stall.

The results for higher pitch rate are shown in Figures 17a and 17b for K = 0.02, and Figures 18a and 18b for K = 0.05. In both Figures, the effect of static stall at onset, which is naturally embedded within the first order indicial responses near $\alpha = 15^\circ$, is apparent in the normal force results. Furthermore, a comparison of Figures 14a and 16a shows that as the pitching rate increases from K = 0.01 to 0.02, the first order indicial response model does not accurately describe the normal force loading for higher angles of attack. This is not too surprising when considering that at a pitch rate of K = 0.02 the flow does not separate until near $\alpha = 27^\circ$, prior to which the flow is more or less attached. This means that for the duration of the ramp motion between the dynamic stall angle of attack and the static stall angle of attack, $16^\circ < \alpha < 27^\circ$, Equation 33 has been computed using indicial responses which do not contain the physically

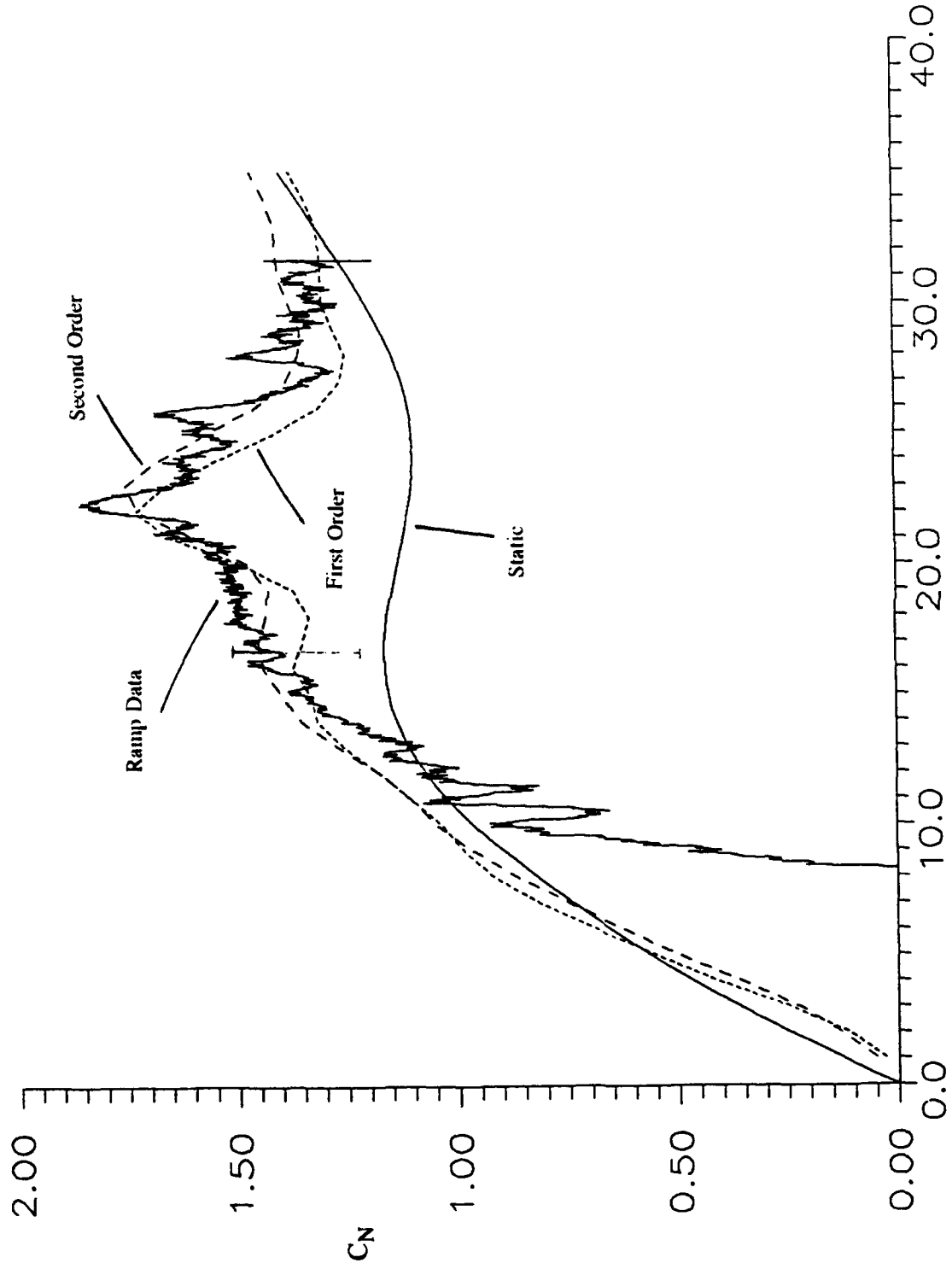

Figure 15. Integrated Normal Force Results for a Ramp Up Motion at K = 0.0075.

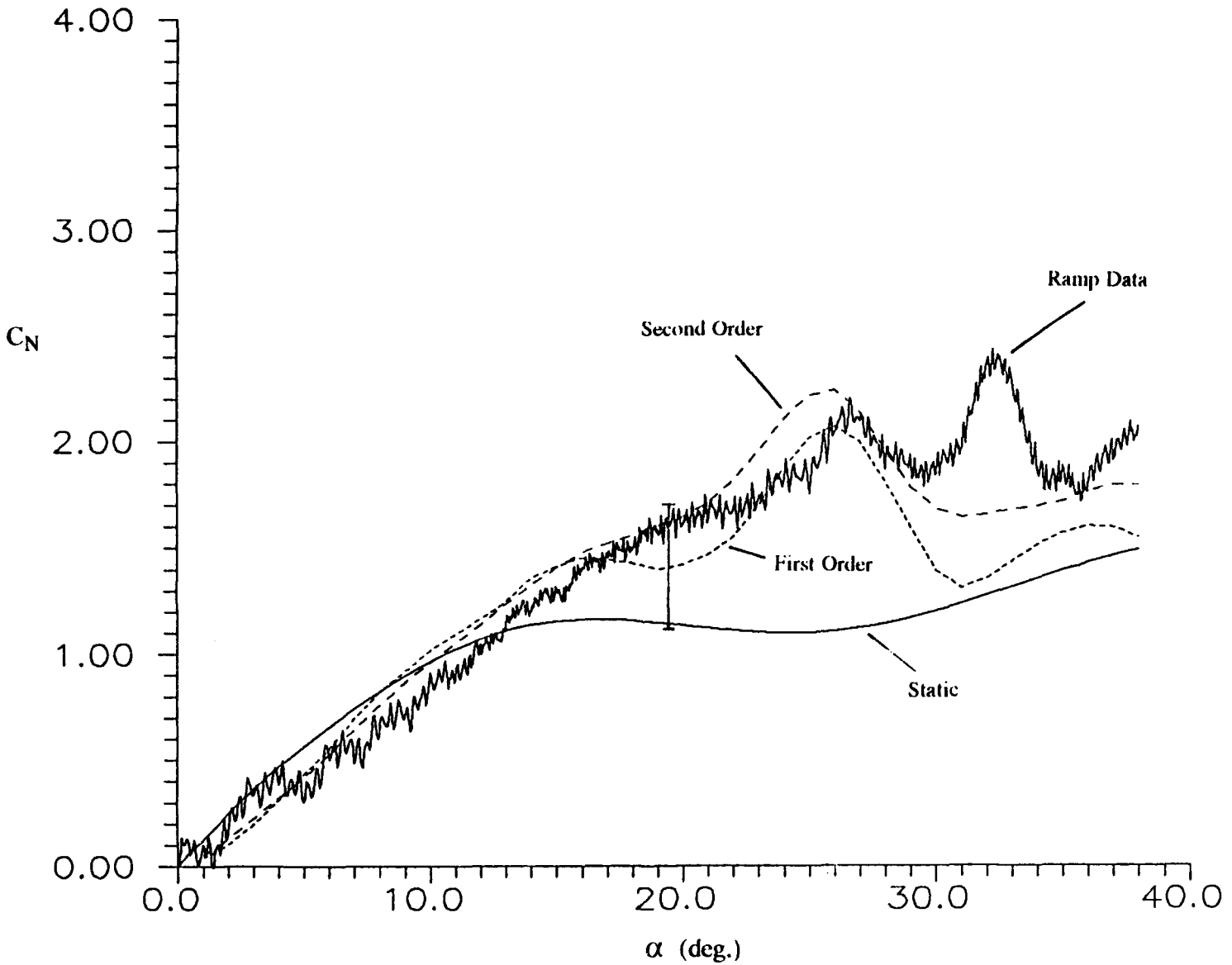

Figure 16a. Integrated Normal Force Results for a Ramp Up Motion at K = 0.015.

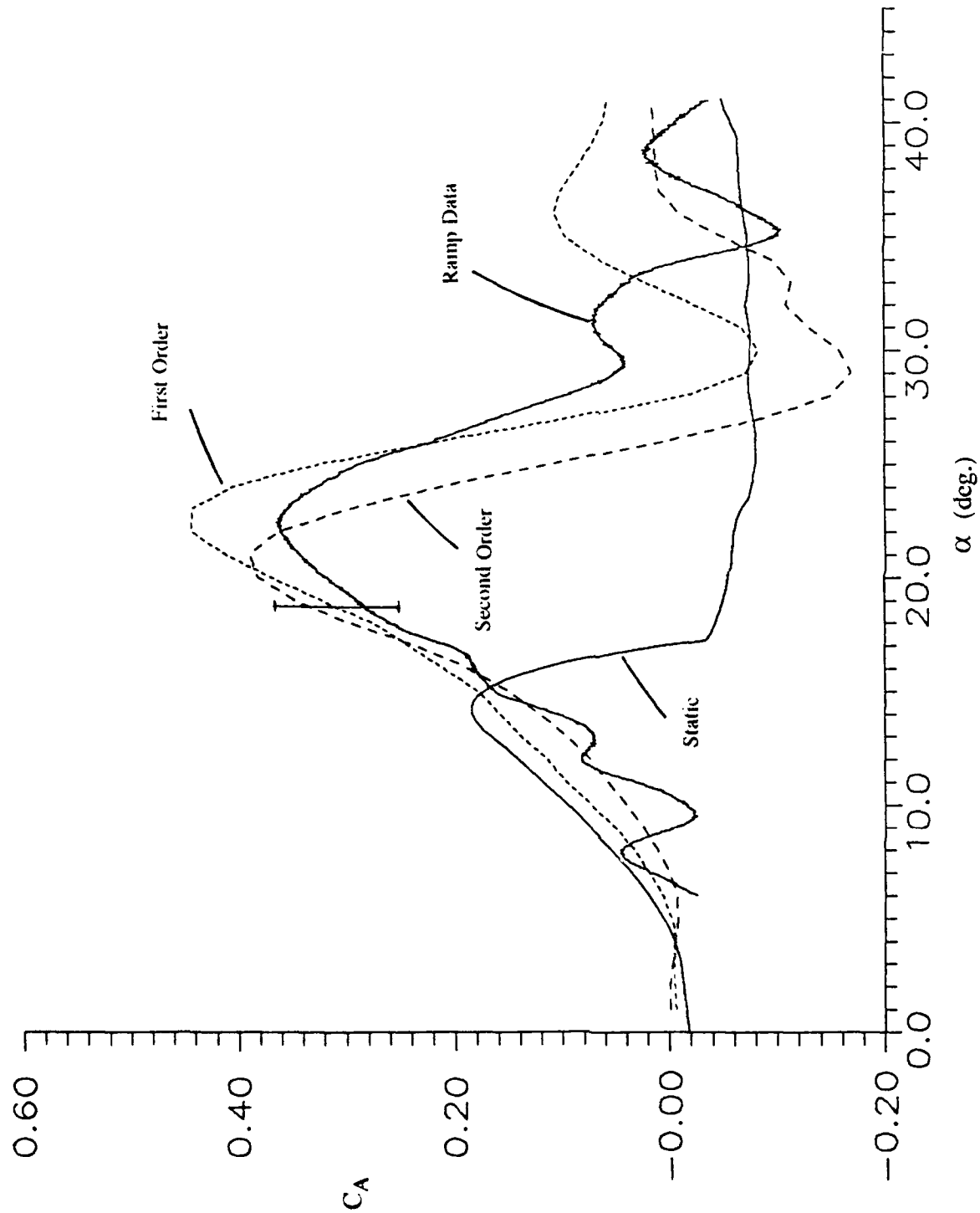

Figure 16b. Integrated Axial Force Results for a Ramp Up Motion at K = 0.015.

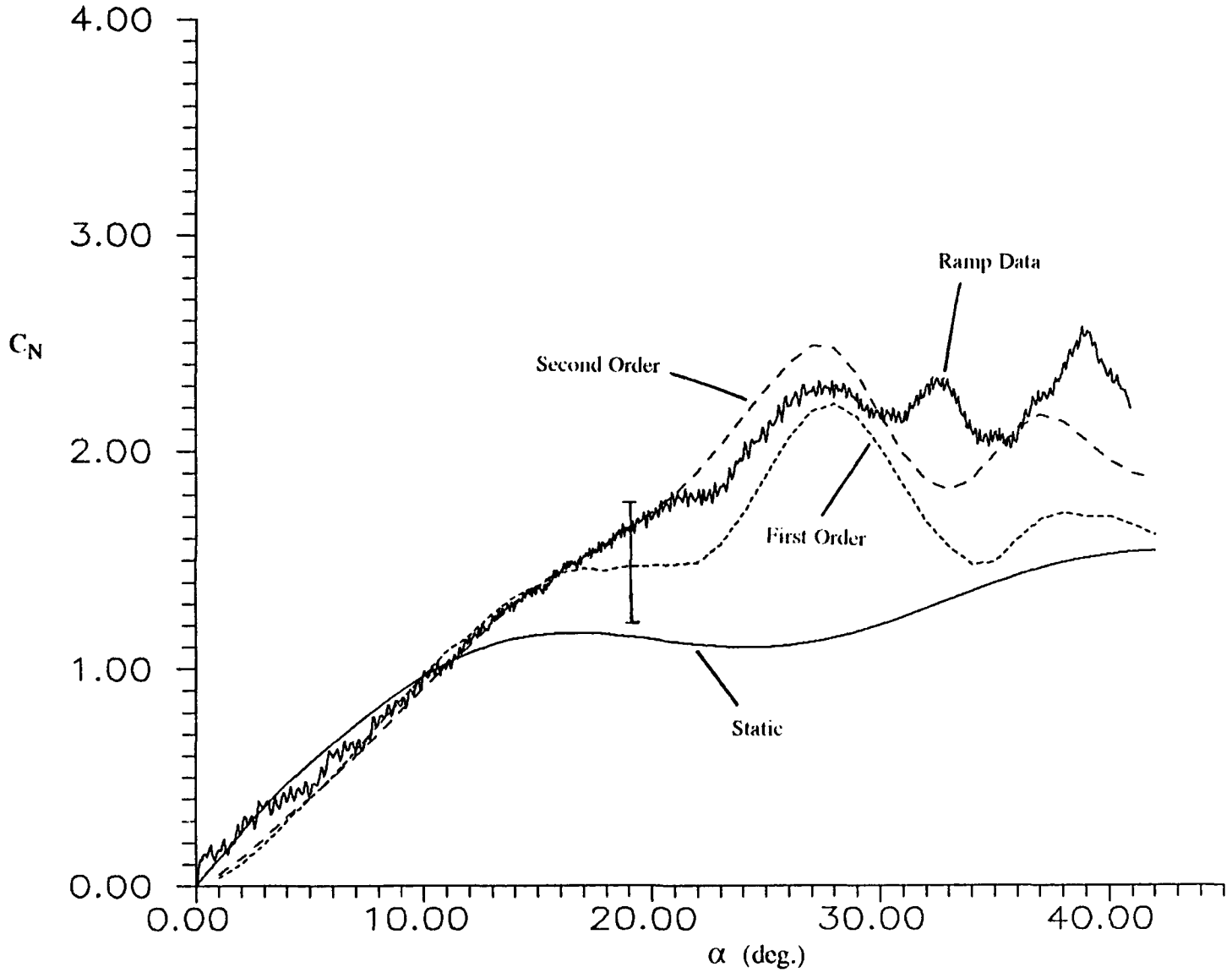

Figure 17a. Integrated Normal Force Results for a Ramp Up Motion at K = 0.02.

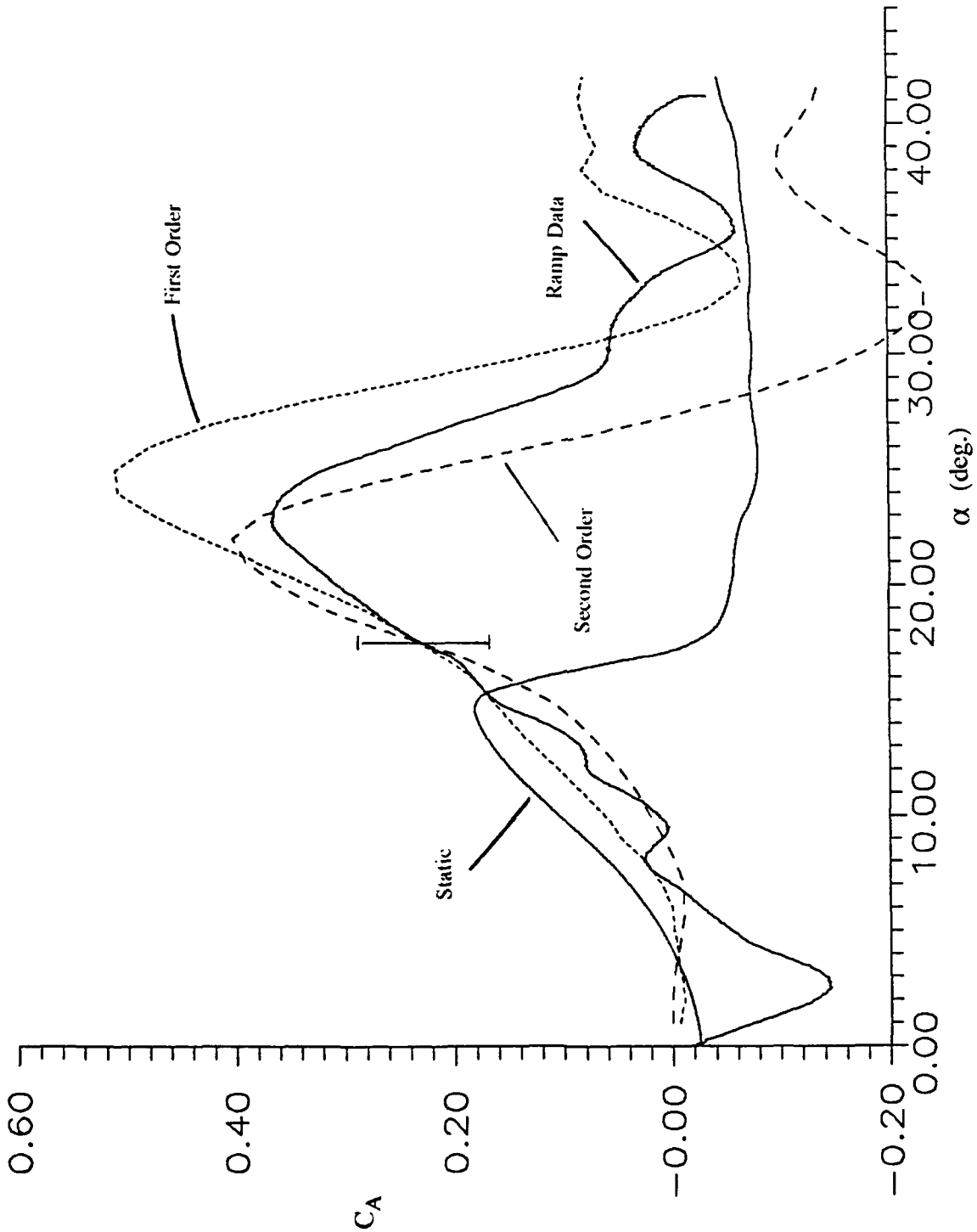

Figure 17b. Integrated Axial Force Results for a Ramp Up Motion at K = 0.02.

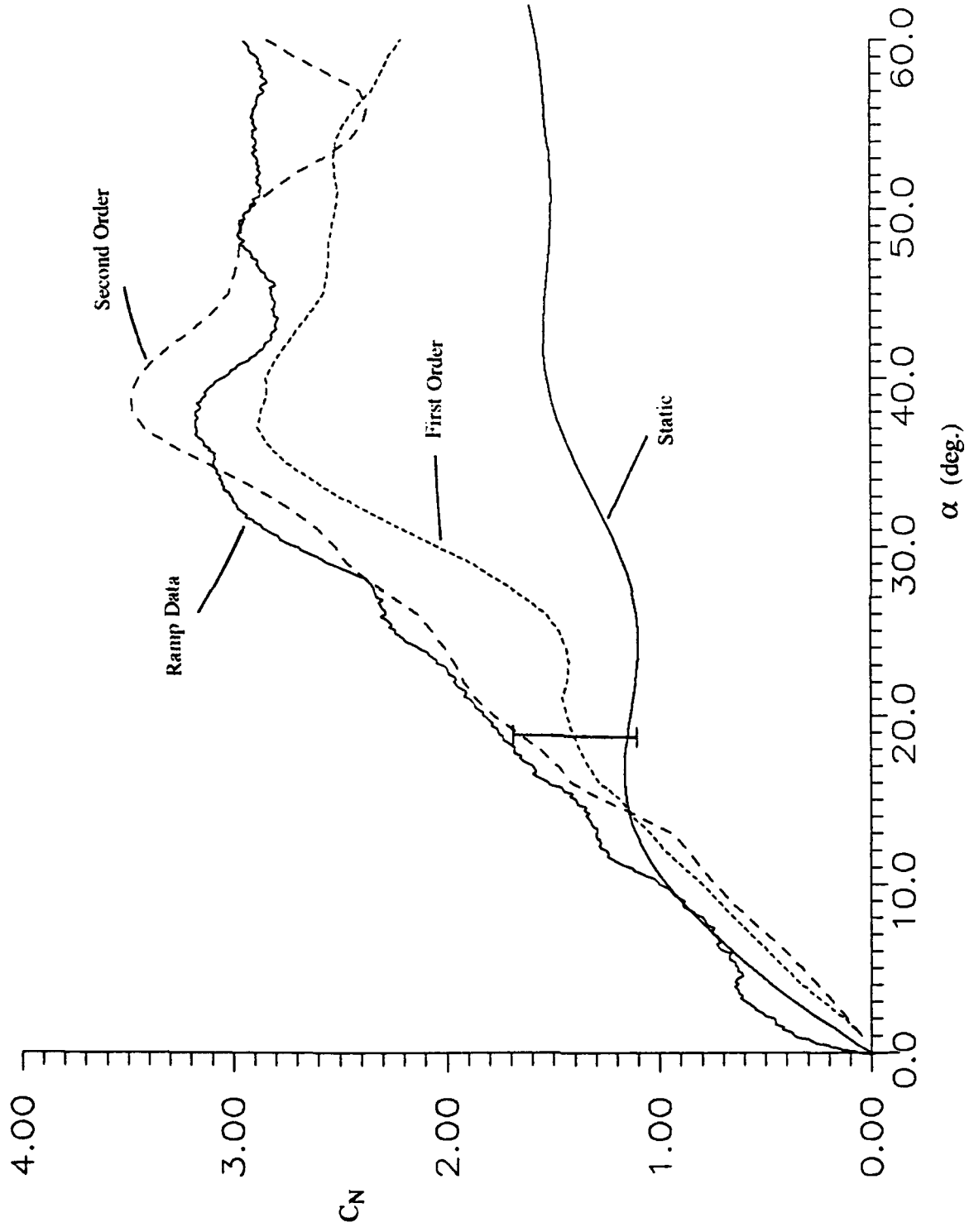

Figure 18a. Integrated Normal Force Results for a Ramp Up Motion at K = 0.05.

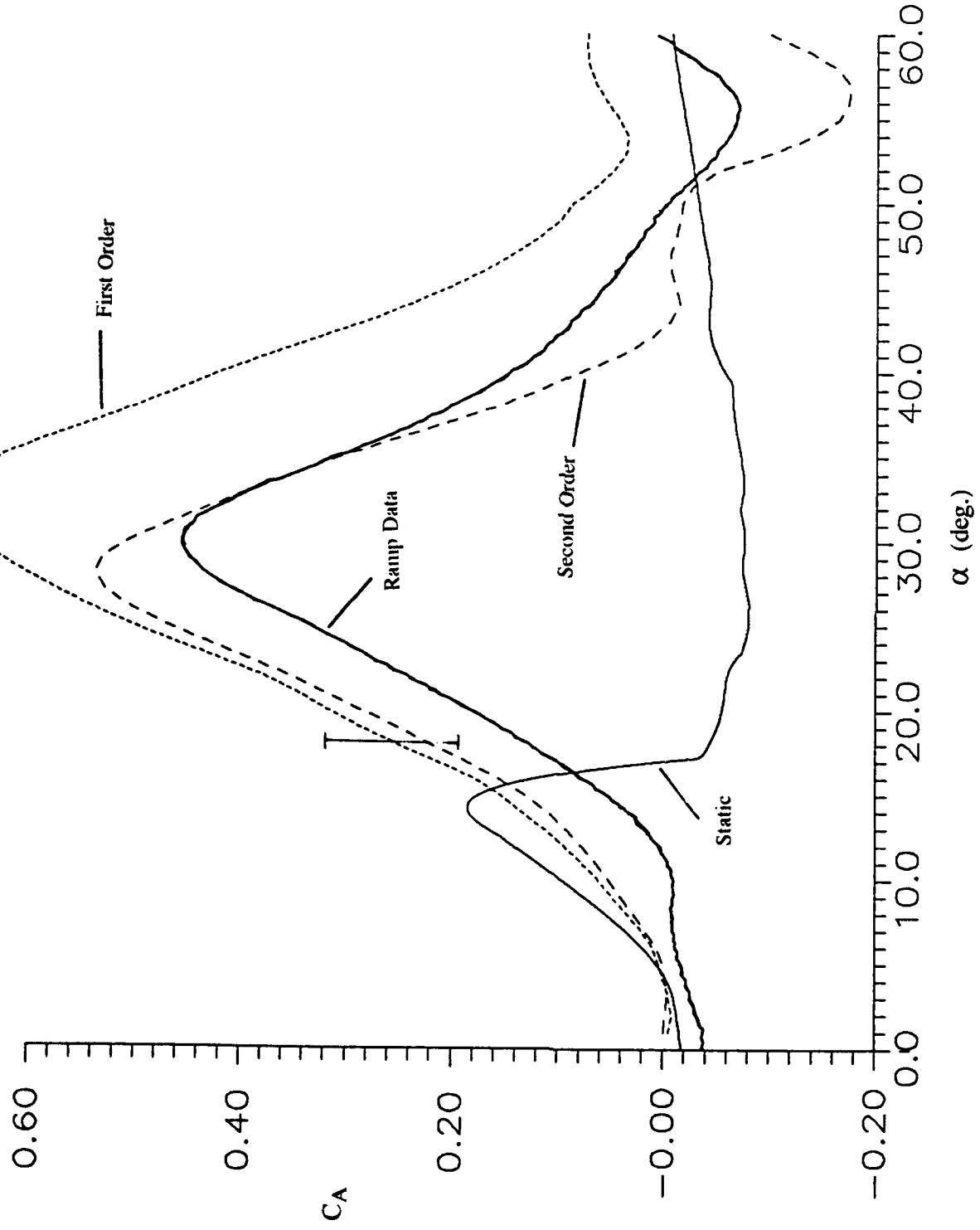

Figure 18b. Integrated Axial Force Results for a Ramp Up Motion at K = 0.05.

correct step onset conditions. Furthermore, as a consequence of the convolution process these errors will propagate throughout the calculation for subsequent measuring times. Rate effects on the indicial response become important for motions in which the angle of attack at which separation actually occurs differs significantly from the static stall angle. This occurs at high pitch rates. The normal force results for K = 0.05 given in Figure 18a also show the consequences of neglecting rate effects on the flow separation. For K = 0.05, leading edge separation occurs near 33°. Improvement can only be achieved by including higher order terms in the indicial response representation of Equation 6. The agreement between the integrated first order axial forces and the ramp data is also seen to deteriorate as the pitch rate increases from K = 0.01 to 0.05.

X. Second Order Response Study

X.1 Integrated Results for the Ramp Up Motion

Second order normal and axial force indicial responses have been measured using a ramp up motion from a substall angle of attack to the step onset angle of attack as has been discussed in Section V. Pitching rates of K = 0.02, 0.05, and 0.1 were studied. The results have been integrated for the ramp up motion by rewriting Equation 33 as:

$$C_N(t) = \sum_{i=1}^{N} \phi^*_{N\alpha}[\tau_{ei}, \alpha_o(\tau_i), \dot{\alpha}(\tau_i)]\,\Delta\alpha_i \qquad (34)$$

For comparison, the second order results are also shown in Figures 14a-b, 16a-b, 17a-b, and 18a-b. The second order responses for K < 0.02 at any particular onset angle were computed by interpolating by pitch rate between the measured second order responses at K = 0.02 and the first order responses (K = 0) at the same onset angle. Referring to Figure 14a, for the case of K = 0.01 the second order result is only a slight improvement over the first order model. For K = 0.05 in Figure 18a, however, at an angle of attack near 16° the second order result is clearly in better agreement with the ramp data. This suggests that including the proper flow condition at step onset is important at the pitch rate of K = 0.05 wherein separation is significantly delayed. Figure 18b shows a corresponding improvement in the axial force prediction.

Finally, as a rather severe test of the present approach, a ramp up at very high pitch rate of K = 0.1 has been considered. The results are shown in Figure 19a and 19b. The second order

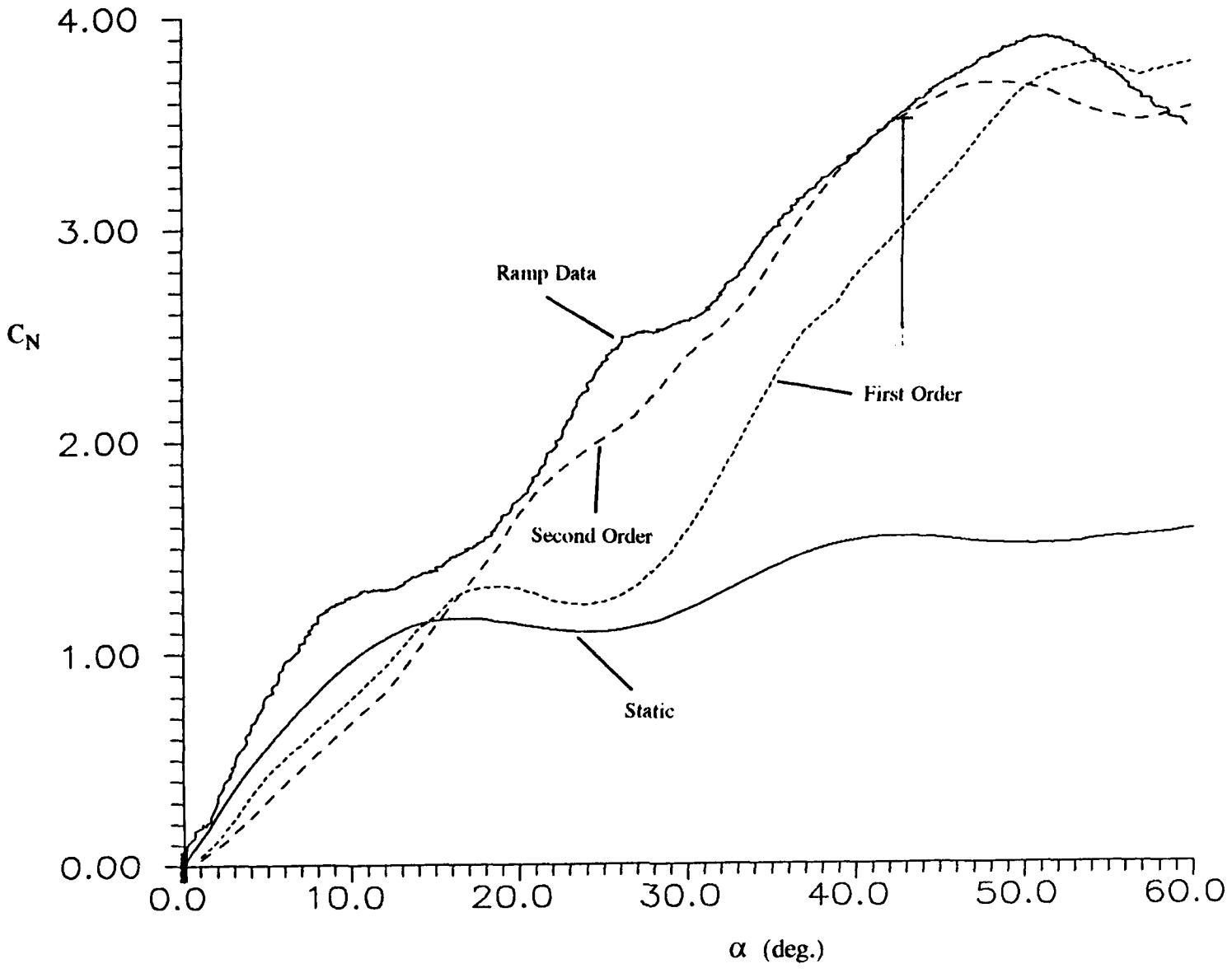

Figure 19a. Integrated Normal Force Results for a Ramp Up Motion at K = 0.1.

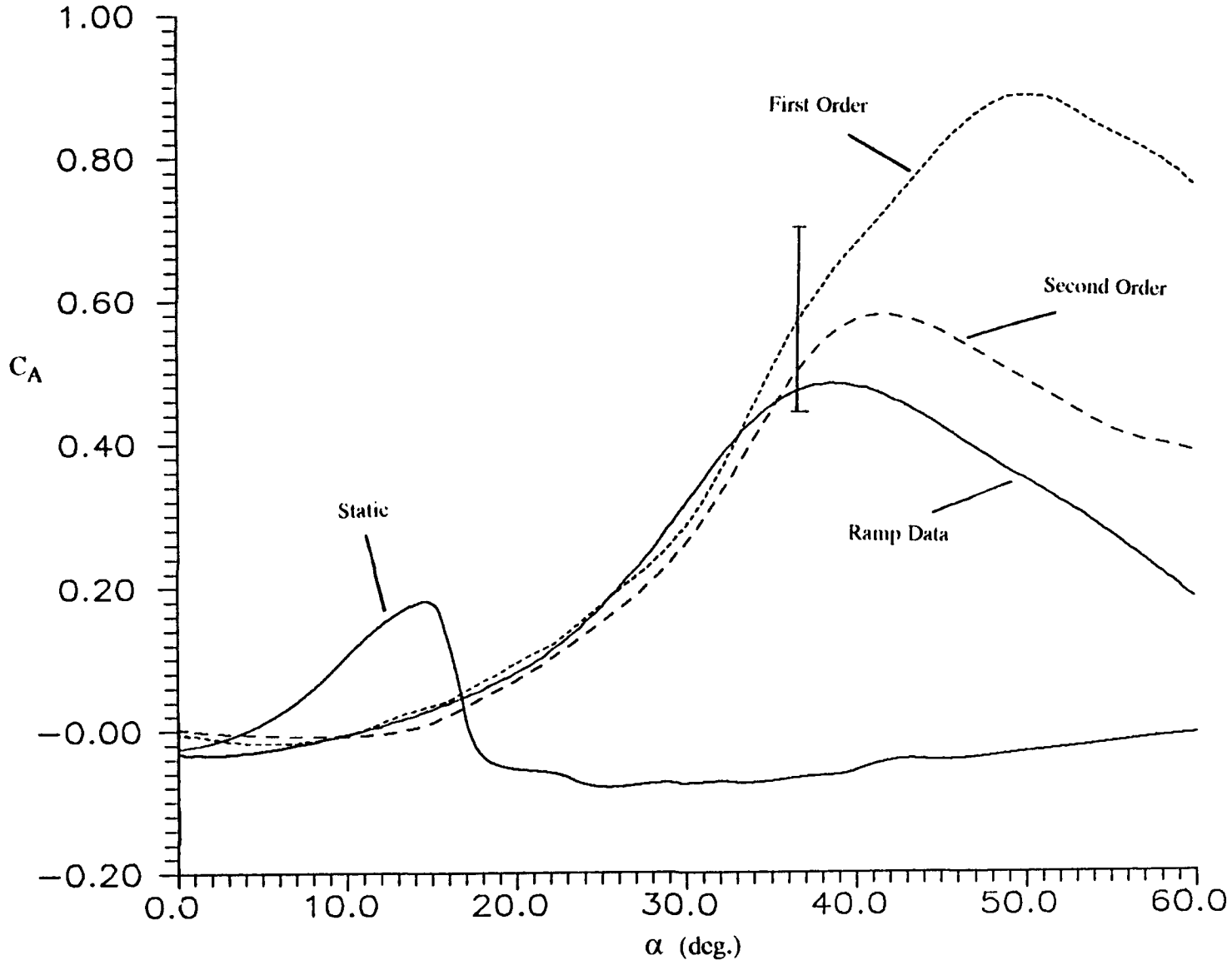

Figure 19b. Integrated Axial Force Results for a Ramp Up Motion at K = 0.1.

results are in general agreement with the ramp data at high angle of attack where first order dependence is not sufficient to accurately describe the loading. It is interesting that for pitch rates of K = 0.05 and 0.1 at low angles of attack the first and second order responses underpredict the loading, and this effect becomes more pronounced as the pitch rate increases (compare, for example, the results at each pitch rate at an angle near 8°). This may be due to neglecting the apparent mass reaction as well as the last term on the RHS of Equation 19 the magnitude of which is directly proportional to pitch rate.

X.2 Comparison of First and Second Order Normal Force Responses

A comparison of first and second order indicial responses provides some insight into the "rate" effects. Shown in Figure 20a are first order and second order (K = 0.05) responses at an onset angle near 11°. The two responses are very similar. The slight difference in the steady state values is due to the fact that the onset angles are not identical. A comparison of other responses for $\alpha_0 < 15°$ shows similar behavior. Notice also from Figure 18a that the integrated first and second order responses are similar below 15°. This suggests that the rate effect, or rather the difference between first and second order responses, is small for onset angles where the flow is initially attached. Figure 20b shows first and second order responses for an onset angle near 20°. For small elapsed time from step onset the second order response increases while the first order response remains small. The measured responses in the range of $16° < \alpha_0 < 25°$ exhibit similar behavior. This is the reason for the improvement in the integrated normal force results near the static stall angle when using second order responses. As noted above, for a pitch rate of K = 0.05 the flow remains more or less attached up to near 33°. It is interesting to note that for elapsed time below 5 chords the general shape of the second order response is similar to the first order responses for substall onset angles of attack; compare for instance with the first order responses in Figure 10d.

Figure 21a shows the second order results for onset angles near 11° for the three pitch rates considered. The pitch rate is seen to have little effect on the normal force response and this behavior is exhibited for other second order responses for α_0 below 15°. Again, differences in the steady state value are believed to be largely due to dissimilar onset angles. At onset angles beyond about 17°, the indicial responses become chaotic due to flow separation, which occurs after the step, and energetic vortex shedding. Figure 21b shows second order normal force responses at onset angles near to 20°. For each pitch rate the flow is more or less attached

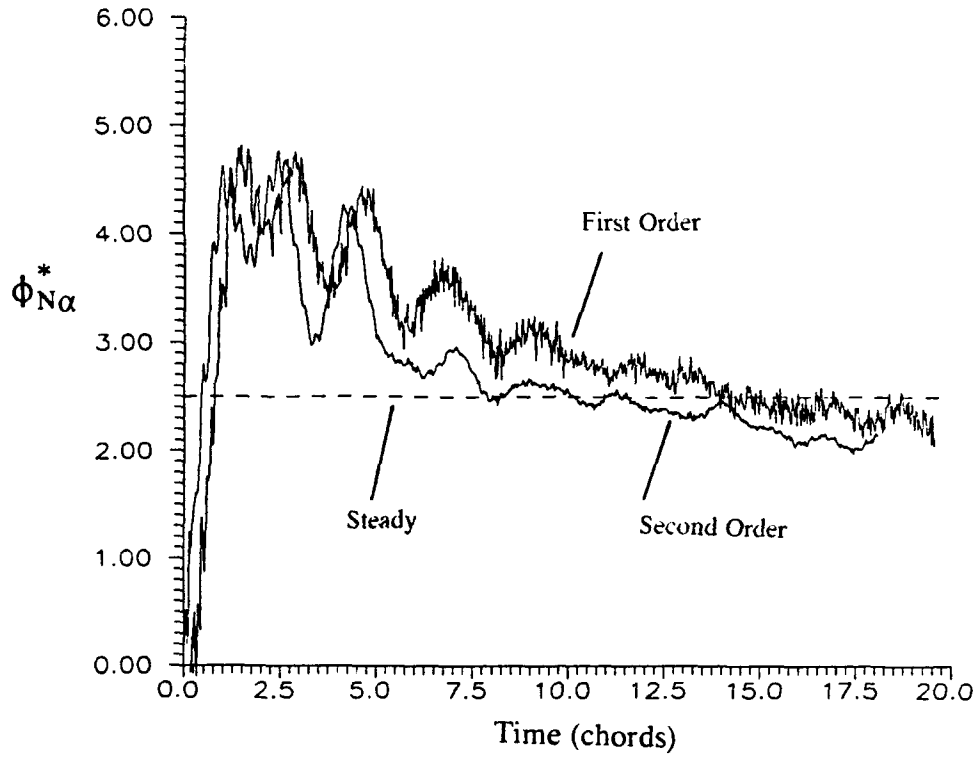

Figure 20a. Comparison of First and Second(K = 0.05) Order Responses for an Onset Angle Near 11°.

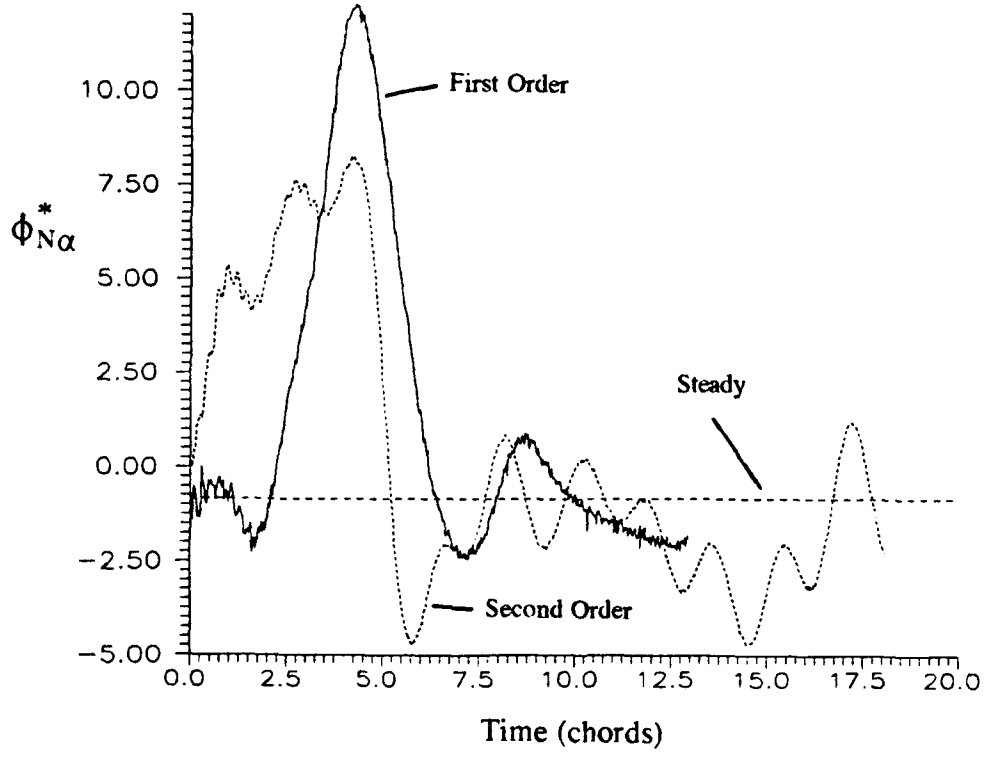

Figure 20b. Comparison of First and Second(K = 0.05) Order Responses for an Onset Angle Near 20°.

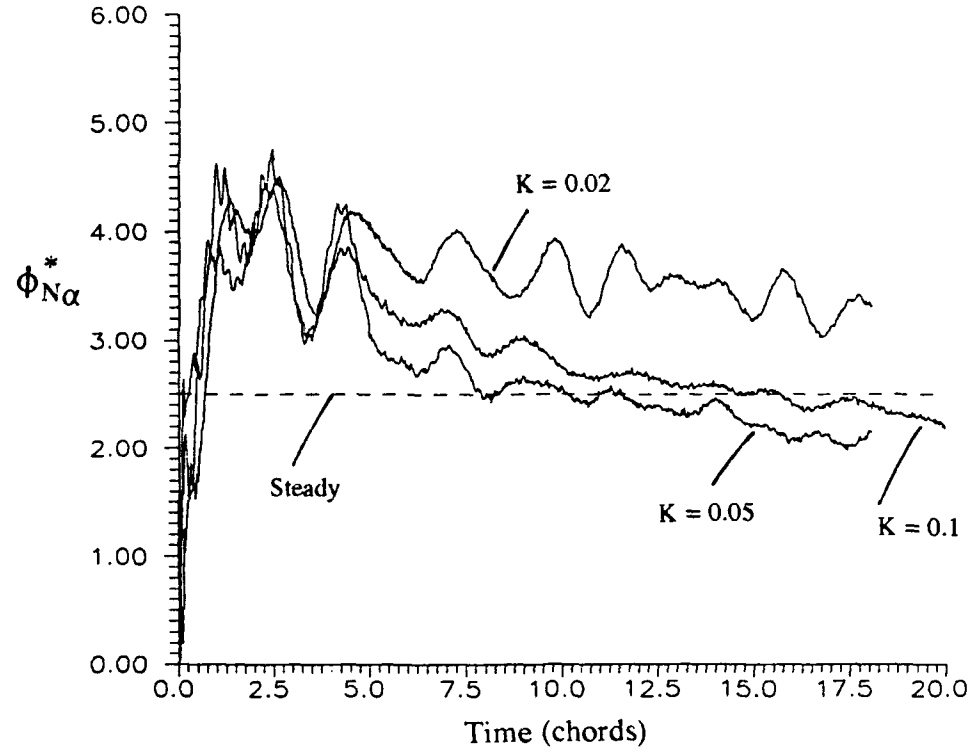

Figure 21a. Comparison of Second Order Responses for K = 0.02, 0.05, and 0.1 for an Onset Angle Near 11°.

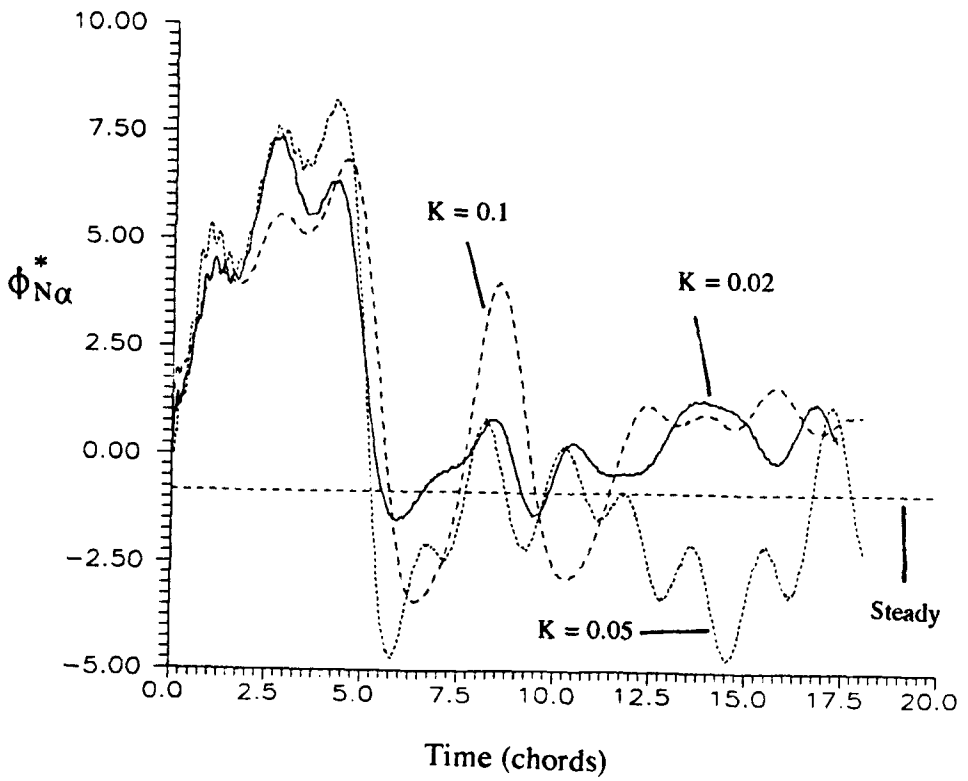

Figure 21b. Comparison of Second Order Responses for K = 0.02, 0.05, and 0.1 for an Onset Angle Near 20°.

at the step onset. Each response is very similar for approximately the first five chords beyond which the responses decrease rapidly. It is difficult to draw conclusions from these data, however, it appears that the attached flow at step onset gives rise initially to a response similar in form to the substall first order responses, and the rapid drop in the response may be due to subsequent flow separation since the onset angle is well beyond the static stall limit. Figure 21c shows second order responses at a high angle of attack near 40° wherein at each pitch rate the flow has undergone dynamic flow separation prior to the step onset. Future flow visualization studies may provide additional information which may help to interpret these data. A complete set of the experimentally measured second order normal and axial force indicial responses for a ramp up to onset at K = 0.05 are given in Appendix B at the end of this report.

XI. Saw Tooth Motion

The loading on an airfoil undergoing a saw tooth motion has been computed by integrating the experimental indicial responses. The saw tooth motion was selected because it contains both positive and negative pitch motion, and could easily be imparted with the current drive train of the O.U. tow tank to provide baseline load data. Figure 22 shows the angle of attack data for the two motions considered. In each motion the pitch occurs at constant rate of $K = \pm 0.05$ and the amplitude in case one is approximately 0° to 10° and in case two 10° to 20°. The saw tooth motion at high pitch rate is an interesting case from the perspective of motion history effects on the flow. Because the pitch rate is constant, only the first and second order terms in Equation 6 will be nonzero. As such, the indicial response at, say, point "A" on Figure 22 will be the same for the saw tooth motion and a pure ramp up motion (or any other constant $\dot{\alpha}$ motion) even though the saw tooth and the pure ramp up will undoubtedly have different motion history effects. The loading results using the first and second(K=0.05) order responses are shown in Figures 23a and 23b for case one. The integrated loads are in good agreement with the baseline data. As has been discussed in relation to Figure 20a, the first and second order indicial responses for low alpha are similar and, therefore, the integrated first and second order loads in Figure 23a are also similar. For case two the integrated loads are shown in Figures 23c and 23d. The integrated loads and the baseline data show clear differences. In Figure 23c the first order results are in better agreement than the second order results. Recall that the second order responses were measured for a ramp up motion ($\dot{\alpha} > 0$) to the onset angle while the saw tooth consists of both

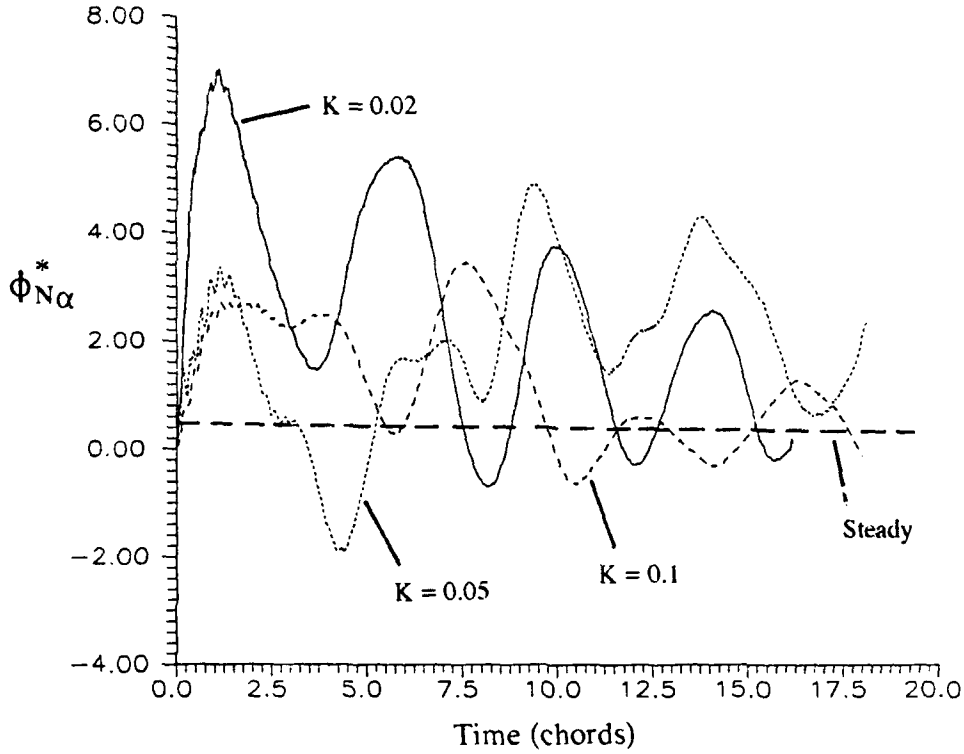

Figure 21c. Comparison of Second Order Responses for K = 0.02, 0.05, and 0.1 for an Onset Angle Near 40°.

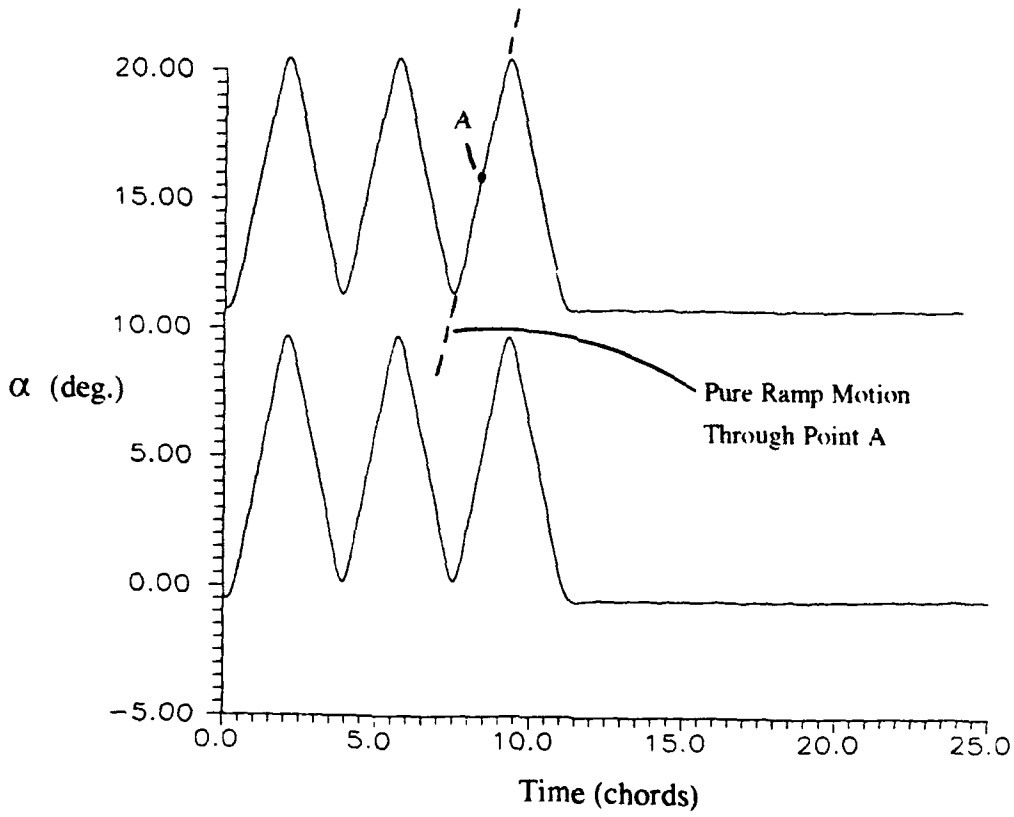

Figure 22. Angle of Attack Data for Saw-Tooth Motion with K = ±0.05.

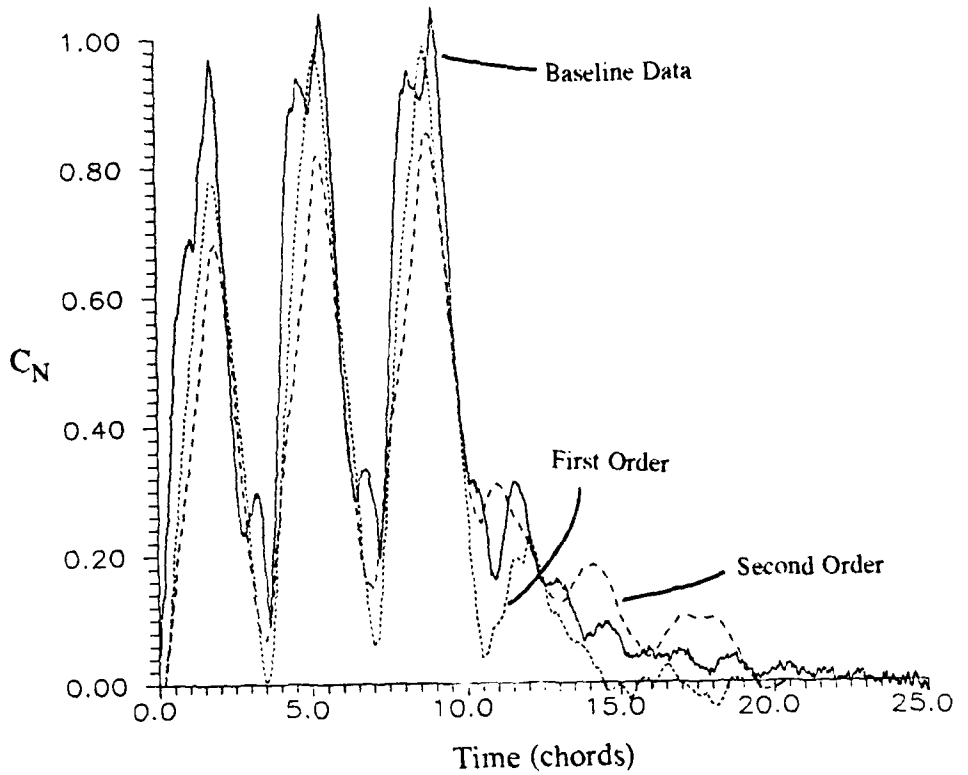

Figure 23a. Integrated Normal Force Loading for Low Amplitude Saw-Tooth Motion.

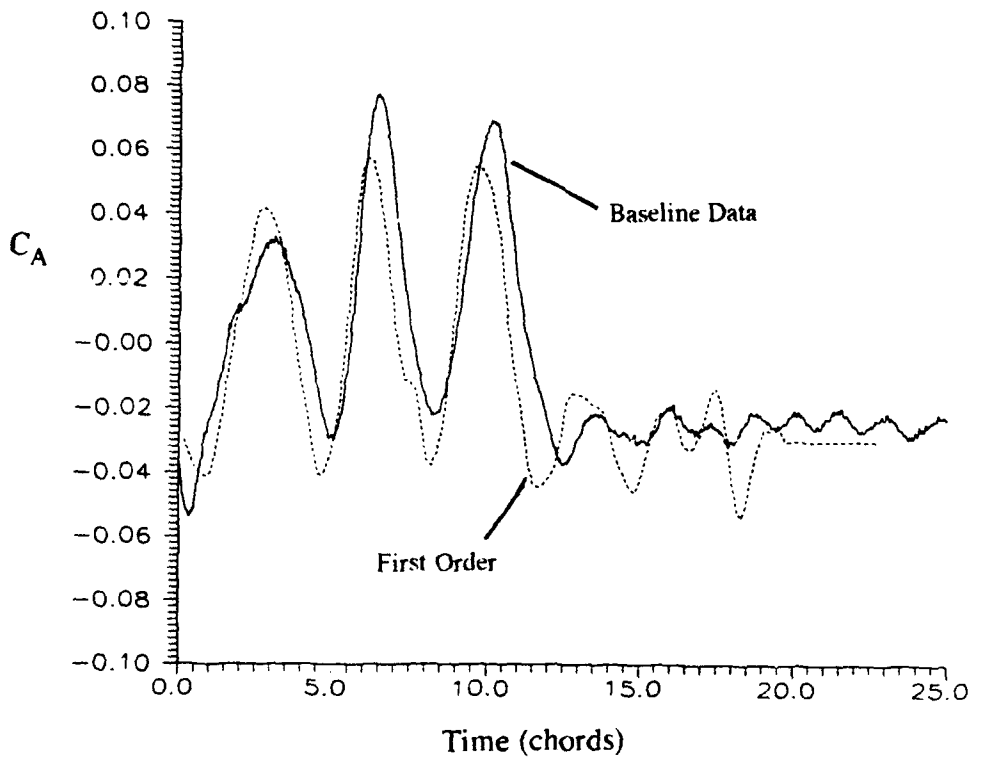

Figure 23b. Integrated Axial Force Loading for Low Amplitude Saw-Tooth Motion.

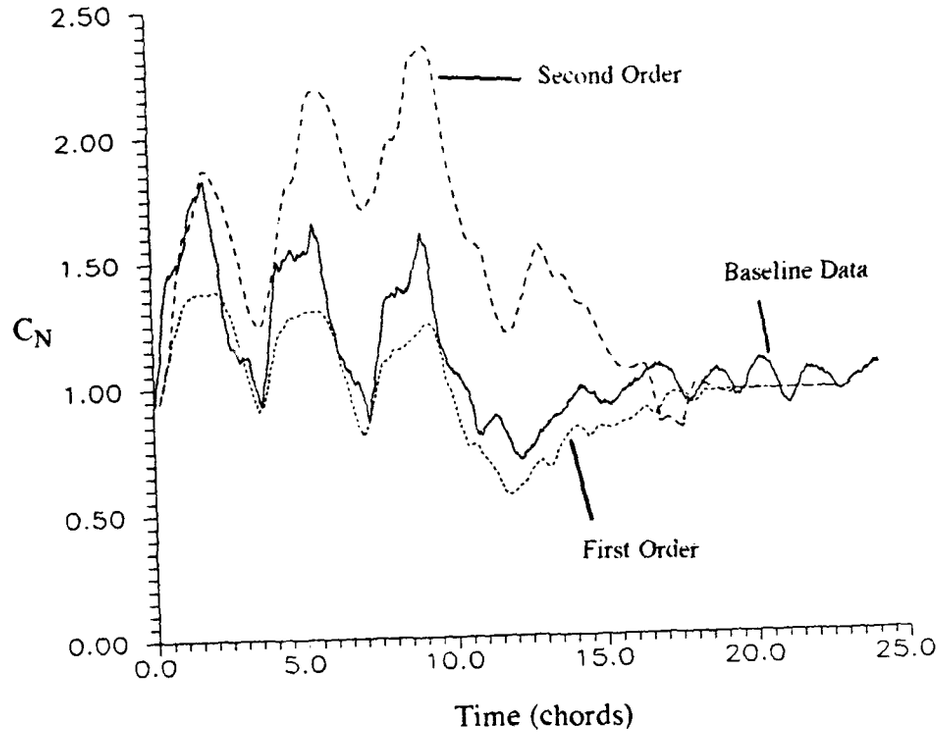

Figure 23c. Integrated Normal Force Loading for High Amplitude Saw-Tooth Motion.

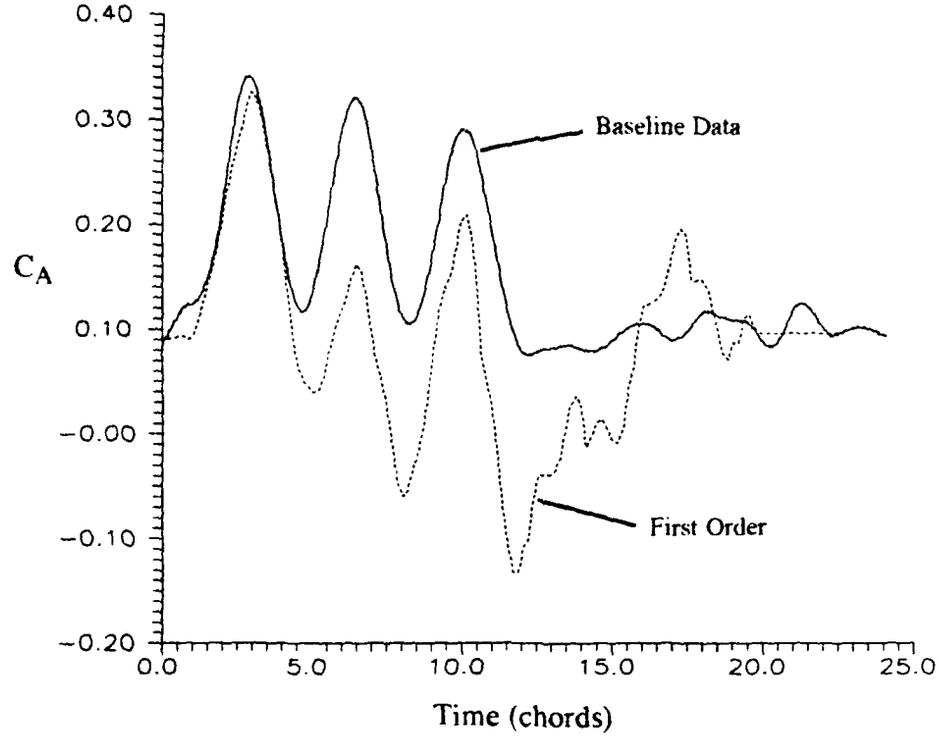

Figure 23d. Integrated Axial Force Loading for High Amplitude Saw-Tooth Motion.

positive and negative pitching motions. The second order integrated normal force results begin to differ from the baseline data as the ramp down motion begins midway through the first cycle. This suggests that the sign of the second order term, $\dot{\alpha}$, in Equation 6 is important. Notice, however, that including the proper sign of $\dot{\alpha}$ may still not be sufficient since, as discussed above, a second order model cannot distinguish between a saw tooth motion or any other constant $\dot{\alpha}$ motion and, therefore, may not include sufficient information about the motion history effects on the flow field. The high alpha motion of case two spans the static stall angle of approximately 15°. As in the case of the ramp up motion considered above, the second order response model gives integrated loads which are higher than the first order results.

XII. Conclusions

* Direct measurements of nonlinear indicial responses in a tow tank facility, along with associated flow visualization, is a promising technique for gaining a fundamental understanding of nonlinear and unsteady flow mechanisms of practical interest. The present study has provided a strong database of indicial response data. The low angle of attack normal force responses have been shown to be in general agreement with the classical theory based on Wagner's function. Numerically integrated indicial responses for certain trial motions have been shown to be in general agreement with baseline data for the same motions. The trial motions which were considered represent a significant challenge for CFD solution methods.

* For large amplitude motions, a large amount of indicial response data may be required. The functional form of the indicial response changes radically over a range of angle of attack of $0° \leq \alpha \leq 60°$. As such, it is difficult to make use of regression techniques and/or curve fitting to simplify the evaluation of the convolution integral. The alternative is to numerically integrate the indicial response data, the accuracy of which depends on the amount of data available.

* Integrated first order indicial responses appear to model dynamic stall effects(for ramp up motion) reasonably well for $K \leq 0.01$. For pitch rates higher than 0.01, the use of only first order responses begins to give increasingly incorrect results. This is primarily due to static stall effects(separated flow at onset) which are naturally embedded within the first order responses. Including second order effects which include flow separation delay has been shown to improve the integrated loads.

* For onset angles below the static stall angle of attack the first order and second order(for $\dot{\alpha}$ >

0) responses measured here are similar. For onset angles above the static stall limit rate effects become increasingly important and this appears to be related to the flow separation delay in dynamic onset conditions.

* The contribution of the apparent mass reaction to the nonlinear indicial response needs to be studied. Without knowledge of the nonlinear noncirculatory effects, full prediction of nonlinear aerodynamic loading using the present method is not possible.

Acknowledgements

This work was sponsored by the Air Force Office of Scientific Research under Grant AFOSR-89-0502. The authors are deeply grateful to Mr. Jerry E. Jenkins of Wright Laboratories for his contributions to this study.

XIII. Bibliography

[1]Tobak, M. and Schiff, L.B., "Aerodynamic Mathematical Modeling-Basic Concepts," AGARD Lecture Series No.114, Paper 1, March 1981.

[2]Tobak, M. and Chapman, G.T.,"Nonlinear Problems in Flight Dynamics Involving Aerodynamic Bifurcations," AGARD CP-386, Paper 25, May 1985.

[3]Beddoes, T.S., "Practical Computation of Unsteady Lift," *Vertica*, Vol.8, No.1, pp.55-71, 1984.

[4]Leishman, J.G., "Validation of Approximate Indicial Aerodynamic Functions for Two-Dimensional Subsonic Flow," AIAA *J. of Aircraft*, Vo.25, No.10, pp.914-922, Oct.1988.

[5]Bisplinghoff, R.L. and Ashley, H., *Principles of Aeroelasticity*, Dover Publications Inc., New York, 1962. p.120.

[6]Jenkins, J.E., "Simplification of Nonlinear Indicial Response Models: Assessment for the 2-D Airfoil Case," AIAA *J.of Aircraft*," Vol. 28, No. 2, pp.131-138, Feb. 1991.

[7]Kaplan, W.K., *Advanced Calculus*, Addison-Wesley Publishing Co., 2nd ed., pp. 515-521.

[8]Currie, I.G., *Fundamental Mechanics of Fluids*, Published by McGraw-Hill, Inc., 1974.

[9]Jacobs, E.J. and Sherman, A., "Airfoil Section Characteristics as Affected by Variations of the Reynolds Number," NACA Report No. 586, 1937.

[10]Tobak, M., Chapman, G.T., and Ünal, A., " Modeling Aerodynamic Discontinuities and

Onset of Chaos in Flight Dynamical Systems," Annales des Telecommunications, tome 42, no. 5-6, pp. 300-314, 1987.

Appendix A. The Indicial Response Due to Rotation

Consider the two motions required to measure the indicial response due to a step change in alpha by rotation about some pitch axis as shown in Figure 1. Notice that in Equation 1 the motion functions are expressed in terms of τ. Motion 1 can be represented by a function of the form:

$$\alpha_1(\tau) = \alpha_o + [\mu(\tau) - \mu(\tau-\tau_o)]\, f(\tau) + \mu(\tau-\tau_o)\, f(\tau_o) \tag{A1}$$

where μ is the unit step function, τ_o is the step onset time and $f(\tau)$ is the reference motion ($\alpha(\xi)$ in Figure 1 expressed in terms of τ) describing the airfoil motion up to the time where motion 1 is constrained to be constant at $f(\tau_o)$. Motion 2 is then given by:

$$\alpha_2(\tau) = \alpha_1(\tau) + \mu(\tau-\tau_o)\Delta\alpha \tag{A2}$$

so that:

$$\frac{d\alpha_2}{d\tau} - \frac{d\alpha_1}{d\tau} = \delta(\tau-\tau_o)\Delta\alpha$$

$$\frac{d\dot{\alpha}_2}{d\tau} - \frac{d\dot{\alpha}_1}{d\tau} = \delta'(\tau-\tau_o)\Delta\alpha \tag{A3}$$

Using Equation 1(with zero plunge) to evaluate the required terms on the RHS of Equation 5 (which defines the indicial response) yields:

$$C_{N2}(t) - C_{N1}(t) = \int_0^t \phi_{N\alpha}\frac{d\alpha_2}{d\tau}d\tau + \int_0^t \phi_{N\dot{\alpha}}\frac{d\dot{\alpha}_2}{d\tau}d\tau - \int_0^t \phi_{N\alpha}\frac{d\alpha_1}{d\tau}d\tau - \int_0^t \phi_{N\dot{\alpha}}\frac{d\dot{\alpha}_1}{d\tau}d\tau \tag{A4}$$

which can be rearranged to give:

$$C_{N2}(t) - C_{N1}(t) = \int_0^t \phi_{N\alpha}\left[\frac{d\alpha_2}{d\tau} - \frac{d\alpha_1}{d\tau}\right]d\tau + \int_0^t \phi_{N\dot{\alpha}}\left[\frac{d\dot{\alpha}_2}{d\tau} - \frac{d\dot{\alpha}_1}{d\tau}\right]d\tau \tag{A5}$$

Substituting Equations A3 into A5 and performing the integrations[7] yields:

$$C_{N2}(t) - C_{N1}(t) = \Delta\alpha\,[\phi_{N\alpha} - \phi'_{N\dot{\alpha}}]\,\Big|_{\tau=\tau_o} \tag{A6}$$

where the prime superscript indicates differentiation with respect to τ. Substituting Equation A6 into Equation 5 and letting $\tau_o = \tau$ yields:

$$\phi^*_{N\alpha}[\alpha(\xi);t,\tau] = \phi_{N\alpha}[\alpha(\xi);t,\tau] - \phi'_{N\dot{\alpha}}[\alpha(\xi);t,\tau] \tag{A7}$$

Reducing the indicial responses to first order and writing in terms of elapsed time in accordance with Equation 6 results in:

$$\phi^*_{N\alpha}[t-\tau,\alpha(\tau)] = \phi_{N\alpha}[t-\tau,\alpha(\tau)] - \phi'_{N\dot{\alpha}}[t-\tau,\alpha(\tau)] \tag{A8}$$

which is identical to Equation 18 which defines $\phi^*_{N\alpha}$.

Appendix B. Second Order Normal and Axial Force Indicial Responses
For A Ramp Up to Step Onset at K = 0.05

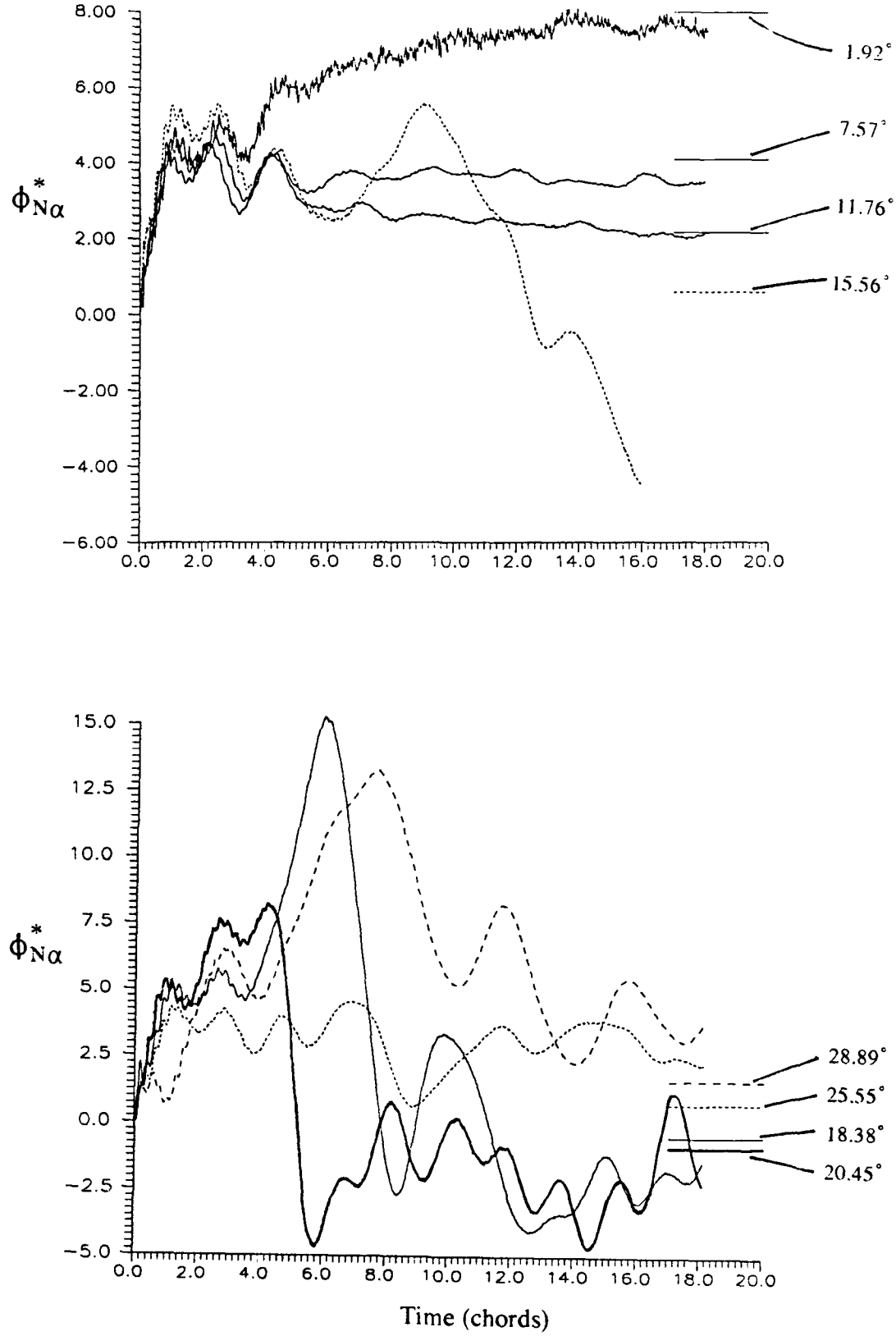
8.00
6.00
4.00
2.00
0.00
−2.00
−4.00
−6.00
$\phi^*_{N\alpha}$
0.0
2.0
4.0
6.0
8.0
10.0
12.0
14.0
16.0
18.0
20.0
1.92°
7.57°
11.76°
15.56°
15.0
12.5
10.0
7.5
5.0
2.5
0.0
−2.5
−5.0
$\phi^*_{N\alpha}$
28.89°
25.55°
18.38°
20.45°
Time (chords)

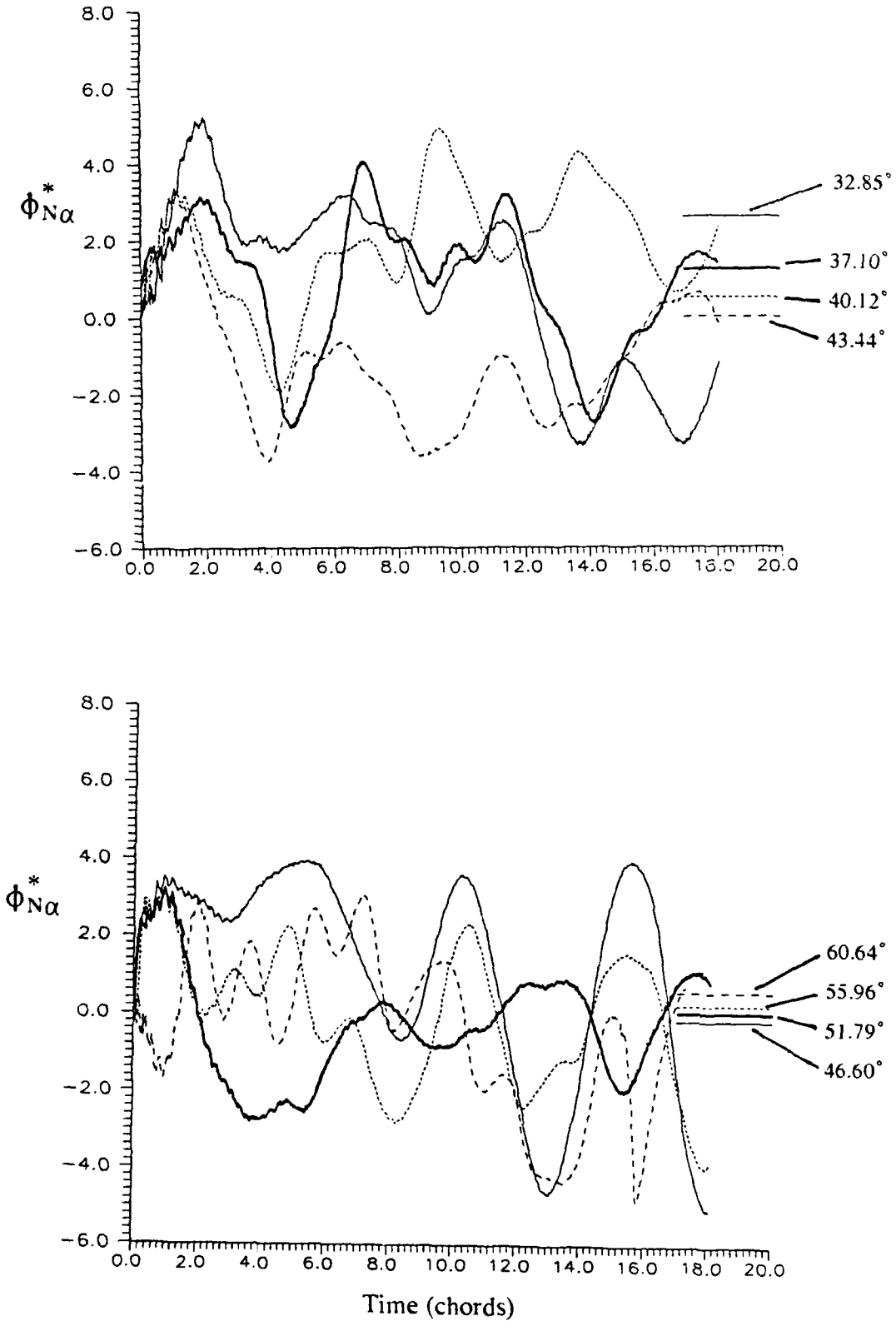
8.0
6.0
4.0
2.0
0.0
−2.0
−4.0
−6.0
$\phi^*_{N\alpha}$
0.0 2.0 4.0 6.0 8.0 10.0 12.0 14.0 16.0 18.0 20.0
32.85°
37.10°
40.12°
43.44°
60.64°
55.96°
51.79°
46.60°
Time (chords)

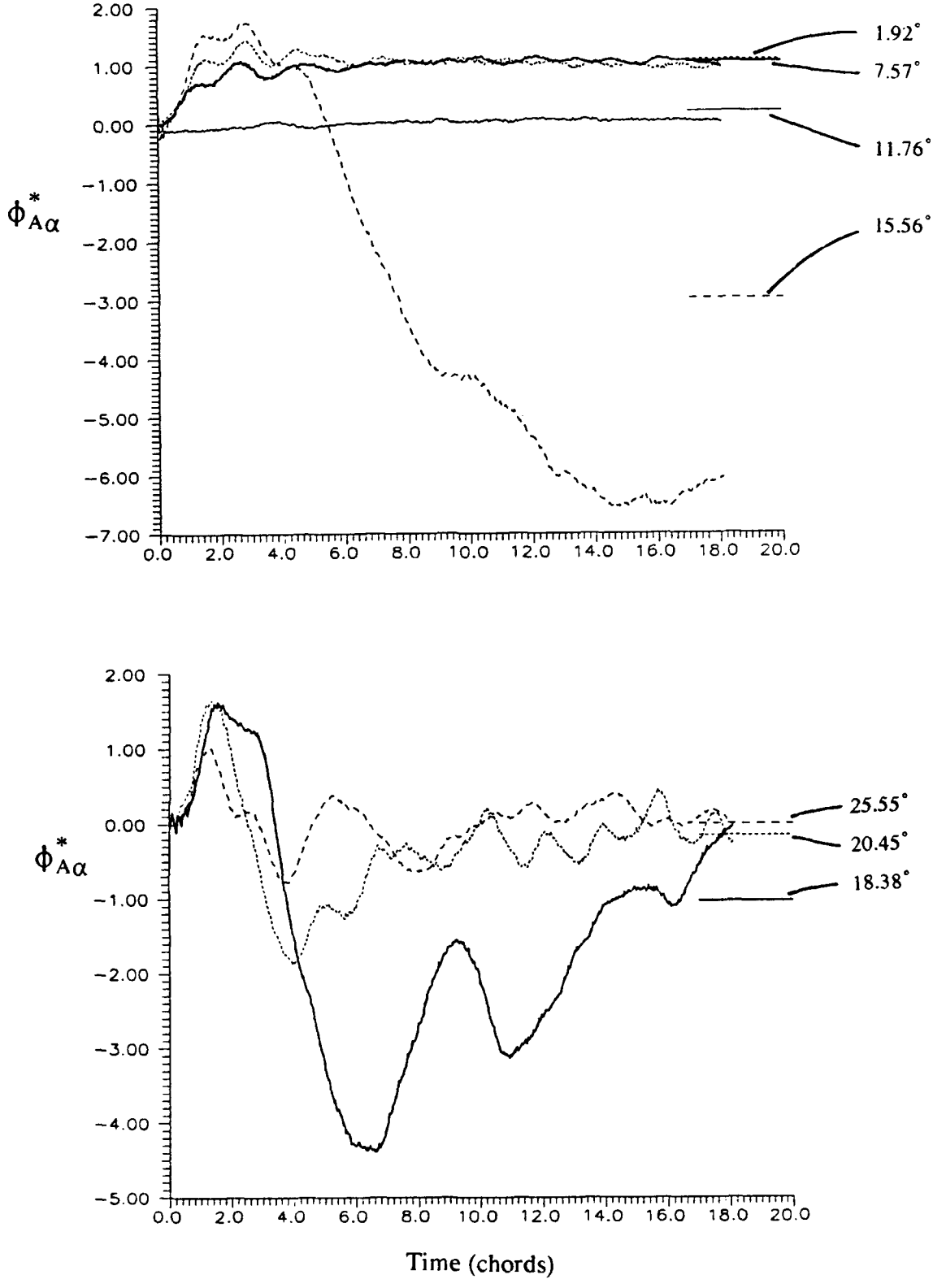
2.00
1.00
0.00
−1.00
−2.00
−3.00
−4.00
−5.00
−6.00
−7.00
$\phi^*_{A\alpha}$
0.0
2.0
4.0
6.0
8.0
10.0
12.0
14.0
16.0
18.0
20.0
1.92°
7.57°
11.76°
15.56°
25.55°
20.45°
18.38°
Time (chords)

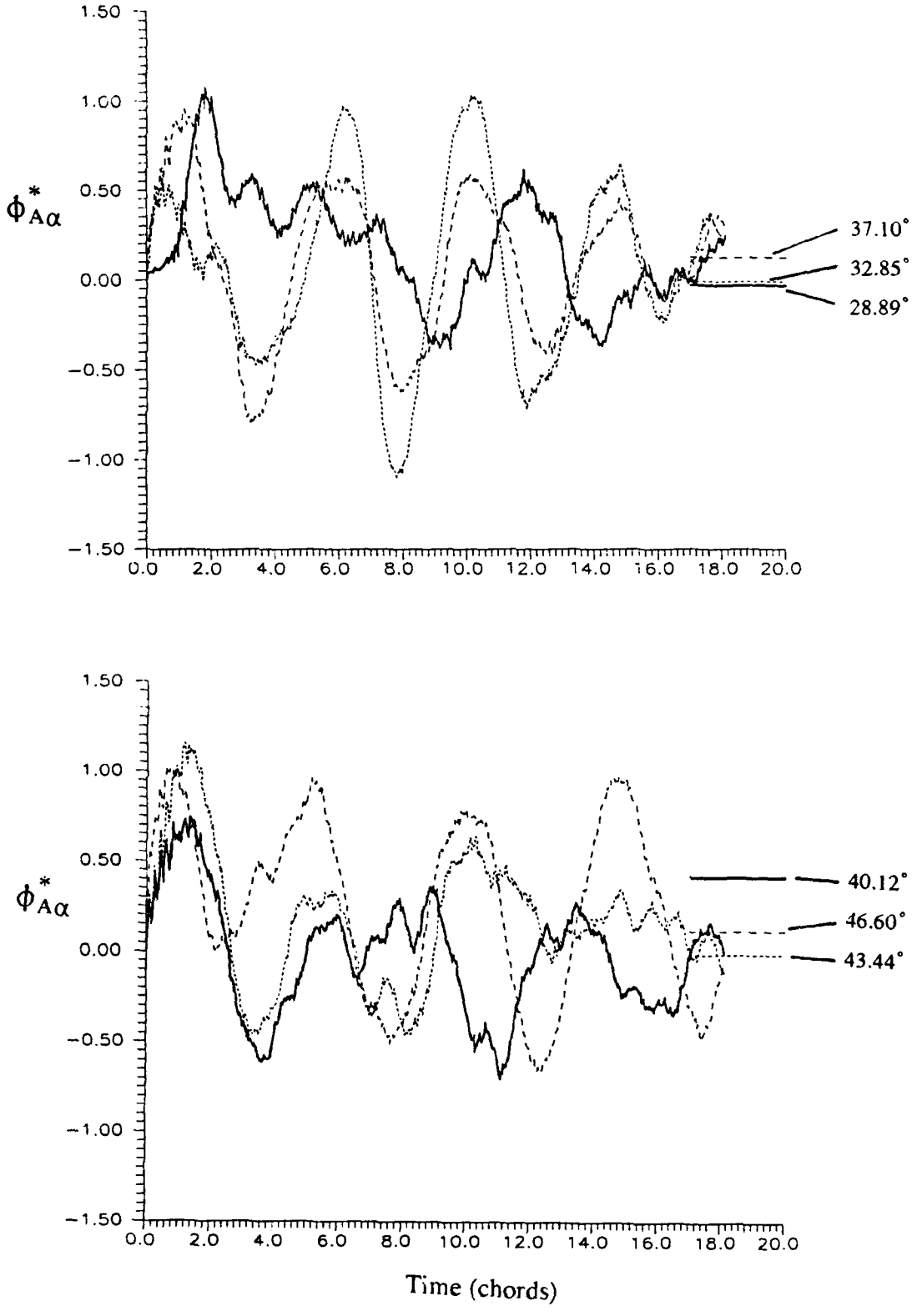
1.50
1.00
0.50
0.00
−0.50
−1.00
−1.50
$\phi^*_{A\alpha}$
0.0
2.0
4.0
6.0
8.0
10.0
12.0
14.0
16.0
18.0
20.0
37.10°
32.85°
28.89°
40.12°
46.60°
43.44°
Time (chords)

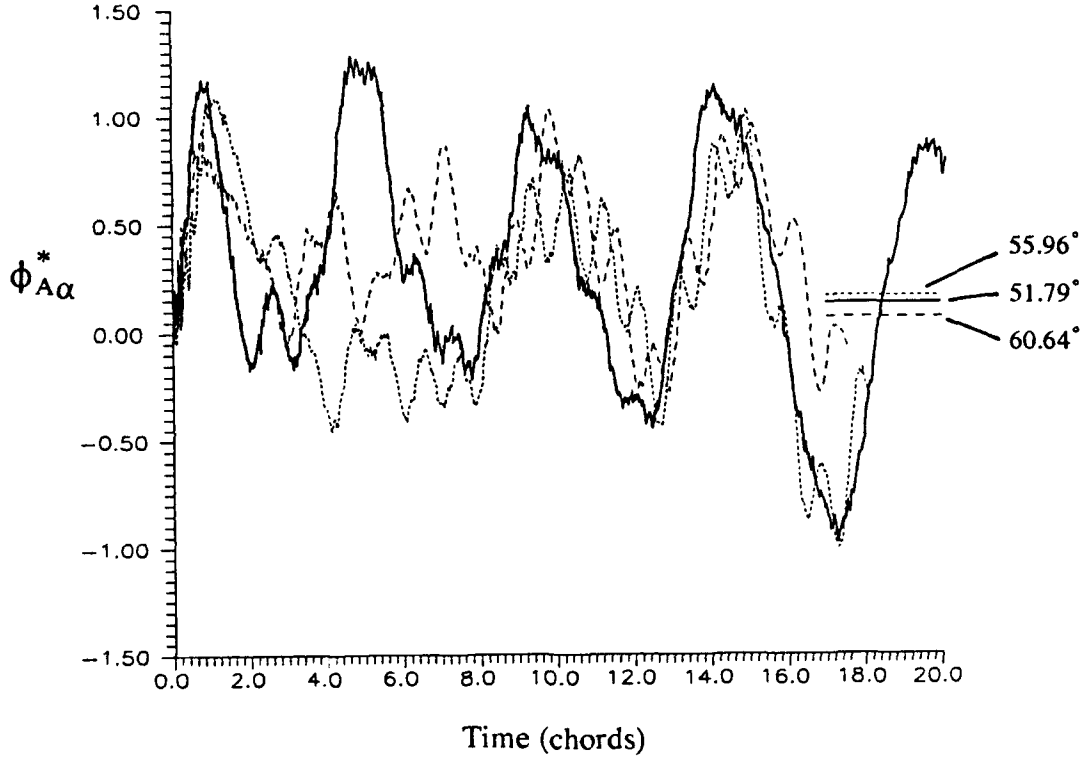
1.50
1.00
0.50
0.00
−0.50
−1.00
−1.50
$\phi^*_{A\alpha}$
0.0
2.0
4.0
6.0
8.0
10.0
12.0
14.0
16.0
18.0
20.0
Time (chords)
55.96°
51.79°
60.64°